Journal of Ophthalmology

Multimodal Imaging in Ophthalmology

Guest Editors: Lisa Toto, Roberto dell'Omo, Gian Marco Tosi, Giuseppe Querques, Sandrine A. Zweifel, and Antoine Labbé

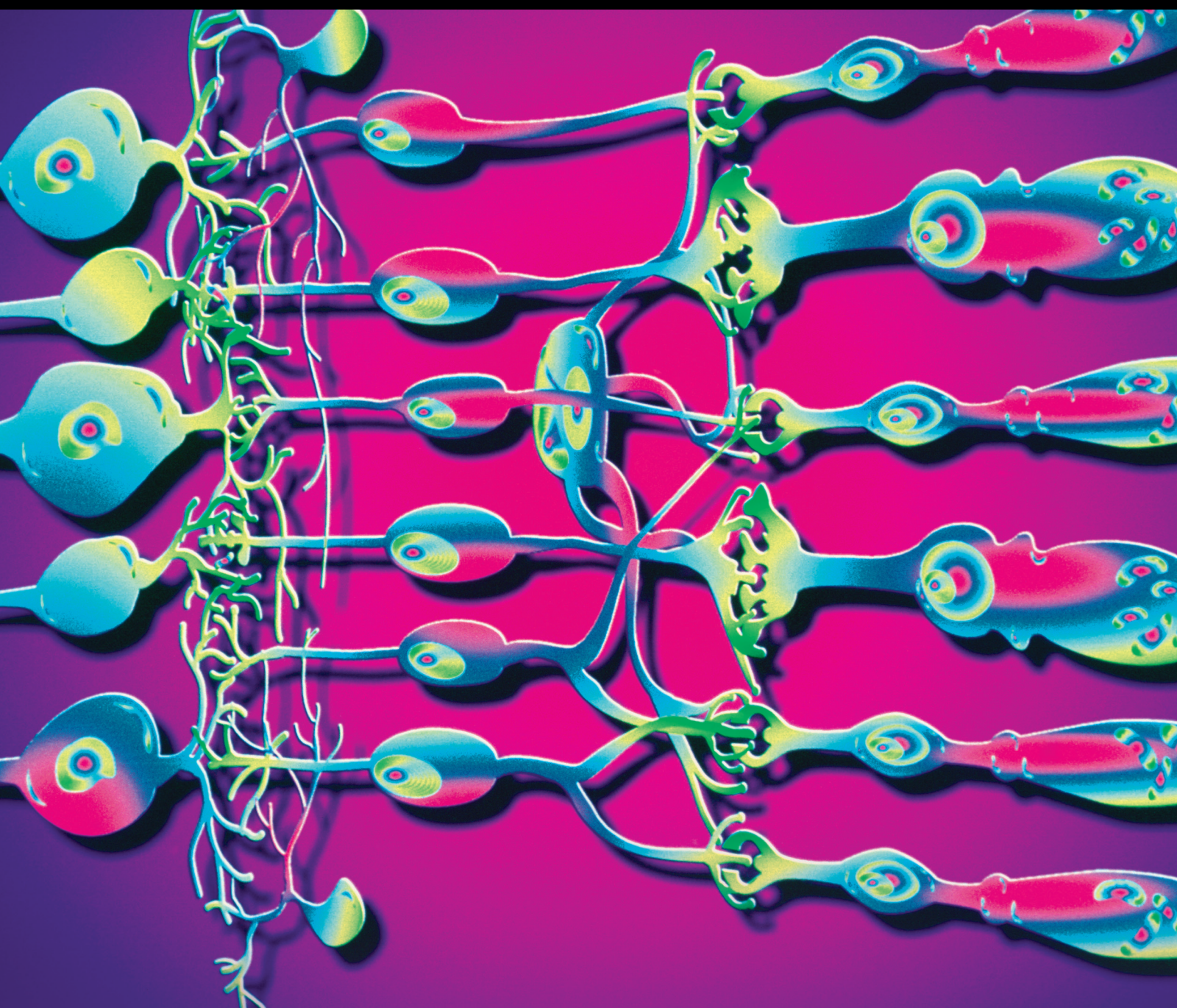

Multimodal Imaging in Ophthalmology

Journal of Ophthalmology

Multimodal Imaging in Ophthalmology

Guest Editors: Lisa Toto, Roberto dell'Omo, Gian Marco Tosi, Giuseppe Querques, Sandrine A. Zweifel, and Antoine Labbé

Copyright © 2016 Hindawi Publishing Corporation. All rights reserved.

This is a special issue published in "Journal of Ophthalmology." All articles are open access articles distributed under the Creative Commons Attribution License, which permits unrestricted use, distribution, and reproduction in any medium, provided the original work is properly cited.

Editorial Board

M. L. Acosta, New Zealand
Hee B. Ahn, Republic of Korea
Luis Amselem, Spain
Usha P. Andley, USA
S. Ansari-Shahrezaei, Austria
Taras Ardan, Czech Republic
F. Arnalich-Montiel, Spain
Takayuki Baba, Japan
Paul Baird, Australia
Antonio Benito, Spain
Mehmet Borazan, Turkey
Francis Carbonaro, Malta
Chi-Chao Chan, USA
Lingyun Cheng, USA
Chung-Jung Chiu, USA
Daniel C. Chung, USA
Colin Clement, Australia
Miguel Cordero-Coma, Spain
Ciro Costagliola, Italy
Vasilios F. Diakonis, USA
Priyanka P. Doctor, India
Michel E. Farah, Brazil
Giulio Ferrari, Italy
Paolo Fogagnolo, Italy
Farzin Forooghian, Canada
Joel Gambrelle, France
M. Gamulescu, Germany
Santiago Garcia-Lazaro, Spain
Ian Grierson, UK
V. Grigoropoulos, Greece
Takaaki Hayashi, Japan
Takeshi Ide, Japan
Vishal Jhanji, Hong Kong
Thomas Klink, Germany
Naoshi Kondo, Japan
Ozlem G. Koz, Turkey
Rachel W. Kuchtey, USA
Hiroshi Kunikata, Japan
Toshihide Kurihara, Japan
George Kymionis, Greece
Neil Lagali, Sweden
Achim Langenbucher, Germany
Van C. Lansingh, Mexico
Paolo Lanzetta, Italy
Theodore Leng, USA
Marco Lombardo, Italy
Tamer A. Macky, Egypt
David Madrid-Costa, Spain
Edward Manche, USA
Flavio Mantelli, USA
E. Mencía-Gutiérrez, Spain
Marcel N. Menke, Switzerland
Lawrence S Morse, USA
Darius M. Moshfeghi, USA
Majid M. Moshirfar, USA
Hermann Mucke, Austria
R. Naranjo-Tackman, Mexico
Magella M. Neveu, UK
Neville Osborne, UK
Ji-jing Pang, USA
Enrico Peiretti, Italy
David P. Piñero, Spain
Jesús Pintor, Spain
Gordon Terence Plant, UK
Pawan Prasher, India
Antonio Queiros, Portugal
Anthony G. Robson, UK
Mario R. Romano, Italy
Dirk Sandner, Germany
Ana R. Santiago, Portugal
Patrik Schatz, Sweden
Kin Sheng Lim, UK
Wisam A. Shihadeh, USA
Bartosz Sikorski, Poland
Katsuyoshi Suzuki, Japan
S. K. Swamynathan, USA
Suphi Taneri, Germany
C. Tappeiner, Switzerland
Stephen C. B. Teoh, Singapore
P. Theodossiadis, Greece
Biju B. Thomas, USA
Lisa Toto, Italy
Manuel Vidal-Sanz, Spain
Gianmarco Vizzeri, USA
David A. Wilkie, USA
Suichien Wong, UK
V. W Y Wong, Hong Kong
Wai T. Wong, USA
Terri L. Young, USA
H. Gon Yu, Republic of Korea
Vicente Zanon-Moreno, Spain

Contents

Hindawi Publishing Corporation
Journal of Ophthalmology
Volume 2016, Article ID 3120129, 1 page
http://dx.doi.org/10.1155/2016/3120129

Editorial
Multimodal Imaging in Ophthalmology

Lisa Toto,[1] Roberto dell'Omo,[2] Gian Marco Tosi,[3] Giuseppe Querques,[4,5] Sandrine A. Zweifel,[6] and Antoine Labbé[7]

[1]*Ophthalmology Clinic, University "G. d'Annunzio" of Chieti-Pescara, 66100 Chieti, Italy*
[2]*University of Molise, 86100 Campobasso, Italy*
[3]*Ophthalmology Section, Department of Medicine, Surgery and Neuroscience, University of Siena, 53100 Siena, Italy*
[4]*Department of Ophthalmology, University Paris Est Creteil, Centre Hospitalier Intercommunal de Creteil, 94010 Creteil, France*
[5]*Department of Ophthalmology, University Vita-Salute, IRCCS Ospedale San Raffaele, Via Olgettina, 60 20132 Milan, Italy*
[6]*Department of Ophthalmology, University Hospital Zurich, University of Zurich, Zurich, Switzerland*
[7]*Department of Ophthalmology III, Quinze-Vingts National Ophthalmology Hospital, 75012 Paris, France*

Correspondence should be addressed to Lisa Toto; totolisa@hotmail.com

Received 14 June 2016; Accepted 14 June 2016

Copyright © 2016 Lisa Toto et al. This is an open access article distributed under the Creative Commons Attribution License, which permits unrestricted use, distribution, and reproduction in any medium, provided the original work is properly cited.

In recent years the use of different, established, and novel imaging techniques provided detailed insight into several retinal diseases. These modalities provide information about anatomy and functional changes in the retina with high resolution images which improve diagnosis and management of retinal pathologies.

The special issue on multimodal imaging in ophthalmology published seven clinical research articles.

Among published articles R. R. Bastos et al. evaluated the usefulness of multimodal image analysis to characterize vitelliform lesions in adult-onset foveomacular vitelliform dystrophy and acquired vitelliform patients. R. Mastropasqua et al. used intraoperative and postoperative spectral domain optical coherence tomography (SD-OCT) to evaluate anatomical results after two different ocriplasmin injection procedures for the treatment of vitreomacular traction. P.-M. Lêvèque et al. used OCT angiography to detect changes in optic nerve head vascularization in glaucoma patients. E.V. Boiko and D. S. Maltsev compared retromode scanning laser ophthalmoscopy images and OCT central retinal thickness maps as a guide for macular laser photocoagulation in patients with macular edema. L. M. Brandao et al. compared two different spectral-domain OCT systems in regard to full macular thickness and ganglion cell layer-inner plexiform layer measures and in regard to structure-function correlation when compared to standard automated perimetry. Q. Liang et al. evaluated the relationship between corneal and conjunctival epithelium thickness evaluated with SD-OCT and ocular surface clinical tests in dry eye disease patients.

I. Yuvaci et al. assessed the effects of mydriatics on choroidal thickness evaluated by means of SD-OCT with Enhanced Depth Imaging modality and anterior chamber changes evaluated using a Pentacam Scheimpflug camera system. All manuscripts underwent a peer review process before publication.

Lisa Toto
Roberto dell'Omo
Gian Marco Tosi
Giuseppe Querques
Sandrine A. Zweifel
Antoine Labbé

Hindawi Publishing Corporation
Journal of Ophthalmology
Volume 2016, Article ID 6037537, 6 pages
http://dx.doi.org/10.1155/2016/6037537

Research Article

Multimodal Image Analysis in Acquired Vitelliform Lesions and Adult-Onset Foveomacular Vitelliform Dystrophy

Ricardo Rocha Bastos,[1] Carla Sofia Ferreira,[1] Elisete Brandão,[1] Fernando Falcão-Reis,[1,2] and Ângela M. Carneiro[1,2]

[1]*Department of Ophthalmology, Hospital São João, Porto, Portugal*
[2]*Department of Sense Organs, Faculty of Medicine, University of Porto, Portugal*

Correspondence should be addressed to Carla Sofia Ferreira; carla.sss.ferreira@gmail.com

Received 5 November 2015; Revised 24 February 2016; Accepted 17 March 2016

Academic Editor: Lisa Toto

Copyright © 2016 Ricardo Rocha Bastos et al. This is an open access article distributed under the Creative Commons Attribution License, which permits unrestricted use, distribution, and reproduction in any medium, provided the original work is properly cited.

Purpose. To characterize vitelliform lesions (VLs) in adult-onset foveomacular vitelliform dystrophy (AOFVD) and acquired vitelliform (AVL) patients using multimodal image analysis. *Methods*. Retrospective study of twenty-eight eyes from nineteen patients diagnosed with AVL or AOFVD. They were evaluated by color fundus photographs, fundus autofluorescence (FAF), fluorescein angiography (FA), and spectral-domain optical coherence tomography (SD-OCT). *Results*. Bilateral VLs were associated with AOFVD ($p = 0.013$). Regular and centered VLs were associated with AOFVD ($p = 0.004$ and $p = 0.016$), whereas irregular and noncentered lesions were more frequent in AVL patients. Visual acuity, greatest linear dimension (GLD), lesion height (LH), and pseudohypopyon were similar between groups. Whereas median LH and GLD in AVL group diminished significantly during follow-up ($p = 0.009$ and $p = 0.001$), AOFVD lesions tended to become larger and thicker. *Conclusions*. When consulting a patient presenting a VL with unknown age of onset, familial history, or previous retinal diseases, some aspects of multimodal imaging assessment may lead the ophthalmologist to a correct diagnosis.

1. Introduction

Vitelliform lesions (VLs) correspond to an accumulation of yellowish material in the subretinal space. This phenotype is shared by different retinal diseases, with distinct genetic background and etiologies [1, 2]. These lesions may evolve over time and may be classified in the following stages:

(i) *Stage I* (previtelliform): normal or only subtle RPE changes (tiny, central honeycomb structure centrally), normal vision.

(ii) *Stage II* (vitelliform): classic "egg-yolk" lesion, normal vision or mild vision loss.

(iii) *Stage III* (pseudohypopyon): layering of lipofuscin, normal vision or mild vision loss.

(iv) *Stage IV* (vitelleruptive): breakup of material gives "scrambled egg" appearance; vision may be mildly decreased.

(v) *Stage V* (atrophic): central RPE and retinal atrophy; vision may range from 20/30 to 20/200.

(vi) *Stage VI* (choroidal neovascularization, CNV): in about 20% of patients; vision often decreased to 20/200 or worse [1, 2].

When detected in younger patients, VLs usually occur in the setting of Best macular dystrophy (Best disease), an autosomal dominant disease associated with a mutation in bestrophin 1 (BEST1) [3, 4].

Adult-onset foveomacular vitelliform dystrophy (AOFVD) is a subtype of macular pattern dystrophies, being associated with mutations in the peripherin 2 (PRPH2) gene, either sporadic or inherited in an autosomal dominant manner [5, 6]. The age of onset is typically between 30 and 50 years, and it is recognized as a pleomorphic disease, with great variability in size, shape, and distribution of the vitelliform material [1, 5].

Acquired vitelliform lesions (AVL) are a different type of VL associated with multiple retinal diseases such as age-related macular degeneration (AMD), cuticular drusen, tractional maculopathies, pseudoxanthoma elasticum, and central serous chorioretinopathy [1, 7].

All the aforementioned diseases share the lack of direct apposition between the photoreceptor outer segments and the retinal pigment epithelium (RPE), which could delay the phagocytosis of shed outer segment photoreceptor tips, and lead to the accumulation of yellowish subretinal vitelliform material [2, 6–9].

Whereas Best disease may be easily distinguished from other VLs by the age of diagnosis or electrophysiological study, the differential diagnosis between AOFVD and AVL may be difficult in patients without familial history of disease or with simultaneous macular diseases.

In this study we characterize the VL in AOFVD and AVL patients using multimodal imaging analysis, exposing similarities and differences that could help in differential diagnosis between the two entities in clinical practice.

2. Methods

This is a retrospective study of patients diagnosed with AVL or AOFVD, who were evaluated in the Department of Ophthalmology of Hospital São João, a tertiary health care center, at Porto, between June 2011 and December 2013. The tenets of the Declaration of Helsinki were followed and local Ethics Committee approval was obtained.

Only eyes having previously undergone multimodal imaging analyses (color fundus photographs, fundus autofluorescence (FAF), fluorescein angiography (FA), and spectral-domain optical coherence tomography (SD-OCT)) were included. Color fundus photographs were obtained with TRC-50EX mydriatic camera (TopCon Medical Systems, Tokyo, Japan). Spectral-domain optical coherence tomography, FAF, and FA were performed using Spectralis HRA + OCT system (Heidelberg Engineering, Heidelberg, Germany).

For each patient we recorded age, type and laterality of VL, associated macular lesions, baseline and final best-corrected visual acuity (VA) using ETDRS charts, and follow-up period. Loss of VA was analyzed as a continuous variable for each letter lost. Vitelliform lesions were evaluated for their stage, integrity of external limiting membrane and the assumed inner segment/outer segment junction (classified as present, absent, or disrupted), intraretinal fluid, and hyporeflective area in the subretinal space both at the baseline and at the final consult. The shape of VL was classified as round or irregular and the location was determined by the foveal topographic relationship and symmetry, being categorized as central or eccentric to the fovea.

Quantitative measurements of anatomical features (greatest linear dimension (GLD) and lesion height (LH)) were recorded using the calipers provided by the review software of the Spectralis HRA + OCT, similar to the method used by Freund et al. [2].

Patients were divided into two groups, AOFVD and AVL, according to familial history and the absence of other previous retinal diseases in the former. In both groups, a normal Arden Index was an obligatory finding. Cases with baseline choroidal neovascularization were excluded. During the follow-up, no patient has received any treatment, such as cataract surgery or CNV intravitreal injections.

Table 1: Summary of clinical findings. Results are expressed as follows: *median, 25th–75th percentiles and †absolute number, %. AVL, acquired vitelliform lesions; AOFVD, adult-onset foveomacular vitelliform dystrophy.

Patient characteristics	AVL	AOFVD	p value
Age (years)*	79 (69–82.50)	73 (61.25–78)	0.210
Male gender†	5 (38.5%)	3 (50%)	0.506
Bilateral cases†	3 (23.1%)	6 (100%)	0.013
Presence of AMD†	7 (53.8%)	0 (0%)	0.044

Statistical calculations were performed using Statistical Package for Social Sciences (version 20.0; SPSS, Inc., Chicago, Illinois, USA). Descriptive analysis was performed for all variables measured. Categoric variables were compared using the chi-square test, and differences for quantitative variables were analyzed by Mann-Whitney U or Kruskal-Wallis test. The association between VA and quantitative measures of lesion was analyzed by Kendall's tau test. The chosen level of statistical significance was $p < 0.05$.

3. Results

Twenty-eight eyes of nineteen patients were included in this study. Thirteen patients were diagnosed with AVL (16 eyes) and six with AOFVD (12 eyes). The median follow-up was 10 months, being the 25th–75th percentiles [5–29]. The groups were followed up by a similar median ($p = 0.782$)—the AVL group was followed up by a median of 9 [7; 22] months and AOFVD by 11 [5; 28] months.

A summary of patient characteristics in each group is presented in Table 1. In our case series, VLs were more frequent in patients in their eighth decade and a slight female predominance was observed. We found no statistical differences in the demographic characteristics between the two groups.

3.1. Fundoscopic Findings. At presentation, the majority of lesions were stage II, with the classic egg-yolk pattern being present in 8 eyes (50%) of AVL patients and in 7 eyes (58.33%) of AOFVD group. This difference did not achieve statistical significance ($p = 0.461$). Pseudohypopyon was observed in 5 patients (31.25%) in AVL group, compared with 2 cases (16.7%) in AOFVD, which also represented a nonsignificant difference between groups ($p = 0.662$). The presence of vitelleruptive stage was also evenly distributed between groups (3 eyes versus 2 eyes, $p = 0.662$). Atrophy was only verified in one AOFVD case.

Unilateral VLs were present only in AVL group. On the other hand, bilateral VLs were found in 3 AVL patients (23.1%) and in 6 AOFVD patients (100%), being significantly associated with the adult-onset disease ($p = 0.013$).

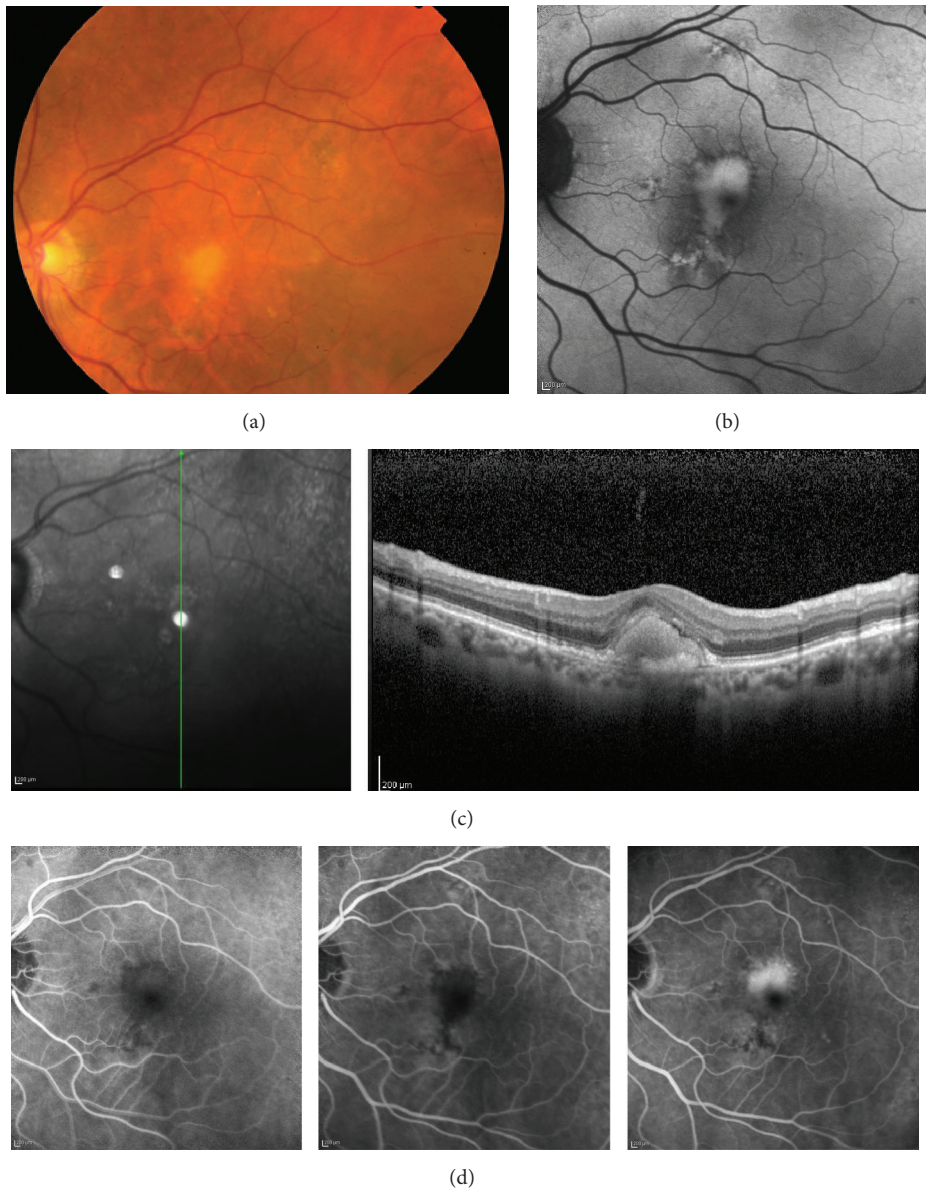

Figure 1: Multimodal imaging of AVL. (a) Color photograph showing an AVL associated with sparse drusen. (b) FAF reveals hyperautofluorescence corresponding to the yellowish material in the color photograph; VL is irregular and in an eccentric position related to the fovea. (c) SD-OCT shows hyperreflective material within the subretinal space. (d) FA revealing blocked fluorescence by material within the subretinal space in the early phases and staining of the AVL during the late phases of angiogram. AVL, acquired vitelliform lesion; FAF, fundus autofluorescence; VL, vitelliform lesion; SD-OCT, spectral-domain optical coherence tomography; FA fluorescein angiography.

The shape and location of the VL were significantly different in the two groups. Regular and centered lesions were associated with adult-onset type ($p = 0.004$ and $p = 0.016$, resp.), whereas irregular and eccentric lesions were more frequent in acquired disease (Figures 1 and 2).

3.2. OCT Findings. Vitelliform lesions observed in the fundoscopic examination were topographically correspondent to hyperreflective material localized between RPE and Ellipsoid Zone or ELM in SD-OCT (Figures 1 and 2). All clinical and OCT findings in the affected eyes are compared in Table 2.

A disrupted Ellipsoid Zone was statistically associated with adult-onset type of disease both at first and at last clinical evaluation ($p = 0.020$ and $p = 0.049$). In acquired form, either the integrity or the absence of this line was more common than a disruption. There was no relation between the integrity of Ellipsoid Zone and the initial or final VA ($p = 0.131$ and $p = 0.384$, resp.).

Initial median LH was 142.5 μm in AVL patients and 118.5 μm in AOFVD cases. This intergroup difference did not achieve statistical significance ($p = 0.452$). At the last follow-up visit, LH measurements were not significantly different

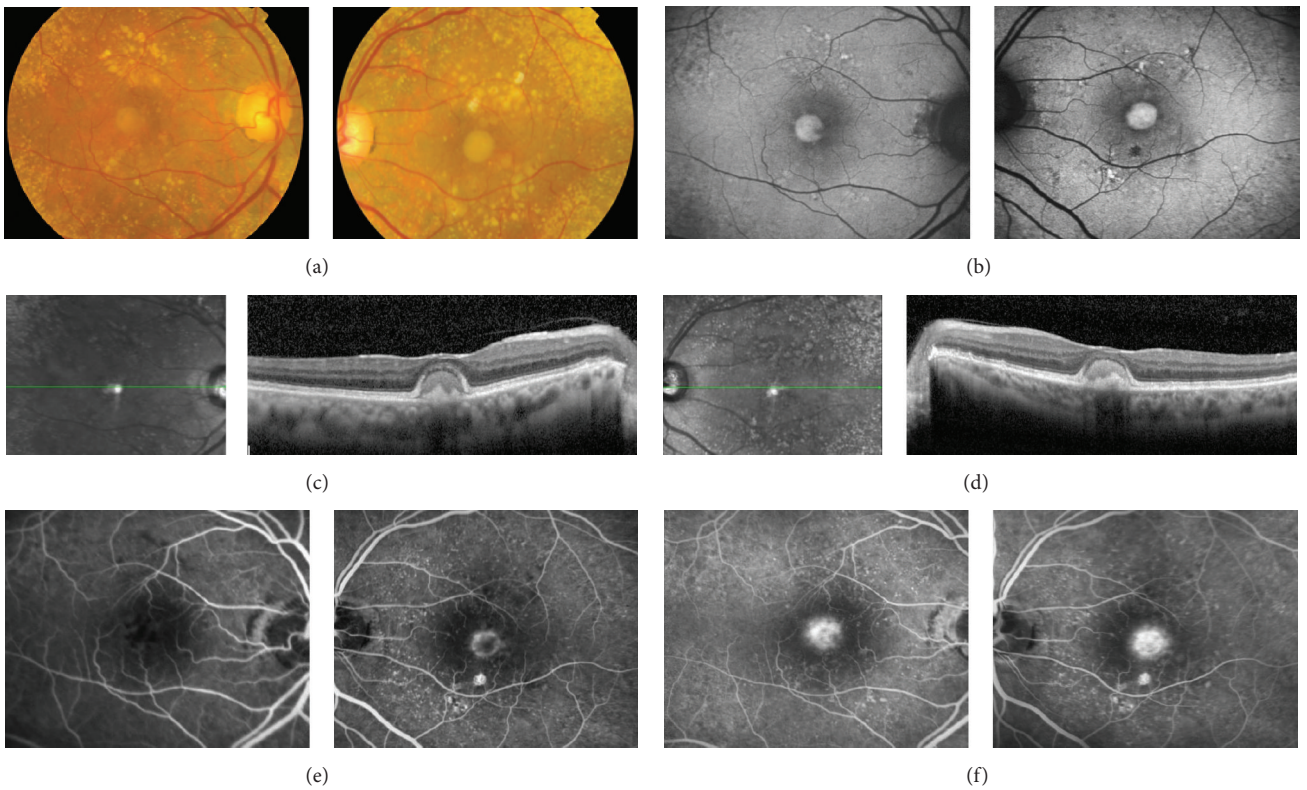

Figure 2: Multimodal imaging of AOFVD. (a) Color photograph showing a VL associated with cuticular drusen. (b) FAF reveals hyperautofluorescence corresponding to the yellowish material in the color photograph; the contours of VL are regular and are centered to the fovea. ((c) and (d)) SD-OCT shows hyperreflective material within the subretinal space in right and left, respectively. (e) FA revealing blocked fluorescence by subretinal material in early phases of angiogram in both eyes, with associated ring of hyperfluorescence in left eye. (f) Staining of VL in the late stages of angiogram. AOFVD, adult-onset foveomacular vitelliform dystrophy; VL, vitelliform lesion; FAF, fundus autofluorescence; SD-OCT, spectral-domain optical coherence tomography; FA, fluorescein angiography.

Table 2: Summary of visual acuity and OCT findings. Results are expressed as follows: *median, 25th–75th percentiles and †absolute number, %. AVL, acquired vitelliform lesions; AOFVD, adult-onset foveomacular vitelliform dystrophy; VA, visual acuity; LH, lesion height; GLD, greatest linear dimension; IS/OS, inner segment/outer segment; ELM, external limiting membrane.

	AVL	AOFVD	p value
Initial VA (letters)*	67.5 (62.25–77)	64.5 (51.25–72.25)	0.347
Final VA (letters)*	65.5 (54.75–73)	61 (54.75–73.75)	0.909
Difference in VA (letters)*	−4 (−9–4.75)	2 (−19.75–18.50)	0.260
Initial LH (μm)*	142.5 (106.5–168)	118.5 (85.75–170.25)	0.452
Final LH (μm)*	125.5 (101.75–226.25)	189 (121.25–285.75)	0.291
Difference in LH (μm)*	27 (−15–44.5)	12 (1–142.25)	0.892
Initial GLD (μm)*	864 (555.25–1505)	736 (487.75–960.75)	0.336
Final GLD (μm)*	761.5 (567.5–1128)	1355 (737.75–2033.75)	0.213
Difference in GLD (μm)*	33.5 (−3.75–273.50)	163.5 (−31–1238)	0.616
Pseudohypopyon†	5 (31.25%)	2 (16.7%)	0.662
Initial interrupted Ellipsoid Zone†	4 (25%)	9 (75%)	0.020
Final interrupted Ellipsoid Zone†	3 (18.75%)	7 (58.5%)	0.049
Initial integrity of ELM†	16 (100%)	12 (100%)	—
Final integrity of ELM†	16 (100%)	7 (87.5%)	0.364
Initial hyporeflective subretinal space†	9 (56.25%)	8 (66.7%)	0.705
Final hyporeflective subretinal space†	9 (64.3%)	4 (50%)	0.662
Regular lesion†	4 (25%)	9 (75%)	0.004
Centered lesion	7 (43.75%)	11 (91.7%)	0.016

between groups ($p = 0.291$). However, in AVL group, when comparing the initial and final measurement of LH, there was significative shrinkage (142.5 versus 125.5, $p = 0.009$), which was not the case in AOFVD group (118.5 versus 189, $p = 0.348$).

Greatest linear dimension of VL was also similar when we compare the two groups, at both the initial and the last follow-up visit ($p = 0.336$ and $p = 0.213$). Once again, in the AVL group there was shrinkage, with initial and final measurements being statistically different (864 versus 761.5, $p = 0.001$), while in AOFVD group growing was not significant (736 versus 1355, $p = 0.188$).

We were not able to measure VL of 10 eyes in the final observation: 4 patients lost follow-up (6 eyes), 1 developed CNV (1 eye), 2 evolved to vitelli-disruptive-like stage of the disease (2 eyes), and 1 AOFVD case presented an atrophic-like stage of the disease in one eye.

3.3. FAF Findings. Vitelliform lesions were hyperautofluorescent in FAF exams (Figures 1 and 2). In some cases with pseudohypopyon, FAF revealed a hypoautofluorescent superior half and a hyperautofluorescent bottom half. Some cases evolved to vitelli-disruptive stage and one AOFVD case presented the atrophic stage of the disease. In either case, residual macular lesions were hypoautofluorescent, revealing damage to the RPE.

3.4. Angiographic Findings. In each patient, FA showed early hypofluorescence of the yellowish subretinal VL (Figure 1), occasionally with a halo of hyperfluorescence (Figure 2). A progressive late staining of VL was observed during the angiogram (Figures 1 and 2). Cuticular drusen presented a typical "stars in the sky pattern" in FA. One case developed CNV during the follow-up period.

3.5. Additional Findings. Concerning AVL group, early AMD was the most frequent concurrent disease, being found in 7 cases.

We found a correlation between loss of VA and increasing GLD ($p = 0.034$) and a tendency to an increase in thickness ($p = 0.058$).

4. Discussion

This study exposed both similarities and differences between AVL and AOFVD patients in a multimodal assessment. Bilateral VLs with regular shape, central location, disrupted Ellipsoid Zone, and the absence of other fundoscopic findings were significantly associated with AOFVD. On the other hand, VA, LH, and GLD did not appear to be distinctive features between these two different clinical entities.

The knowledge about VLs has improved significantly over the last years. In this regard, SD-OCT was determinant to localize vitelliform material in the subretinal space, between RPE and Ellipsoid Zone [3, 8]. Fundus autofluorescence also proved to be useful in the controversial theme regarding the composition of vitelliform material, since typical hyperautofluorescence of VL was consistent with previous histopathological findings of outer segment material, melanin granules, and "lipofuscin-like" material [6, 9]. Fluorescein angiography is a keystone in the diagnosis of retinal disease, and it has been fundamental to identify several distinct entities associated with VL, particularly in AVL patients [2].

It is well known that all VLs share a yellowish appearance in fundoscopic evaluation, a subretinal location and homogeneous hyperreflectivity in SD-OCT, hyperautofluorescence in FAF, and a similar behavior during FA [2, 4, 6, 9, 10]. Theoretically, we can distinguish these patients by the age of diagnosis, familial history, and the presence or absence of associated diseases. However, in clinical practice, this distinction is often difficult since we frequently consult patients for the first time in their sixth to eighth decade, with simultaneous retinal diseases and unknown familial ophthalmological history. In fact, the age of diagnosis in our series was not significantly different between the AVL and AOFVD group. Bilateral disease, although not exclusively, was associated with AOFVD and unilateral disease was present only in the AVL group. This is consistent with a genetic predisposition of AOFVD patients. The association found between AVL and simultaneous retinal diseases, namely, early AMD, was previously reported by several authors and expected according to the diagnostic criteria used for the two groups [2, 6, 9, 11, 12].

We found no statistical difference in VA, LH, and GLD between groups, both at initial and at final observation. However, during the follow-up, we recorded a significant decrease in median LH and GLD in the AVL group. On the other hand, AOFVD lesions became larger and thicker at an apparent larger scale but failed to demonstrate a statistically significant change. This finding could be explained by the different etiologies of these two clinical entities. In AVL patients, VLs are secondary to an underlying retinal disease and could tend to evolve earlier to atrophy. Contrarily, in AOFVD patients VLs occur as a result of a genetic predisposition, becoming atrophic only at later stages. Further studies are necessary to validate this different clinical course between the two entities, namely, the earlier progression to atrophy in AVL patients.

Pseudohypopyon and hyporeflective areas in the subretinal space were not distinctive characteristics between groups. Nevertheless, one must add that pseudohypopyon was observed in 31% of AVL patients, a finding considered to be rare in these patients [2]. A recent report by Gonçalves et al. also presented a case of AVL in a patient with cuticular drusen diagnosed in pseudohypopyon stage [13]. This patient evolved to a stage similar to vitelli-disruptive stage described in Best disease, maintaining a good VA, probably due to a preserved Ellipsoid Zone [1, 2]. In our series, we did not find an association between VA and the integrity of Ellipsoid Zone. Contrasting with previously published series, we found a statistically significant correlation between loss of VA and increasing GLD [2]. These findings could be explained by the size of our sample.

The main distinctive features we found between AVL and AOFVD groups in multimodal imaging were morphological, namely, the shape of VLs and their topographic relationship with the fovea. There was a strong association of centrally located and regular ovoid VL in AOFVD patients, as opposed to irregular shaped and eccentrically located VL in AVL cases. In 1974, Gass first described retinal findings in AOFVD as

"round or oval, yellow, subretinal lesions in the foveal area of each eye" [14]. On the contrary, later studies reported significant variability in size and shape of VL both in AOFVD and in AVL patients [1, 2, 5, 7, 15]. The size of our sample could partially explain the statistical significance of our morphological findings. However, since acquired lesions develop from previous retinal diseases, this could define their variable location and shape, leading us to believe that in clinical practice more VLs will be eccentric and irregular in AVL patients when compared to AOFVD.

Our study has several limitations, mostly related to its retrospective nature. The sample size was also small, limiting our ability to detect further statistic correlations or differences. We included both eyes of some patients in the analysis, which may influence the results, though it is partially controlled by the statistical methods used. We measured VL with the caliper function of SD-OCT, which, despite being used in other studies, could introduce some variability in LH and GLD values.

5. Conclusions

When consulting a patient presenting a VL with unknown age of onset, familial history, or previous retinal diseases, some aspects of multimodal imaging assessment may lead the ophthalmologist to a correct diagnosis of either AVL or AOFVD. These features may comprise laterality, shape, VL location in relation to fovea, and its size evolution.

Competing Interests

The authors declare that they have no competing interests.

References

[1] G. Querques, R. Forte, L. Querques, N. Massamba, and E. H. Souied, "Natural course of adult-onset foveomacular vitelliform dystrophy: a spectral-domain optical coherence tomography analysis," *American Journal of Ophthalmology*, vol. 152, no. 2, pp. 304–313, 2011.

[2] K. B. Freund, K. Laud, L. H. Lima, R. F. Spaide, S. Zweifel, and L. A. Yannuzzi, "Acquired vitelliform lesions: correlation of clinical findings and multiple imaging analyses," *Retina*, vol. 31, no. 1, pp. 13–25, 2011.

[3] G. Querques, M. Regenbogen, C. Quijano, N. Delphin, G. Soubrane, and E. H. Souied, "High-definition optical coherence tomography features in vitelliform macular dystrophy," *American Journal of Ophthalmology*, vol. 146, no. 4, pp. 501–507, 2008.

[4] P. Schatz, D. Sharon, S. Al-Hamdani, S. Andréasson, and M. Larsen, "Retinal structure in young patients aged 10 years or less with Best vitelliform macular dystrophy," *Graefe's Archive for Clinical and Experimental Ophthalmology*, vol. 254, no. 2, pp. 215–221, 2016.

[5] S. R. Hannan, G. de Salvo, A. Stinghe, F. Shawkat, and A. J. Lotery, "Common spectral domain OCT and electrophysiological findings in different pattern dystrophies," *British Journal of Ophthalmology*, vol. 97, no. 5, pp. 605–610, 2013.

[6] I. Chowers, L. Tiosano, I. Audo, M. Grunin, and C. J. F. Boon, "Adult-onset foveomacular vitelliform dystrophy: a fresh perspective," *Progress in Retinal and Eye Research*, vol. 47, pp. 64–85, 2015.

[7] L. H. Lima, K. Laud, K. B. Freund, L. A. Yannuzzi, and R. F. Spaide, "Acquired vitelliform lesion associated with large drusen," *Retina*, vol. 32, no. 4, pp. 647–651, 2012.

[8] G. Querques, M. Regenbogen, G. Soubrane, and E. H. Souied, "High-resolution spectral domain optical coherence tomography findings in multifocal vitelliform macular dystrophy," *Survey of Ophthalmology*, vol. 54, no. 2, pp. 311–316, 2009.

[9] R. Spaide, "Autofluorescence from the outer retina and subretinal space: hypothesis and review," *Retina*, vol. 28, no. 1, pp. 5–35, 2008.

[10] R. F. Spaide, K. Noble, A. Morgan, and K. B. Freund, "Vitelliform macular dystrophy," *Ophthalmology*, vol. 113, no. 8, pp. 1392–1400, 2006.

[11] S. A. Zweifel, R. F. Spaide, and L. A. Yannuzzi, "Acquired vitelliform detachment in patients with subretinal drusenoid deposits (reticular pseudodrusen)," *Retina*, vol. 31, no. 2, pp. 229–234, 2011.

[12] R. F. Spaide and J. M. Klancnik Jr., "Fundus autofluorescence and central serous chorioretinopathy," *Ophthalmology*, vol. 112, no. 5, pp. 825–833, 2005.

[13] N. M. Gonçalves, Â. M. Carneiro, E. Brandão, and F. M. Falcão-Reis, "Multimodal imaging of acquired vitelliform lesion diagnosed at pseudohypopyon stage," *Case Reports in Ophthalmological Medicine*, vol. 2013, Article ID 461758, 4 pages, 2013.

[14] J. D. M. Gass, "A clinicopathologic study of a peculiar foveomacular dystrophy," *Transactions of the American Ophthalmological Society*, vol. 72, pp. 139–156, 1974.

[15] R. Brecher and A. C. Bird, "Adult vitelliform macular dystrophy," *Eye*, vol. 4, no. 1, pp. 210–215, 1990.

Hindawi Publishing Corporation
Journal of Ophthalmology
Volume 2016, Article ID 6521304, 6 pages
http://dx.doi.org/10.1155/2016/6521304

Clinical Study

Comparison of Guided and Unguided Ocriplasmin Injection for the Treatment of Vitreomacular Traction: A Preliminary Study

Rodolfo Mastropasqua,[1] Luca Di Antonio,[2] Vincenzo Ciciarelli,[2] Agbeanda Aharrh-Gnama,[2] Marco Rispoli,[3] and Paolo Carpineto[2]

[1]*Ophthalmology Unit, Department of Neurological, Neuropsychological, Morphological and Movement Sciences, University of Verona, 37100 Verona, Italy*
[2]*Ophthalmology Clinic, Department of Medicine and Aging Science, University "G. d'Annunzio" of Chieti-Pescara, 66100 Chieti, Italy*
[3]*Centro Oftalmologico Mediterraneo, 00195 Roma, Italy*

Correspondence should be addressed to Luca Di Antonio; monsieurluca@yahoo.com

Received 5 November 2015; Revised 16 February 2016; Accepted 22 February 2016

Academic Editor: Bartosz Sikorski

Copyright © 2016 Rodolfo Mastropasqua et al. This is an open access article distributed under the Creative Commons Attribution License, which permits unrestricted use, distribution, and reproduction in any medium, provided the original work is properly cited.

This retrospective quality control study aimed at comparing resolution in patients treated with intravitreal ocriplasmin (IVO) using two injection techniques, classical injection procedure (unguided) and targeted injection using a surgical microscope with a 30-gauge 1-inch needle (guided) for the treatment of focal VMT without macular hole. The two groups presented a statistically significant difference in terms of resolution of VMT within the first month following treatment: 1/7 for the unguided group versus 6/7 for the guided group ($p = 0.0291$). The majority of the guided group presented an earlier resolution than the single resolved case in the unguided group. The results of this preliminary study indicate that the injection of ocriplasmin closer to the site of VMT results in the resolution in a higher number of cases and that this resolution occurs in a short time interval.

1. Introduction

The scaffold of the vitreous is composed of collagen fibers (mostly type II) and hyaluronic acid and the posterior vitreous cortex is a complex structure. In the aging eye, after age 40, the vitreous gel begins to liquefy involving nearly 50% by age 80, a process called synchysis. During this time the posterior vitreous scaffold normally detaches from the retina with fluid filling the intervening space.

Vitreomacular traction (VMT) occurs when the vitreous separates from the retina throughout the peripheral fundus but remains adherent posteriorly, causing an anteroposterior traction on a small region encompassing the macular and optic nerve disc. Symptoms include vision impairment and metamorphopsia, accompanied by photopsia. VMT syndrome is associated with a broad spectrum of maculopathies, including cystoid macular edemas, epiretinal membranes (ERM), and macular holes (MH) [1–3].

Current treatment options include intravitreal injections with pharmacological agents that induce an enzymatic vitreolysis to induce complete VMT resolution. One of these pharmacological agents, ocriplasmin (Jetrea, Thrombogenics, Leuven, Belgium), was approved in October 2012 by the United States Food and Drug Administration for the treatment of symptomatic VMT [4]. It was reported to have a superior efficacy for VMT resolution compared to placebo injection in phase III randomized, controlled trials [4].

Although intravitreal injections are considered a cornerstone of retinal care and one of the most commonly performed procedures across all specialties, the technique is still undergoing evolution. Currently, the principle debates concerning intravitreal injections concern the gauge of the needle and the angle/path of scleral penetration [5, 6]. An important aspect of this procedure that has not been adequately evaluated concerns the site in which the agents are released.

For over twenty years, forensic pathologists have known the importance of extracting all of the vitreous humor for analysis given that it presents variations in solute concentration if sampled in the center or in periphery [7]. Filas et al. reported that in vivo vitreolytic agents cause the vitreous to

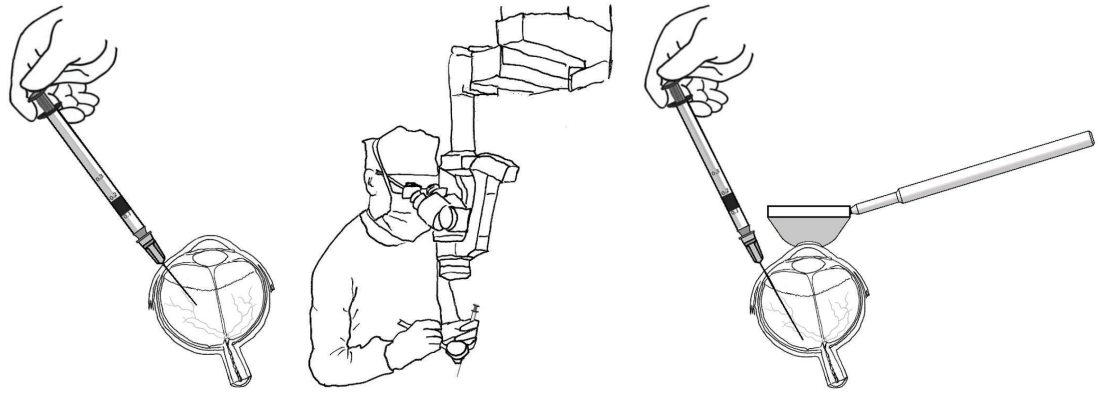

(a) (b) (c)

Figure 1: (a) The unguided injection techniques as suggested by the manufacturer. (b) Additional equipment (30-gauge 1-inch long needle, surgical microscope, and direct contact lens) used for the guided injections. (c) Detail of the injection site release which was not less than 3 mm.

contract and to lose its capacity to bind water with digestion. They also found that proteins spanning the vitreoretinal interface are not affected by hyaluronidase and concluded that these combined effects could exacerbate traction. This could explain why transient vision loss is observed after intravitreal injections [8]. de Smet et al. also recommended injecting the enzyme close to the VMT in order to improve effectiveness [9]. Based on these results we decided to modify our injection procedure by performing a standard intravitreal injection procedure with a surgical microscope equipped with an OCT scanner in an operating room setting and a longer needle in order to release the pharmaceutical agent closer to the VMT.

This retrospective quality control study aimed at comparing resolution in patients treated with intravitreal ocriplasmin (IVO) using two different injecting techniques, standard injection procedure (unguided) and proximal injection using a surgical microscope and a 30-gauge 1-inch needle (guided) for the treatment of focal VMT without macular hole (MH).

2. Patients and Methods

This quality assessment [10] nonrandomized retrospective consecutive case series study adhered to the tenets of the Declaration of Helsinki and received approval from an institution review board. The first fourteen consecutive patients with VMT without MH treated with intravitreal ocriplasmin with two different injecting techniques between June 2014 and September 2015 at the Ophthalmic Clinic of University Chieti-Pescara (Italy) were enrolled. Informed consent was obtained from all patients prior to their enrollment. Patients underwent complete ophthalmic evaluation, including LogMAR visual acuity (VA) testing, and spectral-domain optical coherence tomography (SD-OCT) at baseline and follow-up controls.

2.1. Outcome Measures. The primary outcome measure was VMT resolution. Secondary outcomes were time to resolution, visual acuity, and central macular thickness measured with OCT.

Following injection, patients were visited one day after injection, and at five-day intervals for 30 days. They were also instructed to present within 24 hours if they noted a modification in their vision. During the first follow-up visit the treated eye was uncovered, VA was assessed, and an OCT was acquired. Visual acuity was assessed with the Early Treatment Diabetic Retinopathy Study (ETDRS) chart and standardized measurement criteria [11].

SD-OCT images were acquired through a dilated pupil using an RTVUE XR Avanti (version 2015.100.0.35, Optovue Inc., Fremont, CA) and RTVue-100 (Optovue version 5.1.0.90, Fremont, CA). Each evaluation was performed with both instruments and included a cross-line (10.00 mm scan length) and a 5 mm × 5 mm retinal map for central macular thickness (CMT). In addition, RTVUE XR Avanti was used to obtain enhanced HR line 12 mm scan length. Scans were evaluated by a single experienced ophthalmologist for the presence of VMT (vitreous adhesion within six mm of the fovea and elevation of the posterior vitreous cortex), for VMT release (defined as vitreous release from the macula within a six mm central retinal field), and for the absence of MH.

2.2. Intravitreal Injection Techniques. The unguided standard injection procedure (unguided; Figure 1(a)) was performed according to the manufacturer's instructions (http://jetrea.com/wp-content/uploads/JETREAPrescribingInformation.pdf). Briefly, after the content of the vial reached room temperature, it was diluted with 0.2 mL of 0.9% w/v sodium chloride (sterile, preservative-free) using an aseptic technique. Then 0.1 mL (equivalent of 0.125 mg of ocriplasmin) was injected in the mid-vitreous area using a 30-gauge 1/2-inch injection needle, inserted 3.5–4.0 mm posterior to the limbus and aimed towards the center of the vitreous cavity, avoiding the horizontal meridian. The injections were performed in a sterile operating room but without using a surgical microscope.

The guided injections (Figures 1(b) and 1(c)) were performed in a similar manner except a 30-gauge 1-inch needle was used for the injection. Also, a surgical microscope and

Table 1: Comparison of group characteristics at baseline.

	Unguided	Guided	p
Age (years)	71.7 ± 10.3	73.1 ± 10.2	0.799*
Male, n (%)	1/7	2/7	1.000*
Adhesion size, maximum length (μm)	293.27 ± 59.06	326.75 ± 48.02	0.267**
Epiretinal membrane (presence)	2/7	2/7	1.000*
Phakic lens status, n (%)	7/7	6/7	1.000*
BCVA baseline (logMAR)	0.43 ± 0.26	0.23 ± 0.22	0.121**
Central macular thickness (μm)	368 ± 79	405 ± 89	0.406**

* Fisher's Exact Test; ** two-tailed independent sample t-test.

a contact retinal lens were used to determine the depth of insertion in order to guarantee that the area of release corresponded to the site of VMT (not less than 3 mm from the retinal plane). An intraoperative spectral-domain OCT system integrated into a surgical microscope (Rescan 700 iOCT: Zeiss, Oberkochen, Germany) and evaluation of the shadow produced by the needle on the retinal surface were used to determine the distance from the retina during intravitreal injection.

2.3. Statistical Analysis. All statistical analyses were performed using SPSS 22 (IBM, Armonk, NY) and evaluated at an alpha level of 0.05. Differences in baseline parameters were evaluated with Fisher's Exact Test (qualitative parameters) and two-tailed independent sample t-test with correction for results of Levene's Test for Equality of Variances (quantitative parameters). The primary outcome was evaluated with Fisher's Exact Test. The statistical significance of differences in the temporal distribution of VMT resolution was evaluated using Kaplan-Meier Survival Curves. Statistically significant variations of VA and CMT within group between time points and between groups with single time points were evaluated using two-tailed pair t-tests and Mann-Whitney Tests, respectively.

3. Results

All patients successfully completed follow-up. The two groups of seven patients did not present statistically significant differences in terms of age, sex, phakic lens status, and best corrected visual acuity (Table 1).

The two groups presented a statistically significant difference in the main outcome measure (resolution of VMT) within the first month following treatment: 1/7 for the unguided injection group versus 6/7 for the guided injection group ($p = 0.0291$, Fisher's Exact Test, Figure 2). The Kaplan-Meier Survival Curve analysis of the temporal distribution of VMT resolution indicated a statistically significant difference between the two groups ($p = 0.004$, Figure 3). The majority of the guided injection group (Figure 4) presented an earlier resolution than the single resolved case in the unguided injection group.

Statistically significant intergroup differences for VA and CMT at the three time points were not observed (Figure 5).

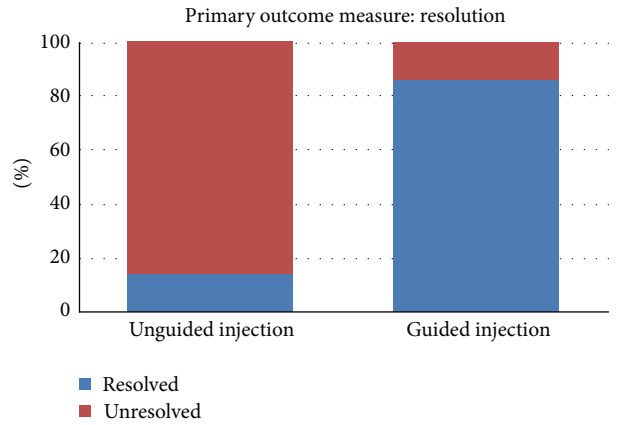

Figure 2: Distribution of patients presenting resolution of VMT within the first month following injection.

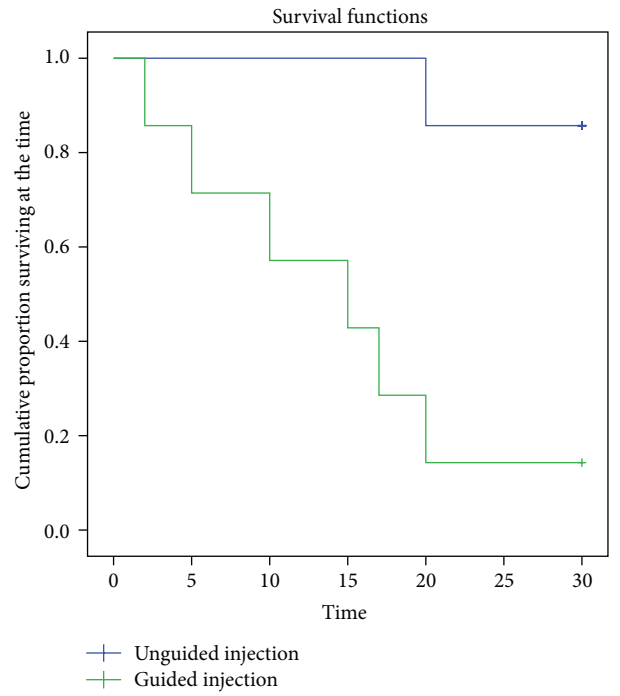

Figure 3: Kaplan-Meier Survival Curves of the temporal distribution of VMT resolution.

Table 2: Secondary outcome measurements: Group mean of the modifications in visual acuity (logMAR) and central macular thickness (μm) of individual patients between time points.

	Time (days)					
	0 versus 5 days		0 versus 30 days		5 versus 30 days	
VA (logMAR)	Mean variation	p	Mean variation	p	Mean variation	p
Unguided injection	0.1	0.111	0.2	0.011	0.1	0.045
Guided injection	0.3	0.003	0.3	0.003	0.3	0.356
CMT (μm)	Mean percentage variation	p	Mean percentage variation	p	Mean percentage variation	p
Unguided injection	23	0.251	46	0.045	48	0.293
Guided injection	85	0.004	66	0.005	−20	0.218

p: two-tailed pair t-test.

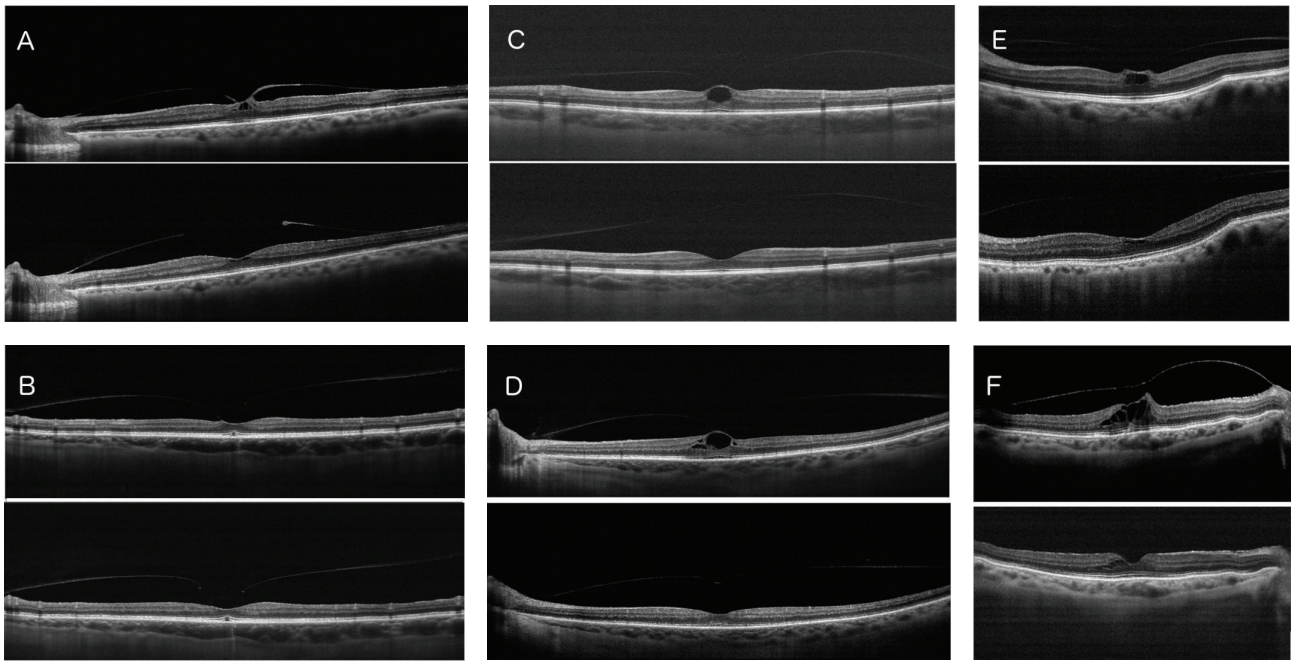

Figure 4: Cross-sectional optical coherence tomography images showing patients (from A to F) before (top) and after (bottom) resolution of vitreomacular traction after intravitreal guided injection of ocriplasmin.

When the intrapatient variation was evaluated, statistically significant differences in VA were observed between baseline and five and thirty days for the unguided group and between baseline and five and thirty days for the guided group (Table 2).

Statistically significant differences in CMT were observed between baseline and thirty days for the unguided group and between baseline and five and thirty days for the guided group (Table 2).

4. Discussion

In this study we investigated the efficacy of ocriplasmin for VMT when using two different injecting procedures. The resolution of VMT was observed in 1/7 of patients in the unguided injection group and in 6/7 of patients in the guided injection group. In phase III clinical trials, the resolution of VMT after ocriplasmin injection was reported to be 26.5% ranging from 41% to 75% with higher percentages in patients with age less than 65 years, focal adhesions less than or equal to 1500 mm, phakic lens status, and absence of epiretinal membrane [12–14].

Previous studies reported comparable percentages of VMT resolution ranging from 42.1% to 66.7% [13, 15]. In our case series, patients did not differ significantly for baseline characteristics such as age (14/14 were more than 65-year-old), sex distribution (6/7 and 5/7 were female in the unguided and guided group, resp.), type of VMT (focal in 14/14 of eyes without ERM and/or MH), and lens status (pseudophakic in 14/14 patients); thus these aspects could not account for the differences between the two groups in resolution rate.

It was demonstrated that injected ocriplasmin has a high autolytic activity in vitreous and that the presence of partially liquefied vitreous may reduce the rate of autolysis prolonging the enzyme activity [9]. During aging the vitreous

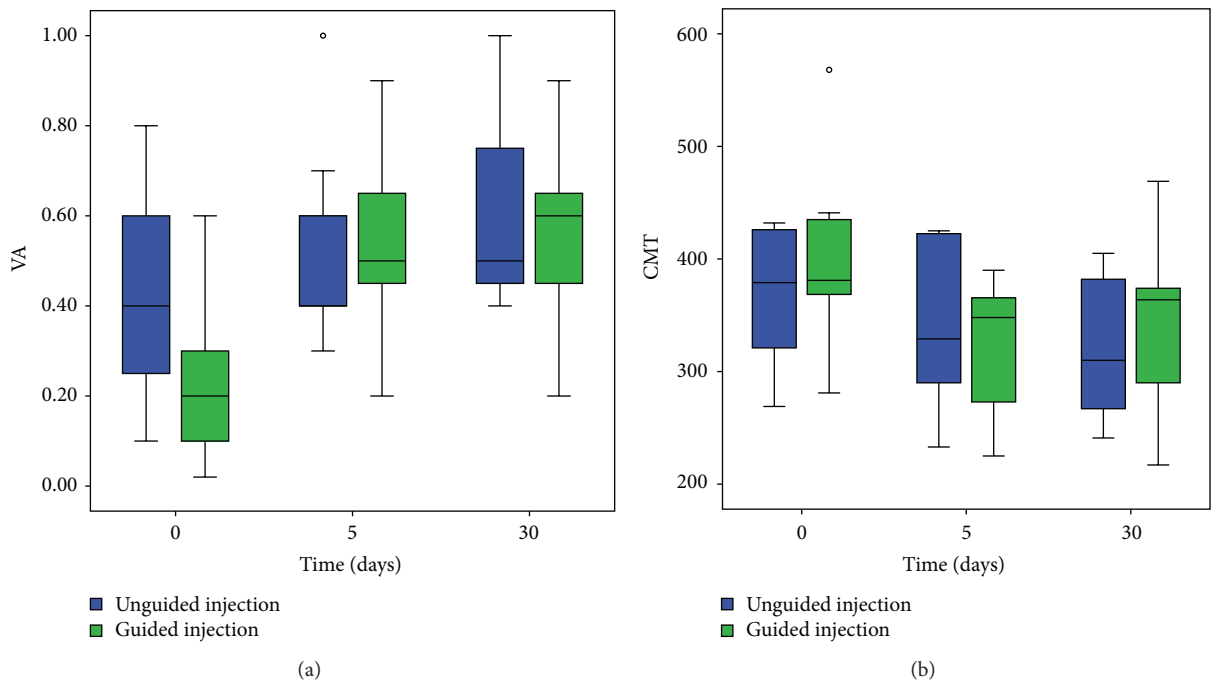

Figure 5: Box plot of visual acuity and central macular thickness. Intergroup differences at the three time points are not statistically significant.

physiologically liquefies and separates from the retina; thus it is possible to hypothesize that, by placing the enzyme deep inside the vitreous cavity close to the site of VMT, increasing the probability that it will be in an area that has already undergone liquefaction, it will result in a high concentration and a prolonged action of the enzyme, accounting for the quicker and higher percentage of resolution in the ocriplasmin guided injection group.

The lower percentage of resolution in the ocriplasmin unguided injection group compared to clinical trials and real life studies was probably due to the small sample size rather than a real difference in the study population [13, 14].

The anatomic resolution of VMT was related to a significant CMT decrease with a mean percentage variation of 85% from 0 to 5 days ($p < 0.04$) and of 66% from 0 to 30 days ($p < 0.005$) in the guided group compared to a mean percentage variation of 23% from 0 to 5 ($p < 0.251$) and 46% from 0 to 30 days ($p < 0.045$) in the unguided group. The related increase of VA showed a mean variation of 0.3 logMAR from 0 to 5 and 0 to 30 days ($p < 0.03$) in the guided group compared to a mean variation of 0.1 decimal in the unguided group from 0 to 5 ($p < 0.11$) and of 0.2 from 0 to 30 days ($p < 0.011$).

Other authors demonstrated a similar improvement of macular anatomy after ocriplasmin injection. Chatziralli et al. described a decrease of macular thickness from 389 ± 152 μm to 263 ± 99 μm for cases with VMT release [15].

Favorable results in terms of visual acuity increase in the guided group were comparable to VA increase observed in phase III clinical trial showing at six months: a gain of two or more lines in 23.7% of patients treated with ocriplasmin compared to 11.2% of patients in the placebo group ($p < 0.001$) [12]. Sharma et al. observed an improvement of two or more lines at one month of follow-up and a gain of three lines or more for a mean follow-up of 258 days in patients treated with ocriplasmin for VMT [16].

This study presents several limits. Adverse events were not evaluated in this study given the low incidence with which they occur and the small sample size. Transitory vision loss was not evaluated since treated eyes were patched for the first 24 hours. Another limit of this study was the sample size. Therefore, prior to drawing conclusive results, a similar study should be performed in a larger study population using a multicenter randomized case-control design.

The results of this preliminary study indicate that the injection of ocriplasmin closer to the site of VMT results in the resolution in a higher number of cases and that this resolution occurs in a shorter time interval compared to a standard injection technique.

Competing Interests

None of the authors have a financial or proprietary interest in the products and materials presented in this paper.

Authors' Contributions

Rodolfo Mastropasqua and Luca Di Antonio contributed equally to this work and should be considered co-first authors.

References

[1] W. E. Smiddy, R. G. Michels, and W. R. Green, "Morphology, pathology, and surgery of idiopathic vitreoretinal macular disorders. A review," *Retina*, vol. 10, no. 4, pp. 288–296, 1990.

[2] D. L. Shechtman and M. T. Dunbar, "The expanding spectrum of vitreomacular traction," *Optometry*, vol. 80, no. 12, pp. 681–687, 2009.

[3] M. W. Johnson, "Posterior vitreous detachment: evolution and complications of its early stages," *American Journal of Ophthalmology*, vol. 149, no. 3, pp. 371–382.e1, 2010.

[4] F. R. Stefanini, M. Maia, P. Falabella et al., "Profile of ocriplasmin and its potential in the treatment of vitreomacular adhesion," *Clinical Ophthalmology*, vol. 8, pp. 847–856, 2014.

[5] E. B. Rodrigues, A. Grumann Jr., F. M. Penha et al., "Effect of needle type and injection technique on pain level and vitreal reflux in intravitreal injection," *Journal of Ocular Pharmacology and Therapeutics*, vol. 27, no. 2, pp. 197–203, 2011.

[6] A. Özkaya, Z. Alkin, U. Çelik et al., "Comparing the effects of three different intravitreal injection techniques on vitreous reflux and intraocular pressure," *Journal of Ocular Pharmacology and Therapeutics*, vol. 29, no. 3, pp. 325–329, 2013.

[7] J. I. Coe, "Postmortem chemistry update. Emphasis on forensic application," *The American Journal of Forensic Medicine and Pathology*, vol. 14, no. 2, pp. 91–117, 1993.

[8] B. A. Filas, Q. Zhang, R. J. Okamoto, Y.-B. Shui, and D. C. Beebe, "Enzymatic degradation identifies components responsible for the structural properties of the vitreous body," *Investigative Ophthalmology and Visual Science*, vol. 55, no. 1, pp. 55–63, 2014.

[9] M. D. de Smet, B. Jonckx, M. Vanhove, J. van Calster, P. Stalmans, and J. M. Stassen, "Pharmacokinetics of ocriplasmin in vitreous," *Investigative Ophthalmology & Visual Science*, vol. 53, no. 13, pp. 8208–8213, 2012.

[10] J. Lynn, M. A. Baily, M. Bottrell et al., "The ethics of using quality improvement methods in health care," *Annals of Internal Medicine*, vol. 146, no. 9, pp. 666–673, 2007.

[11] F. L. Ferris III and I. Bailey, "Standardizing the measurement of visual acuity for clinical research studies: guidelines from the Eye Care Technology Forum," *Ophthalmology*, vol. 103, no. 1, pp. 181–182, 1996.

[12] P. Stalmans, M. S. Benz, A. Gandorfer et al., "Enzymatic vitreolysis with ocriplasmin for vitreomacular traction and macular holes," *New England Journal of Medicine*, vol. 367, no. 7, pp. 606–615, 2012.

[13] B. T. Kim, S. G. Schwartz, W. E. Smiddy et al., "Initial outcomes following intravitreal ocriplasmin for treatment of symptomatic vitreomacular adhesion," *Ophthalmic Surgery Lasers & Imaging Retina*, vol. 44, no. 4, pp. 334–343, 2013.

[14] R. P. Singh, A. Li, R. Bedi et al., "Anatomical and visual outcomes following ocriplasmin treatment for symptomatic vitreomacular traction syndrome," *The British Journal of Ophthalmology*, vol. 98, no. 3, pp. 356–360, 2014.

[15] I. Chatziralli, G. Theodossiadis, E. Parikakis, I. Datseris, and P. Theodossiadis, "Real-life experience after intravitreal ocriplasmin for vitreomacular traction and macular hole: a spectral-domain optical coherence tomography prospective study," *Graefe's Archive for Clinical and Experimental Ophthalmology*, vol. 254, no. 2, pp. 223–233, 2016.

[16] P. Sharma, A. Juhn, S. K. Houston et al., "Efficacy of intravitreal ocriplasmin on vitreomacular traction and full-thickness macular holes," *American Journal of Ophthalmology*, vol. 159, no. 5, pp. 861–867, 2015.

Hindawi Publishing Corporation
Journal of Ophthalmology
Volume 2016, Article ID 6956717, 9 pages
http://dx.doi.org/10.1155/2016/6956717

Research Article

Optic Disc Vascularization in Glaucoma: Value of Spectral-Domain Optical Coherence Tomography Angiography

Pierre-Maxime Lévêque,[1] Pierre Zéboulon,[1] Emmanuelle Brasnu,[1,2] Christophe Baudouin,[1,2,3] and Antoine Labbé[1,2,3,4]

[1]*CHNO des Quinze-Vingts, DHU Sight Restore, INSERM-DHOS CIC, 28 rue de Charenton, 75012 Paris, France*
[2]*Sorbonne Universités, UPMC, INSERM, CNRS, Institut de la Vision, 17 rue Moreau, 75012 Paris, France*
[3]*Department of Ophthalmology, Ambroise Paré Hospital (AP-HP), University of Versailles Saint-Quentin-en-Yvelines, 55 Avenue de Paris, 78000 Versailles, France*
[4]*Department of Ophthalmology III, Quinze-Vingts National Ophthalmology Hospital, 28 rue de Charenton, 75012 Paris, France*

Correspondence should be addressed to Antoine Labbé; dr.antoinelabbe@gmail.com

Received 30 October 2015; Revised 21 January 2016; Accepted 24 January 2016

Academic Editor: Paolo Fogagnolo

Copyright © 2016 Pierre-Maxime Lévêque et al. This is an open access article distributed under the Creative Commons Attribution License, which permits unrestricted use, distribution, and reproduction in any medium, provided the original work is properly cited.

Purpose. To detect changes in optic nerve head (ONH) vascularization in glaucoma patients using spectral-domain OCT angiography (OCT-A). *Material and Method*. Fifty glaucoma patients and 30 normal subjects were evaluated with OCT-A (AngioVue®, Optovue). The total ONH vessel density and temporal disc vessel density were measured. Clinical data, visual field (VF) parameters, and spectral-domain OCT evaluation (RNFL: retinal nerve fiber layer thickness, GCC: ganglion cell complex thickness, and rim area) were recorded for glaucoma patients. Correlations among total and temporal ONH vessel density and structural and VF parameters were analyzed. *Results*. In the glaucoma group, total and temporal ONH vessel density were reduced by 24.7% (0.412 versus 0.547; $p < 0.0001$) and 22.88% (0.364 versus 0.472; $p = 0.001$), respectively, as compared with the control group. Univariate analysis showed significant correlation between rim area (mm^2) and temporal ONH vessel density ($r = 0.623$; $p < 0.0001$) and total ONH vessel density ($r = 0.609$; $p < 0.0001$). Significant correlations were found between temporal and total ONH vessel density and RNFL, GCC, VF mean deviation, and visual field index. *Conclusion*. In glaucoma patients OCT-A might detect reduced ONH blood vessel density that is associated with structural and functional glaucomatous damage. OCT-A might become a useful tool for the evaluation of ONH microcirculation changes in glaucoma.

1. Introduction

Although elevated intraocular pressure (IOP) is the main risk factor for glaucoma, high numbers of patients also develop glaucoma with normal IOP levels [1]. Therefore, other risk factors and in particular vascular risk factors have been implicated in the pathogenesis of glaucoma [2]. These vascular factors include autoregulation of the blood flow (BF) in the optic nerve head (ONH), local vasospasm, arterial hypertension, and nocturnal hypotension [3]. Impaired microcirculation in the ONH may contribute to the initiation and progression of glaucomatous neuropathy. BF in the ONH is supplied by two arterial systems: the central retinal artery in superficial layers and the posterior ciliary artery in deeper layers (prelaminar and lamina cribrosa and retrolaminar structures) [4]. It has been proposed that the main pathologic changes in glaucoma are located in the deep ONH region, supplied by ciliary arteries [5].

Consequently, several techniques have been proposed to measure optic disc perfusion [6, 7]. Laser Doppler velocimetry has been used to identify the maximum BF velocity present in large retinal vessels [6]. Other methods such as scanning laser Doppler flowmetry [8] and laser speckle flowgraphy [9] were also developed to measure disc perfusion. Doppler optical coherence tomography (OCT) has been used to measure the total retinal blood flow around the ONH [10]. Using this imaging technique, BF in large vessels of the ONH can be quantified, but the study of the microvascular structure is impossible due to the low velocity of the BF in small vessels. The microsphere method, a method

based on radioactive solid microspheres injected into the systemic circulation, has also provided evidence that the laser speckle flowgraphy is capable of assaying BF in the deep ONH region but only in experimental glaucoma models [11].

More recently, Jia et al. developed a new method to study in vivo the ONH microcirculation in glaucoma patients: the split spectrum amplitude-decorrelation angiography (SSADA) algorithm [12]. It provides high-quality three-dimensional (3D) angiography using ultra-high-speed swept-source OCT [13]. These authors found reduced disc perfusion in a group of patients with early glaucoma and established a link between ONH vessel density and visual field pattern standard deviation (PSD) using a custom swept-source OCT device [14]. The OCT angiography with SSADA may be more reliable than LSFG or LDF, offering better intravisit repeatability and intervisit reproducibility [14–16].

The objective of the present study was to detect changes in ONH vascularization by comparing normal subjects and glaucoma patients using a commercial spectral-domain OCT angiography (OCT-A) device.

2. Methods

2.1. Study Population. This cross-sectional observational study was conducted at the Quinze-Vingts National Ophthalmology Hospital, Paris, France, from January to September 2015 after approval of our Institutional Review Board. The study adhered to the tenets of the Declaration of Helsinki and informed consent was obtained from all subjects. Patients followed up at the Quinze-Vingts National Ophthalmology Hospital for glaucoma were consecutively included. Inclusion criteria were chronic glaucoma defined as glaucomatous optic disc neuropathy and characteristic visual field (VF) loss based on the criteria of the Ocular Hypertension Treatment Study [17]. The glaucomatous VF loss was defined as a glaucoma hemifield test graded "outside normal limits" and a cluster of three contiguous points at the 5% level on the pattern deviation plot, using the threshold test strategy with the 24-2 test pattern of the Humphrey Field Analyzer II [18]. Patients with diabetic retinopathy, other diseases that may cause visual field loss or optic disc abnormalities, and inability to clinically view or photograph the optic discs due to media opacity or poorly dilating pupil were excluded.

For all glaucoma patients, the following data were recorded: age, gender, best corrected visual acuity (BCVA) on a logarithmic scale, IOP (mmHg), central corneal thickness (CCT), type of glaucoma, and cup/disc ratio. IOP was measured using the Goldmann applanation tonometer. For each eye, IOP value represented the mean value of two IOP readings. CCT was measured with an A-scan ultrasound (A-Scan Pachymeter, Ultrasonic, Exton, PA, USA). The mean retinal nerve fiber layer (RNFL) thickness, mean ganglion cell complex (GCC) thickness, and disc rim area were also evaluated (Cirrus® spectral-domain OCT, Carl Zeiss Meditec Inc., Dublin, IE). VF tests were performed with a Humphrey Field Analyzer II (Carl Zeiss Meditec Inc.) set for 24-2 to collect mean deviation (MD), pattern standard deviation (PSD), and the visual field index (VFI). The Bascom Palmer (Hodapp-Anderson-Parrish) glaucoma staging system (GSS) based on VF results was selected to classify patients as having mild, moderate, and severe glaucoma [19].

Healthy age-matched controls were also included. Normal subjects had IOP < 21 mmHg with clinically normal ONH and no history of ocular or systemic disease. For control subjects, demographic data and IOP were recorded.

2.2. Optical Coherence Tomography. We used the commercially available spectral-domain OCT RT XR Avanti with the AngioVue software (Optovue, Inc., Fremont, CA, USA). It detects BF in an acquired volume using the SSADA [12]. The instrument used for OCT-A images is based on the AngioVue Imaging System (Optovue, Inc., Fremont, CA, USA) to obtain amplitude decorrelation angiography images. This instrument has an A-scan rate of 70,000 scans per second, using a light source centered on 840 nm and a bandwidth of 50 nm. Each OCT-A volume contains 304 × 304 A-scans with two consecutive B-scans captured at each fixed position before proceeding to the next sampling location. Split spectrum amplitude-decorrelation angiography was used to extract the OCT angiography information. Each OCT-A volume is acquired in three seconds and two orthogonal OCT-A volumes were acquired in order to perform motion correction to minimize motion artifacts arising from microsaccades and fixation changes.

The software analyzes the amplitude of variation of the OCT signal over time for every location acquired and calculates decorrelation. Static tissue yields low decorrelation values as the signal varies a little over time, and BF yields high decorrelation values because moving red blood cells cross the OCT beam and cause the signal amplitude to vary rapidly over time. A threshold decorrelation value is therefore used to discriminate BF from static tissue [20, 21]. The angiography information displayed was the average of the decorrelation values when viewed perpendicularly through the thickness evaluated. This maps all the detected vessels in the acquired volume. The AngioVue software (Optovue) can then calculate a quantitative variable: the total surface of the flowing vessel on the en face projection. The right eye from each normal subject was scanned. For glaucoma patients, we decided to analyze the most severe eye as determined by the MD 24-2.

2.3. Image Acquisition and Processing. First, each subject underwent one set of two scans on the macular region. The SSADA algorithm requires the user to define a threshold of detection of circulating vessels [13]. Jia et al. described a method to calculate the appropriate threshold. The central avascular zone was defined as a noise region and the mean decorrelation value of the whole avascular zone was calculated. A threshold one standard deviation above the mean avascular decorrelation value was defined as circulating vessels.

Then we performed one set of two 3 × 3 mm scans on the ONH. We used the neural canal opening, which is the termination of the retinal pigment epithelium/Bruch membrane complex, to define the ONH margin [22]. The volumes analyzed were defined by both a circular surface on the en face projection and the anteroposterior boundaries, thus creating a cylinder. A circle on the en face projection

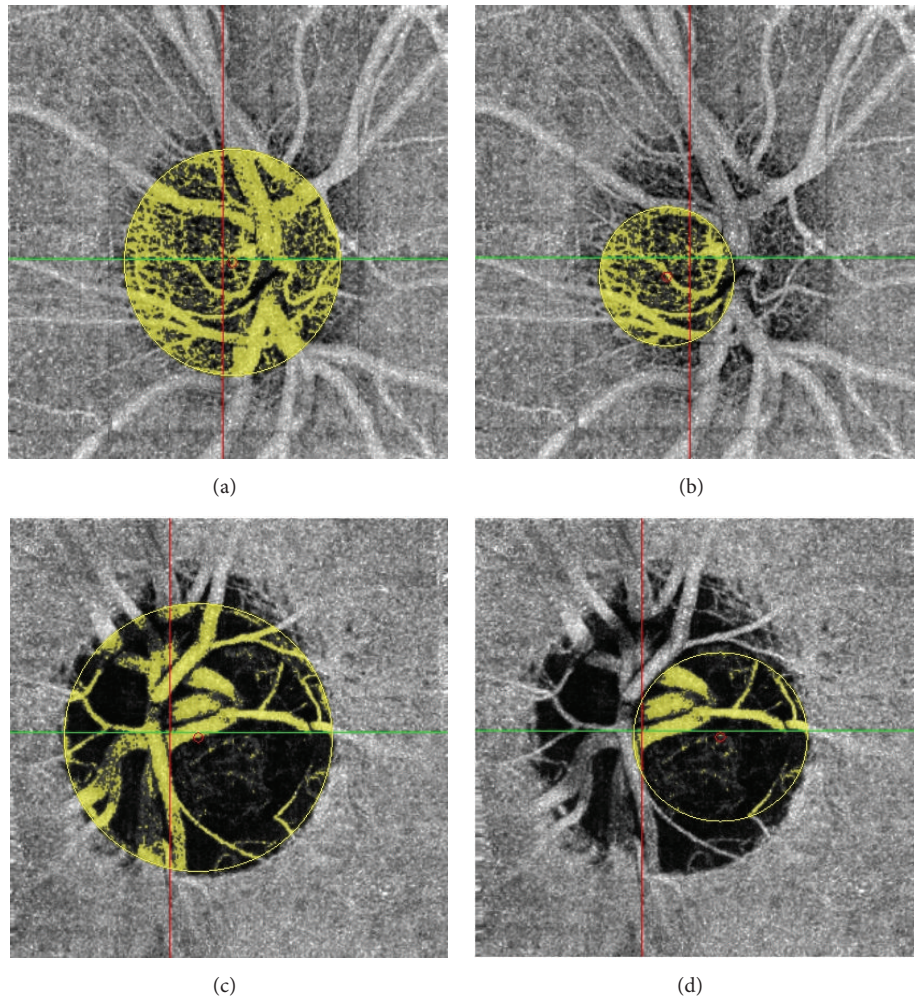

Figure 1: Total (a) and temporal (b) ONH acquisition in a normal patient. Total (c) and temporal (d) ONH acquisition in a glaucoma patient.

and anteroposterior limits defines each cylinder. We studied the total ONH flow area (mm^2), representing the number of vessels, detected from all the depths of the disc, from the top of the ONH (inner surface) to the lamina cribrosa. Next, the total ONH vessel density (%) was calculated by dividing flow area by the optic disc surface (πR^2). The ONH temporal region (determined by the temporal disc between the temporal arteries and veins) was also studied to avoid BF due to major superior and inferior branches of retinal vessels in order to focus on the ONH laminar microvasculature (Figure 1). Then we measured the temporal disc flow area (mm^2) and calculated the temporal disc vessel density by dividing the temporal disc flow area by the temporal disc surface (πR^2 temporal). The total and temporal optic disc vessel densities, obtained as the ratio of the optic disc flow area to the optic disc surface, were calculated to account for the intereye differences in total and temporal optic disc surface areas. Image quality was determined for all OCT-A scans. Poor quality images with a signal strength index (SSI) < 40 or image sets with remaining motion artifacts were excluded from the study analysis [23].

2.4. Reproducibility and Repeatability. Measurement repeatability of the disc flow area was evaluated from three sets of acquisitions from a subset of 6 normal subjects within a single visit. The intravisit coefficient of variation (CV) was calculated by comparing these three measurements. Intervisit reproducibility was obtained from three sets of scans performed on three separate visits from the same subset of normal subjects.

2.5. Statistical Analysis. Mann-Whitney tests were used to compare the average values of the measurements between normal and glaucomatous eyes. Linear regression analysis was used in the control group to investigate whether the measurement of ONH vessel density was affected by age, gender, and IOP. Univariate analysis with the Pearson correlation test and multivariate analysis with the ANCOVA test were performed to study the correlation between ONH vessel density and other variables: age, RNFL thickness, GCC, rim area, MD 24-2, and PSD 24-2.

3. Results

3.1. Demographic and Clinical Data. Fifty glaucoma patients and 30 normal subjects were included in this study. There was

Table 1: Qualitative and quantitative demographic data. IOP: intraocular pressure; F: female, M: male.

	Normal		Glaucoma		p value
Qualitative demographic data	($n = 30$)	%	($n = 50$)	%	
Gender					
F	17	56.7	23	46	NS
M	13	43.3	27	54	
Family history of glaucoma					
0	27	90	24	48	$p < 0.0001$
1	3	10	26	52	
Ethnic origin					
African	8	26.7	11	22	—
Caucasian	20	66.7	33	66	
Asian	0	0	2	4	
Hispanic	0	0	2	4	
Maghrebi	2	6.7	2	4	
Quantitative demographic data	Mean	SD	Mean	SD	
Age (years)	51.1	18.1	58.4	15.9	NS
IOP (mmHg)	14.4	2.59	17.6	6.41	0.022

no difference between the two groups concerning age, gender, and ethnic origin. A family history of glaucoma was found in 52% of glaucoma patients and 10% of control subjects ($p < 0.0001$). IOP was 17.6 mmHg and 14.4 mmHg in the glaucoma and control group, respectively ($p = 0.022$). The demographic data are summarized in Table 1.

Regarding the type of glaucoma, 43 patients (86%) had open-angle glaucoma (OAG) and seven patients (14%) had angle-closure glaucoma (ACG). Twenty-three patients (46%) had mild glaucoma, eight (16%) had moderate glaucoma, and 19 (38%) had severe glaucoma. Mean RNFL thickness, GCC thickness, and rim area were $66.48 \pm 12.6\,\mu$m, $63.6 \pm 9.07\,\mu$m, and $0.786 \pm 0.291\,\text{mm}^2$ in the glaucoma group, respectively. The results of the glaucoma patients' clinical data are summarized in Table 2.

3.2. ONH Blood Flow Evaluation. The en face projection angiograms showed that normal discs had a denser microvascular network, especially in the temporal region, compared with glaucomatous discs (Figure 1). Total ONH vessel density was reduced by 24.7% (0.412 ± 0.117 versus 0.547 ± 0.077, $p < 0.0001$) in the glaucoma group as compared with the control group. Temporal disc vessel density was significantly reduced by 22.88% (0.364 ± 0.150 versus 0.472 ± 0.105, $p = 0.001$) in the glaucoma group as compared with the control group. Moreover, SSI and the decorrelation threshold were higher in the control group (72.3 versus 61.8, $p < 0.0001$, and 0.095 versus 0.085, $p = 0.001$, resp.). The intravisit CV was 6.17%. The intervisit CV was 6.48%. The results of the ONH BF evaluation are summarized in Table 3.

In the glaucoma group, univariate analysis showed that total ONH vessel density was significantly associated with structural variables including rim area ($r = 0.609$; $p < 0.0001$), RNFL thickness ($r = 0.406$; $p < 0.003$), and GCC thickness ($r = 0.337$; $p = 0.017$) (Figure 2). Total ONH vessel density was also associated with the functional variables VFI ($r = 0.339$; $p = 0.017$) and MD 24-2 ($r = 0.301$; $p = 0.038$). The results of these correlations are summarized in Table 4. In the multivariate analysis where total ONH vessel density was considered as a dependent variable, rim area was the dominant explanatory variable, accounting for 38.9% of the variance (R^2). In this multivariate model, RNFL thickness, GCC thickness, and VF parameters (MD 24-2 and VFI)

Table 2: Quantitative and qualitative clinical data. OAG: open-angle glaucoma; ACG: angle-closure glaucoma. Visual field and OCT spectral-domain testing. MD: mean deviation; PSD: pattern standard deviation; VFI: visual field index; RNFL: retinal nerve fiber layers; GCC: ganglion cell complex.

	Glaucoma	
Qualitative clinical data	($n = 50$)	%
Type		
OAG	43	86
ACG	7	14
Stage		
Mild	23	46
Moderate	8	16
Severe	19	38
Quantitative clinical data	Mean	SD
log AV	0.142	0.239
Corneal central thickness (μm)	525.8	46
Cup/disc ratio	0.821	0.153
MD 24-2 (dB)	−10.5	8.91
PSD 24-2 (dB)	6.81	4.7
VFI	70.87	27.6
RNFL thickness (μm)	66.48	12.6
GCC thickness (μm)	63.6	9.07
Rim area (mm^2)	0.786	0.29

Table 3: OCT angiography measurements. SSI: strength signal index.

OCT angiography measurements	Normal		Glaucoma		p value
	Mean	SD	Mean	SD	
Threshold	0.095	0.012	0.085	0.012	0.001
SSI	72.3	8.41	61.8	7	<0.0001
Total ONH vessel density	0.547	0.154	0.412	0.117	<0.0001
Temporal disc vessel density	0.472	0.105	0.364	0.15	0.0001
Glaucoma stage	Total ONH vessel density		Temporal disc vessel density		
	Mean	SD	Mean	SD	
Mild	0.441	0.145	0.404	0.178	
Moderate	0.439	0.067	0.414	0.110	
Severe	0.365	0.076	0.293	0.096	

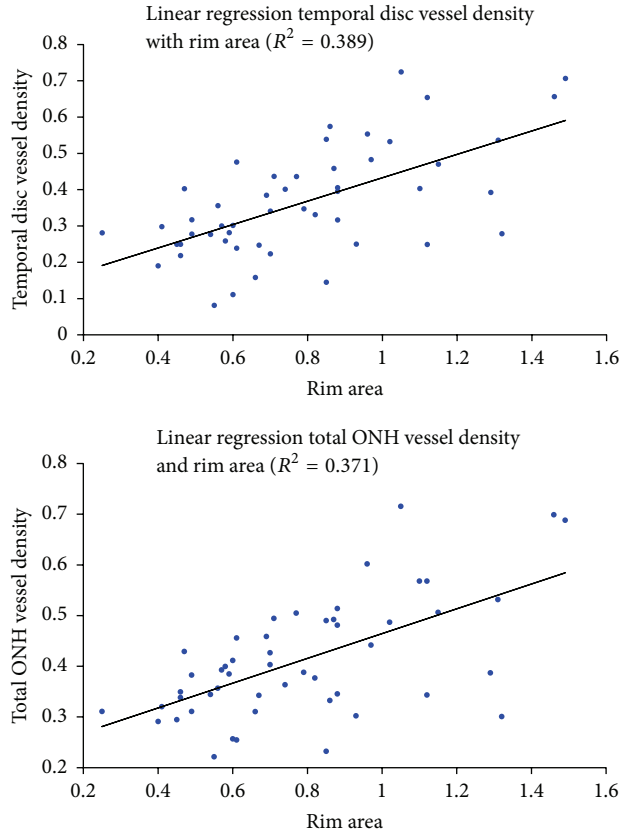

Figure 2: Linear regression analysis for temporal disc vessel density, total ONH vessel density, and rim area.

were not statistically associated with ONH vascular density (Table 5).

Considering temporal disc vessel density, in univariate analysis, a correlation was observed with rim area ($r = 0.624$; $p < 0.0001$) (Figure 2), RNFL thickness ($r = 0.448$; $p = 0.001$), and GCC thickness ($r = 0.395$; $p = 0.004$). Temporal disc vessel density was also associated with VFI ($r = 0.423$; $p = 0.002$), MD 24-2 ($r = 0.385$; $p = 0.007$), but not with PSD 24-2 (Table 6). In a multivariate model studying temporal disc vessel density as a dependent variable, rim area was also the dominant explanatory variable, accounting for 39% of the variance (R^2). RNFL thickness, GCC thickness, and VF parameters (MD 24-2, VFI) were not associated with temporal disc vessel density (Table 7).

4. Discussion

In this study, we report the use of spectral-domain OCT angiography to measure ONH perfusion in glaucoma. We targeted two regions, the whole disc and a temporal disc area, to compare the two groups. We showed a significant difference in ONH vascular density between glaucoma and normal patients. The difference was similar for the total and temporal vascular area, with a decrease of ONH perfusion as compared with controls by 24.7% and 22.9%, respectively. We observed a significant correlation between ONH perfusion and structural and functional glaucoma damage. Moreover, the multivariate regression models confirmed the relation between disc rim area and ONH perfusion (total and temporal vessel density). These results emphasized the relation between ONH BF and structural loss in glaucoma.

In a previous similar study using a prototype of swept-source angio-OCT, Jia et al. studied ONH total BF with the SSADA. These authors found a correlation between the disc flow index and PSD, but they did not observe a correlation with structural variables such as the C/D ratio, rim area, or RNFL thickness [14]. Although altered microcirculation is reported to be associated with optic nerve head changes in glaucoma [24], these authors suggested that the flow index was independent information on glaucoma severity that is not explained by structural variables alone. The differences between our two studies can be explained by random variations due to the small sample size of the study reported by Jia et al. (24 normal subjects and 11 glaucoma patients). Moreover, most of their glaucoma patients had early-stage disease. In our study, 38% of the patients had severe glaucoma with advanced structural changes. The correlations we observed between ONH perfusion and structural parameters such as rim area, RNFL thickness, and GCC thickness could be explained by the more advanced glaucoma cases included in the present study. Interestingly, in these more advanced glaucoma patients, we also found a low but significant

Table 4: Pearson correlation coefficient matrix for visual field, structural variables, and ONH total vessel density in subjects with glaucoma. MD: mean deviation; PSD: pattern standard deviation; VFI: visual field index; RNFL: retinal nerve fiber layers; GCC: ganglion cell complex; total ONH density: total ONH vessel density; SSI: strength signal index. Statistically significant correlations with total ONH vessel density are in bold.

Variable		Total ONH density	SSI	VFI	PSD 24-2	MD 24-2	GCC	Rim area	RNFL	Age
Total ONH density	r	**1**								
	p	**0**								
SSI	r	**0.318**	1							
	p	**0.026**	0							
VFI	r	**0.339**	0.248	1						
	p	**0.017**	0.089	0						
PSD 24-2	r	−0.192	−0.090	−0.595	1					
	p	0.185	0.544	<0.0001	0					
MD 24-2	r	**0.301**	0.202	0.986	−0.685	1				
	p	**0.038**	0.173	<0.0001	<0.0001	0				
GCC thickness	r	**0.337**	0.230	0.580	−0.472	0.532	1			
	p	**0.017**	0.111	<0.0001	0.001	0.000	0			
Rim area	r	**0.609**	0.187	0.622	−0.581	0.628	0.598	1		
	p	**<0.0001**	0.198	<0.0001	<0.0001	<0.0001	<0.0001	0		
RNFL thickness	r	**0.406**	0.201	0.649	−0.533	0.664	0.789	0.661	1	
	p	**0.003**	0.166	<0.0001	<0.0001	<0.0001	<0.0001	<0.0001	0	
Age	r	0.166	−0.308	0.268	−0.285	0.350	0.047	0.267	0.244	1
	p	0.248	0.031	0.063	0.047	0.015	0.746	0.061	0.088	0

Table 5: Multivariate model for total ONH vessel density R^2 = 0.387.

Variable	Slope	p value
MD 24-2	−0.002	0.870
VFI	−0.001	0.955
GCC thickness	−0.002	0.484
Rim area	**0.269**	**0.000**
RNFL thickness	0.002	0.445

MD: mean deviation; VFI: visual field index; RNFL: retinal nerve fiber layers; GCC: ganglion cell complex. Statistically significant correlations with total ONH vessel density are in bold.

correlation with VF variables in univariate analysis, as did Jia et al. These results are also in accordance with the study by Liu et al. using OCT-A (RTVue-XR; Optovue, Inc.) that showed reduced peripapillary vessel density in glaucoma patients correlated with VF indexes [23]. In a recent study, Wang et al. comparing optic disc perfusion with OCT-A between 62 glaucoma patients and 20 control subjects found similar results with reduced disc vessel density in the glaucoma group correlated with structural parameters such as the GCC [25].

The SSADA algorithm requires the user to define a threshold of circulating vessel detection. Jia et al. described a method to calculate the appropriate threshold using the central avascular zone as a noise region and calculating the mean decorrelation value of the whole avascular zone. With their OCT-A prototype, they set the threshold two standard deviations above the mean avascular zone decorrelation. In the present study, using the commercially available spectral-domain OCT RT XR Avanti with the AngioVue software (Optovue, Inc. Fremont, CA, USA), we could not detect obvious circulating vessels using the same threshold as Jia et al. Therefore we set our threshold one standard deviation above the mean avascular decorrelation value. This difference might be explained by the difference in OCT-A hardware and software used in the two studies.

The results obtained with OCT-A confirmed the findings of several other techniques that reported ONH BF changes in glaucoma. Harris et al. measured ONH BF with different imaging technologies including color Doppler imaging, confocal scanning laser ophthalmoscopic angiography, laser blood flowmetry, or scanning laser Doppler flowmetry and demonstrated reduced ONH perfusion in glaucoma patients [6, 7]. Disc BF was also investigated by fluorescein angiography (FA) in several studies showing diffuse disc hypoperfusion and ONH fluorescein filling defects in glaucomatous patients [26]. Nevertheless, FA is not commonly used for monitoring glaucoma because of quantification problems and its potential side effects as an invasive technique [27]. Decreased ONH BF in glaucoma patients versus controls and increased viscosity in the papillary microvascular network were reported with the use of the laser Doppler velocimeter [28]. Using scanning laser Doppler flowmetry, Michelson et al. showed decreased peripapillary retinal BF and neuroretinal BF comparing glaucoma patients to control subjects [29]. Hafez et al. also found lower ONH BF in glaucoma patients and suggested a correlation between visual field defects and ONH perfusion [30]. Using laser speckle flowgraphy, other authors reported reduced BF in glaucoma patients and found a correlation between BF and MD and RNFL thickness [31]. Wang et al. confirmed a high correlation between the BF reduction measured by laser speckle flowgraphy and the microsphere method, providing evidence that this technique is capable of assaying BF for a critical deep ONH region [11].

Table 6: Pearson correlation coefficient matrix for visual field, structural variables, and temporal disc vessel density in subjects with glaucoma. MD: mean deviation; PSD: pattern standard deviation; VFI: visual field index; RNFL: retinal nerve fiber layers; GCC: ganglion cell complex; SSI: strength signal index. Statistically significant correlations with temporal disc vessel density are in bold.

Variable		Temporal disc density	SSI	VFI	PSD 24-2	MD 24-2	GCC	Rim area	RNFL	Age
Temporal disc density	r	**1**								
	p	**0**								
SSI	r	0.235	1							
	p	0.105	0							
VFI	r	**0.423**	0.248	1						
	p	**0.002**	0.089	0						
PSD 24-2	r	−0.171	−0.090	−0.595	1					
	p	0.241	0.544	<0.0001	0					
MD 24-2	r	**0.385**	0.202	0.986	−0.685	1				
	p	**0.007**	0.173	<0.0001	<0.0001	0				
GCC thickness	r	**0.396**	0.230	0.580	−0.472	0.532	1			
	p	**0.004**	0.111	<0.0001	0.001	0.000	0			
Rim area	r	**0.624**	0.187	0.622	−0.581	0.628	0.598	1		
	p	**<0.0001**	0.198	<0.0001	<0.0001	<0.0001	<0.0001	0		
RNFL thickness	r	**0.448**	0.201	0.649	−0.533	0.664	0.789	0.661	1	
	p	**0.001**	0.198	<0.0001	<0.0001	<0.0001	<0.0001	<0.0001	0	
Age	r	0.185	−0.308	0.268	−0.285	0.350	0.047	0.267	0.244	1
	p	0.199	0.031	0.063	0.047	0.015	0.746	0.061	0.088	0

Table 7: Multivariate model for temporal disc vessel density R^2 = 0.390.

Variable	Slope	p value
MD 24-2	0.005	0.717
VFI	−0.002	0.680
GCC thickness	−0.001	0.690
Rim area	**0.311**	**0.001**
RNFL thickness	0.001	0.648

MD: mean deviation; VFI: visual field index; RNFL: retinal nerve fiber layers; GCC: ganglion cell complex. Statistically significant correlations with temporal disc vessel density are in bold.

The use of OCT-A to evaluate ONH BF may provide a new tool to investigate the role of the microvasculature in the pathophysiology of glaucoma and its changes with glaucoma progression. One of the longstanding questions is whether reduced BF is a preexisting pathologic change or a consequence of glaucomatous optic atrophy [32]. This is difficult to determine in part because a substantial portion of retinal ganglion cells/axons may have already become degenerated, even at an early stage of glaucoma [33]. Compromised blood supply and therefore reduced ocular BF due to increased IOP or vascular dysregulation has been implicated in the pathogenesis of the disease [7, 32]. In terms of laminar capillary volume flow, Burgoyne et al. hypothesized that, within the lamina, connective tissue IOP-related strain has both direct and indirect effects on axonal nutrition and that axonal ischemia can result from either IOP-induced occlusion of the laminar capillaries (direct effect) or decreased diffusion of nutrients (indirect effect), or both. In terms of only the retrolaminar effects on BF, the level of IOP-related strain within the peripapillary sclera may significantly affect volume flow through the scleral branches of the short posterior ciliary arteries. This hypothesis suggests that vascular mechanisms damaging the ONH are not necessarily IOP-independent and proposes a logic for understanding the complicated interaction between these three important factors (IOP, volume BF, and nutrient delivery) within the tissues of the ONH [34].

Our study has limitations that need to be considered when interpreting the results. Normal and glaucomatous eyes have been classified according to the visualization the ONH and no visual field was performed to control subjects. As OCT-A was used to evaluate ONH vascularization, we may have increased the chance of finding significant differences between groups. Similarly, by selecting the worst eye of glaucomatous patients we may have influenced the results. Nevertheless, this limitation has not influenced the analysis of correlation of OCT-A results and optic nerve parameters for glaucoma patients as this group was classified according to the results of VF.

The results of the present study suggest that spectral-domain OCT angiography might detect reduced ONH blood flow in glaucoma patients. These ONH blood flow changes were associated with structural and functional glaucomatous alterations. New studies are needed to evaluate the exact potential of OCT-A in glaucoma.

Conflict of Interests

The authors declare that there is no conflict of interests regarding the publication of this paper.

References

[1] D. C. Broadway and S. M. Drance, "Glaucoma and vasospasm," *British Journal of Ophthalmology*, vol. 82, no. 8, pp. 862–870, 1998.

[2] B. L. Petrig, C. E. Riva, and S. S. Hayreh, "Laser Doppler flowmetry and optic nerve head blood flow," *American Journal of Ophthalmology*, vol. 127, no. 4, pp. 413–425, 1999.

[3] C. Prünte, S. Orgül, and J. Flammer, "Abnormalities of microcirculation in glaucoma: facts and hints," *Current Opinion in Ophthalmology*, vol. 9, no. 2, pp. 50–55, 1998.

[4] O.-Y. Tektas, E. Lütjen-Drecoll, and M. Scholz, "Qualitative and quantitative morphologic changes in the vasculature and extracellular matrix of the prelaminar optic nerve head in eyes with POAG," *Investigative Ophthalmology and Visual Science*, vol. 51, no. 10, pp. 5083–5091, 2010.

[5] S. S. Hayreh, "Blood supply of the optic nerve head and its role in optic atrophy, glaucoma, and oedema of the optic disc," *British Journal of Ophthalmology*, vol. 53, no. 11, pp. 721–748, 1969.

[6] E. Rechtman, A. Harris, R. Kumar et al., "An update on retinal circulation assessment technologies," *Current Eye Research*, vol. 27, no. 6, pp. 329–343, 2003.

[7] A. Harris, L. Kagemann, R. Ehrlich, C. Rospigliosi, D. Moore, and B. Siesky, "Measuring and interpreting ocular blood flow and metabolism in glaucoma," *Canadian Journal of Ophthalmology*, vol. 43, no. 3, pp. 328–336, 2008.

[8] C. P. Jonescu-Cuypers, H. S. Chung, L. Kagemann, Y. Ishii, D. Zarfati, and A. Harris, "New neuroretinal rim blood flow evaluation method combining Heidelberg retina flowmetry and tomography," *British Journal of Ophthalmology*, vol. 85, no. 3, pp. 304–309, 2001.

[9] T. Sugiyama, M. Araie, C. E. Riva, L. Schmetterer, and S. Orgul, "Use of laser speckle flowgraphy in ocular blood flow research," *Acta Ophthalmologica*, vol. 88, no. 7, pp. 723–729, 2010.

[10] Y. Wang, B. A. Bower, J. A. Izatt, O. Tan, and D. Huang, "Retinal blood flow measurement by circumpapillary Fourier domain Doppler optical coherence tomography," *Journal of Biomedical Optics*, vol. 13, no. 6, Article ID 064003, 2008.

[11] L. Wang, G. A. Cull, C. Piper, C. F. Burgoyne, and B. Fortune, "Anterior and posterior optic nerve head blood flow in nonhuman primate experimental glaucoma model measured by laser speckle imaging technique and microsphere method," *Investigative Ophthalmology and Visual Science*, vol. 53, no. 13, pp. 8303–8309, 2012.

[12] Y. Jia, O. Tan, J. Tokayer et al., "Split-spectrum amplitude-decorrelation angiography with optical coherence tomography," *Optics Express*, vol. 20, no. 4, pp. 4710–4725, 2012.

[13] Y. Jia, J. C. Morrison, J. Tokayer et al., "Quantitative OCT angiography of optic nerve head blood flow," *Biomedical Optics Express*, vol. 3, no. 12, pp. 3127–3137, 2012.

[14] Y. Jia, E. Wei, X. Wang et al., "Optical coherence tomography angiography of optic disc perfusion in glaucoma," *Ophthalmology*, vol. 121, no. 7, pp. 1322–1332, 2014.

[15] Y. Tamaki, M. Araie, K. Tomita, M. Nagahara, A. Tomidokoro, and H. Fujii, "Real-time measurement of human optic nerve head and choroid circulation, using the laser speckle phenomenon," *Japanese Journal of Ophthalmology*, vol. 41, no. 1, pp. 49–54, 1997.

[16] A. S. Hafez, R. L. G. Bizzarro, M. Rivard et al., "Reproducibility of retinal and optic nerve head perfusion measurements using scanning laser Doppler flowmetry," *Ophthalmic Surgery, Lasers & Imaging*, vol. 34, no. 5, pp. 422–432, 2003.

[17] M. O. Gordon, J. A. Beiser, J. D. Brandt et al., "The Ocular Hypertension Treatment Study: baseline factors that predict the onset of primary open-angle glaucoma," *Archives of Ophthalmology*, vol. 120, no. 6, pp. 714–730, 2002.

[18] J. L. Keltner, C. A. Johnson, K. E. Cello et al., "Classification of visual field abnormalities in the ocular hypertension treatment study," *Archives of Ophthalmology*, vol. 121, no. 5, pp. 643–650, 2003.

[19] E. Hodapp, R. K. Parrish II, and D. R. Anderson, *Clinical Decisions in Glaucoma*, The CV Mosby, St Louis, Miss, USA, 1993.

[20] R. F. Spaide, J. M. Klancnik, and M. J. Cooney, "Retinal vascular layers imaged by fluorescein angiography and optical coherence tomography angiography," *JAMA Ophthalmology*, vol. 133, no. 1, pp. 45–50, 2015.

[21] R. F. Spaide, J. M. Klancnik, and M. J. Cooney, "Retinal vascular layers in macular telangiectasia type 2 imaged by optical coherence tomographic angiography," *JAMA Ophthalmology*, vol. 133, no. 1, pp. 66–73, 2015.

[22] N. G. Strouthidis, H. Yang, J. F. Reynaud et al., "Comparison of clinical and spectral domain optical coherence tomography optic disc margin anatomy," *Investigative Ophthalmology and Visual Science*, vol. 50, no. 10, pp. 4709–4718, 2009.

[23] L. Liu, Y. Jia, H. L. Takusagawa et al., "Optical coherence tomography angiography of the peripapillary retina in glaucoma," *JAMA Ophthalmology*, vol. 133, no. 9, pp. 1045–1052, 2015.

[24] N. Chiba, K. Omodaka, Y. Yokoyama et al., "Association between optic nerve blood flow and objective examinations in glaucoma patients with generalized enlargement disc type," *Clinical Ophthalmology*, vol. 5, no. 1, pp. 1549–1556, 2011.

[25] X. Wang, C. Jiang, T. Ko et al., "Correlation between optic disc perfusion and glaucomatous severity in patients with open-angle glaucoma: an optical coherence tomography angiography study," *Graefe's Archive for Clinical and Experimental Ophthalmology*, vol. 253, no. 9, pp. 1557–1564, 2015.

[26] R. A. Hitchings and G. L. Spaeth, "Fluorescein angiography in chronic simple and low tension glaucoma," *British Journal of Ophthalmology*, vol. 61, no. 2, pp. 126–132, 1977.

[27] M. R. Stein and C. W. Parker, "Reactions following intravenous fluorescein," *American Journal of Ophthalmology*, vol. 72, no. 5, pp. 861–868, 1971.

[28] P. Hamard, H. Hamard, J. Dufaux, and S. Quesnot, "Optic nerve head blood flow using a laser Doppler velocimeter and haemorheology in primary open angle glaucoma and normal pressure glaucoma," *British Journal of Ophthalmology*, vol. 78, no. 6, pp. 449–453, 1994.

[29] G. Michelson, M. J. Langhans, and M. J. Groh, "Perfusion of the juxtapapillary retina and the neuroretinal rim area in primary open angle glaucoma," *Journal of Glaucoma*, vol. 5, no. 2, pp. 91–98, 1996.

[30] A. S. Hafez, R. L. G. Bizzarro, and M. R. Lesk, "Evaluation of optic nerve head and peripapillary retinal blood flow in glaucoma patients, ocular hypertensives, and normal subjects," *American Journal of Ophthalmology*, vol. 136, no. 6, pp. 1022–1031, 2003.

[31] Y. Yokoyama, N. Aizawa, N. Chiba et al., "Significant correlations between optic nerve head microcirculation and visual field defects and nerve fiber layer loss in glaucoma patients with myopic glaucomatous disk," *Clinical Ophthalmology*, vol. 5, no. 1, pp. 1721–1727, 2011.

[32] J. Flammer, S. Orgül, V. P. Costa et al., "The impact of ocular blood flow in glaucoma," *Progress in Retinal and Eye Research*, vol. 21, no. 4, pp. 359–393, 2002.

[33] L. A. Kerrigan-Baumrind, H. A. Quigley, M. E. Pease, D. F. Kerrigan, and R. S. Mitchell, "Number of ganglion cells in

glaucoma eyes compared with threshold visual field tests in the same persons," *Investigative Ophthalmology and Visual Science*, vol. 41, no. 3, pp. 741–748, 2000.

[34] C. F. Burgoyne, J. Crawford Downs, A. J. Bellezza, J.-K. Francis Suh, and R. T. Hart, "The optic nerve head as a biomechanical structure: a new paradigm for understanding the role of IOP-related stress and strain in the pathophysiology of glaucomatous optic nerve head damage," *Progress in Retinal and Eye Research*, vol. 24, no. 1, pp. 39–73, 2005.

Hindawi Publishing Corporation
Journal of Ophthalmology
Volume 2016, Article ID 3726353, 7 pages
http://dx.doi.org/10.1155/2016/3726353

Research Article

Retro-Mode Scanning Laser Ophthalmoscopy Planning for Navigated Macular Laser Photocoagulation in Macular Edema

Ernest V. Boiko[1,2] and Dmitrii S. Maltsev[2]

[1]*St. Petersburg Branch of the S. Fyodorov Eye Microsurgery Federal State Institution, 21 Yaroslav Gashek Street, Saint Petersburg 192283, Russia*
[2]*Department of Ophthalmology, Military Medical Academy, 5 Klinicheskaya Street, Saint Petersburg 194044, Russia*

Correspondence should be addressed to Dmitrii S. Maltsev; glaz.med@yandex.ru

Received 7 October 2015; Revised 26 December 2015; Accepted 27 January 2016

Academic Editor: Lisa Toto

Copyright © 2016 E. V. Boiko and D. S. Maltsev. This is an open access article distributed under the Creative Commons Attribution License, which permits unrestricted use, distribution, and reproduction in any medium, provided the original work is properly cited.

Purpose. To compare treatment areas and navigated macular laser photocoagulation (MLP) plans suggested by retro-mode scanning laser ophthalmoscopy (RM-SLO) image versus optical coherence tomography (OCT) central retinal thickness map and treatment planning among retina specialists. *Methods*. Thirty-nine eyes with diabetic or branch retinal vein occlusion-related ME undergoing navigated MLP with navigated photocoagulator had OCT and RM-SLO taken. OCT map and RM-SLO image were imported to the photocoagulator and aligned onto the retina. Two retina specialists placed laser spot marks separately based on OCT and RM-SLO images in a random fashion. The spots placed by each physician were compared between OCT and RM-SLO and among physicians. The areas of retinal edema on OCT and RM-SLO of the same eye were also compared. *Results*. The average number of laser spots using RM-SLO and OCT template was 189.6 ± 77.4 and 136.6 ± 46.8, respectively, $P = 0.003$. The average area of edema on RM-SLO image was larger than that on OCT map ($14.5 \pm 3.9\ mm^2$ versus $10.3 \pm 2.8\ mm^2$, $P = 0.005$) because of a larger scanning area. There was narrow variability in treatment planning among retina specialists for both RM-SLO ($P = 0.13$) and OCT ($P = 0.19$). *Conclusion*. The RM-SLO image superimposed onto the fundus of the same eye can be used to guide MLP with narrow variability in treatment planning among retina specialists. The treatment areas suggested by RM-SLO-guided MLP plans for ME were shown to be larger than those suggested by OCT-guided plans.

1. Introduction

Laser treatment [1] and intravitreal therapy with antiangiogenic agents and steroids [2] are the two standard treatment options for macular edema (ME) secondary to diabetes and retinal vein occlusion (RVO). The latter option, although shown by multiple studies [3, 4] to be efficacious for this condition, involves numerous intravitreal injections, which is associated with the cumulative risk of endophthalmitis [5]. Additionally, intravitreal antiangiogenic agents and steroids result in an increased financial burden for the patient [6] and increased rates of elevated intraocular pressure and cataract [7], respectively.

Therefore, laser therapy, either alone, as an adjunct to intravitreal antiangiogenic and steroid therapy [1, 2, 8, 9] or as a switching therapy for non-responders to pharmacotherapeutic-only options [10] is still important in treating ME. Central scotoma, loss of central vision, and decreased color vision [11, 12] associated with progressive retinal pigment epithelial atrophy are possible adverse effects of macular laser photocoagulation (MLP). Novel navigated MLP has however been shown to be safe and to improve accuracy in photocoagulation treatments of diabetic retinopathy lesions compared to conventional manual-technique laser treatment [13].

Currently, the standard approach to MLP involves treating individual-leaking microaneurysms (ILMs) and/or diffuse vascular leakage (DVL) [14] regions. For decades, fluorescein retinal angiography (FA) was the only technique to demonstrate reliably ILMs, DVL regions and associated ME. Since retinal edema develops mainly as a result of retinal vascular leakage [15], in some cases of this disease, FA-guided planning for MLP may be changed for OCT-guided planning. Moreover, OCT-guided planning has been

already used for navigated MLP [16–18], and it is reasonable to expect an increase in the use of such an approach. OCT-guided planning for MLP (for macular edema) has shown similar results as FA-guided planning, with visualization of the retinal edema regions of similar area and location [16, 19].

Retro-mode (RM) scanning laser ophthalmoscopy (SLO) is another new method for visualizing the retinal edema regions and also may have the potential to be used to guide navigated MLP. In RM-SLO, the scattered light that passes a deviated aperture gives a shadow to the silhouetted cystoid spaces, allowing for clear visualization of intraretinal cystoid spaces in retinal edema [20].

The purpose of the study was (1) to compare treatment areas suggested by RM-SLO versus OCT and (2) to compare navigated MLP plans using RM-SLO images superimposed onto a color fundus photograph versus OCT thickness map superimposed onto a color fundus photograph among retina specialists.

2. Materials and Methods

The study was approved by the Ethics Committee of Military Medical Academy and followed the tenets of the Declaration of Helsinki. All patients gave written informed consent for both participation in the study and for MPL. Before treatment, they were explained the cause of the disease, treatment options available to address macular edema, as well as advantages and disadvantages of these options. Patients' decision in favor of having MLP was free, conscious and voluntary (and based mostly on economic reasons).

The inclusion criteria for this prospective, randomized study included OCT (central foveal B scan) evidence of diabetic or RVO-related macular edema or RM-SLO evidence of retinal edema (diabetic or RVO-related macular edema) for which MLP was to be performed. Exclusion criteria included evidence of acute or chronic uveitis, vitreoretinal traction, fibrosis of the internal limiting membrane (with macular involvement), central RVO, and apparent optic media opacity (resulting in OCT images with a Signal Strength Index reduced to less than 40).

2.1. MLP Technique. In all eyes of the study, navigated MLP (NAVILAS, OD-OS Inc, Berlin, Germany) with 1% tropicamide (Mydriacyl; Alcon-Couvreur, Puurs, Belgium)-induced mydriasis was planned and performed following RM-SLO and OCT imaging. The MLP-related treatment decisions were to deliver laser to areas of retinal edema, as per Early Treatment Diabetic Retinopathy Study (ETDRS) guidelines. The parameters used included a spot size of 50 μm, burn spacing of 2 burn-widths apart, and areas to avoid including the optic nerve head and central macular 2000-μm diameter area.

2.2. RM-SLO Images. RM-SLO image obtained with SLO F-10 (NIDEK, Gamagori, Japan) was imported into the NAVILAS system, superimposed onto the baseline image (i.e., NAVILAS color fundus image), and utilized for treatment planning. In RM-SLO images, retinal edema was defined as the zones with intraretinal microcysts visible as raised structures with clearly defined boundaries.

2.3. OCT Maps. An OCT retinal thickness map (Enhanced Macular Map 5 (EMM5) protocol) and background SLO-type fundus photograph (7 mm × 7 mm) were acquired on the spectral domain OCT system (RTVue-100, Optovue, Fremont, CA) and imported into the NAVILAS system to overlay them on a baseline color fundus image and to utilize for treatment planning. In the OCT retinal thickness map, retinal edema was defined as the zones with retinal thickness greater than 250 μm indicated by colors warmer than green. All OCT images were obtained by a single, experienced technician. Macular thickness map artifacts were assessed, focusing on automatic segmentation and off-center errors, and corrected manually as soon as scanning was completed. Errors in automatic segmentation were corrected by manual boundary segmentation of images on B scans. Off-center errors, if any, were corrected through manual repositioning of the foveal center using B scan landmarks that allow its identification. If it was impossible to correct a retinal thickness map manually in a proper way, rescanning and manual post-scan correction of such errors was performed until obtaining an adequate map for the treatment planning for MLP.

2.4. Measurement of the Retinal Edema Area and Planning. Two MLP specialists independently measured the area of retinal edema on OCT maps and RM-SLO images in a random order using the ImageJ software (NIH, Bethesda, MD). Additionally, they performed preplanning which involved placing laser spot marks after superimposing the OCT map or RM-SLO image onto the baseline image (i.e., NAVILAS color fundus image). The spots placed by each physician were compared between RM-SLO and OCT and among physicians. In addition, the areas of retinal edema measured by each physician were compared between RM-SLO and OCT and among the physicians.

2.5. Statistics. Unless otherwise stated, all the data are expressed as the mean standard deviation (SD). The paired t-test was used to compare equivalent parameters (the area of retinal edema and the number of spots placed by the physician) obtained with RM-SLO and OCT. Additionally, it was used to compare the area of retinal edema and the number of spots placed among physicians.

3. Results

Thirty-two patients (20 women and 12 men, mean age: 65.3 ± 8.7 years) were included into the study. In 22 patients (29 eyes), the examination revealed diabetic macular edema which had not been treated with MLP. Ten patients (10 eyes) were diagnosed with macular edema secondary to branch RVO.

3.1. Quality of OCT Maps and RM-SLO Images. Seventeen out of 39 final OCT retinal thickness maps (43.6%) were found

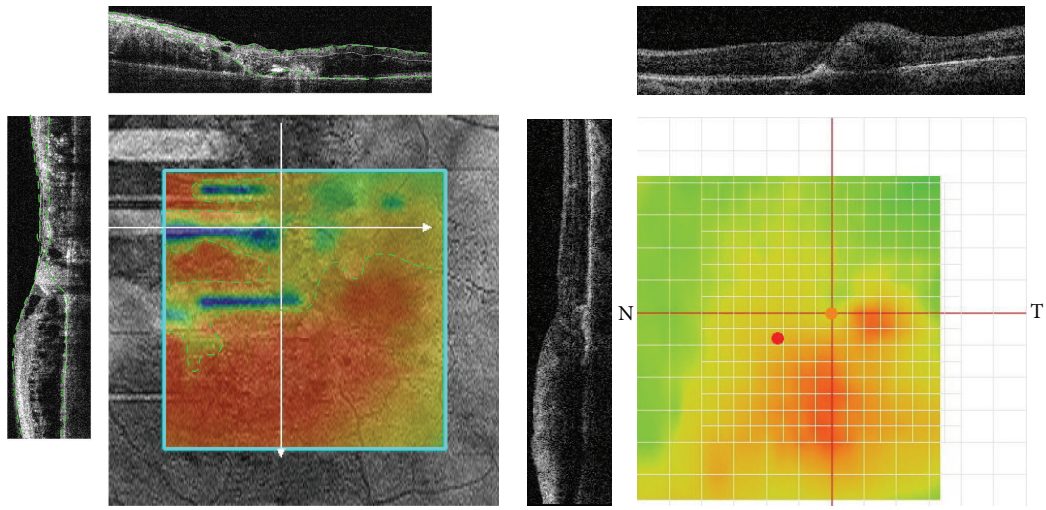

Figure 1: Artifacts in OCT retinal thickness maps that impede OCT-guided planning for navigated MLP. (a) Incorrect automated segmentation (in B scans, a green dashed line represents automated segmentation boundaries; white arrows on the map indicate the locations of B scans) resulting in the occurrence of zones with underestimated retinal thickness (indicated by map colors colder than red and limited by a yellow dashed line). (b) Off-center artifact due to fixation error (green mark represents the true foveal center identified with B scans; red mark represents the foveal center identified automatically; black lines on the map represent the locations of B scans).

to be inadequate for immediate import into the NAVILAS system with the following overlay on a baseline fundus image. The reasons for this were incorrect automated segmentation (with underestimation of the true retinal thickness due to misidentification of outer retinal layers [21, 22]) in 14/17 eyes, misidentification of foveal center (off-center artifact [21, 22]) due to incompliance with the gaze fixation requirement in 2 cases, and the combination of the first two reasons in 1 case (Figure 1). In all these 14 eyes, after manual correction of retinal boundary segmentation errors in OCT B scans, retinal thickness maps were regenerated and found to be adequate (i.e., having no retinal thickness measurement errors) for OCT-guided planning for MLP. In 2 out of the 3 cases of misidentified foveal center, a scan was slightly off-center, and correction was made through manual repositioning of the foveal center, whereas another case required repeating the scan followed by manual repositioning of the foveal center. Neither corrections nor retakes were required for RM-SLO images, all of which were found to be adequate for RM-SLO-guided planning for MLP. In 2/39 eyes, neither of the two retinal specialists managed to identify the zone of edema with confidence and to perform the treatment planning based on OCT findings only. This was caused by the insignificant edema height (and, consequently, poor identification of the edema on the color map) in one case, and both the out-of-scan-area location of retinal edema and the insignificant edema height in another case (Figure 2). In both these eyes, the retinal edema was clearly visualized on RM-SLO images, which allowed for RM-SLO-guided planning for MLP (Figure 2); these eyes were excluded from statistical analysis. In the rest of the eyes ($n = 37$; 94.9%), rather large intraretinal cysts (i.e., larger than those at the adjacent extrafoveal sites) were found in the foveal zone on RM-SLO images.

3.2. Measurement of the Retinal Edema Area. The area of edema on RM-SLO image was found to be statistically significantly larger than that on OCT map of the same eye by each physician (physician 1, $P = 0.004$; physician 2, $P = 0.003$). The average area of edema on RM-SLO image was larger than that on OCT map ($14.5 \pm 4.3\,\text{mm}^2$ versus $9.1 \pm 1.9\,\text{mm}^2$, $P = 0.015$). However, in 24 eyes (61.5%), OCT mapping did not allow to visualize the entire area of retinal edema, since the edema territory exceeded the boundaries of a 5 mm × 5 mm scan area (Figure 3). Therefore, in these eyes, the comparison of the retinal edema area was redone for OCT retinal thickness map and RM-SLO image solely within a 5 mm × 5 mm scan area aligned against the foveal center (Figure 3).

The retinal edema area measured within a 5 mm × 5 mm zone of RM-SLO image (i.e., within a zone identical to a 5 mm × 5 mm OCT scan area) was not statistically significantly different from that measured on OCT of the same eye by each physician (physician 1, $P = 0.25$; physician 2, $P = 0.28$). The average retinal edema area measured within a 5 mm × 5 mm zone of RM-SLO image was statistically insignificantly larger than that measured on OCT maps ($10.5 \pm 2.2\,\text{mm}^2$ versus $9.1 \pm 1.9\,\text{mm}^2$, $P = 0.11$).

In comparison of measuring edema area on RM-SLO images, there was no statistically significant difference among the 2 physicians ($P = 0.17$). No statistically significant difference among the 2 physicians was also present in comparison of measuring edema area on OCT maps ($P = 0.19$).

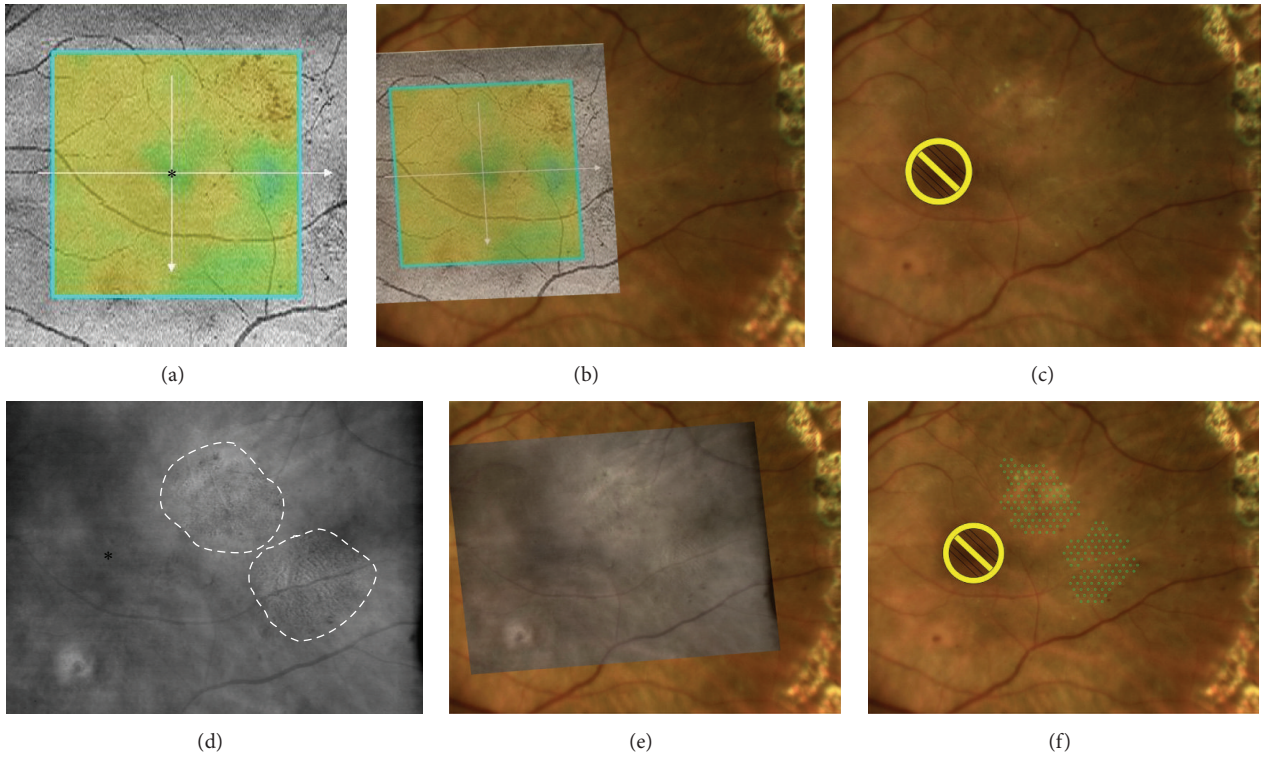

Figure 2: OCT- versus RM-SLO-guided treatment plan for macular laser photocoagulation. (a) Retinal edema is visualized on the OCT retinal thickness map (asterisk represents the foveal center). (b) OCT map is superimposed onto the baseline image. (c) Placing laser spot marks is impossible in this case of OCT-guided planning for macular laser photocoagulation. (d) Retinal edema zones (total area, 13.12 mm^2) are identified on the RM-SLO image (white dashed line represents the zone boundary; asterisk represents the foveal center). (e) RM-SLO image is superimposed onto the baseline image. (f) In RM-SLO-guided planning for macular laser photocoagulation, the number of laser spot marks was 198.

3.3. Spot Placing. The average number of spots using RM-SLO images and OCT maps was 189.6 ± 77.4 and 136.6 ± 46.8, respectively, $P = 0.003$ (Figure 3). In comparison of placing laser spots based on RM-SLO images, there was no statistically significant difference among the two physicians ($P = 0.13$). No statistically significant difference among the 2 physicians was also present in comparison of placing laser spots based on OCT maps ($P = 0.19$).

4. Discussion

This study demonstrates that MLP treatment planning for diabetic or RVO-related ME can be guided by RM-SLO, with the spots placed at the zones of visualized intraretinal microcysts, and these zones generally conforming in size and shape to those of increased retinal thickness (secondary to edema) on OCT.

A key RM-SLO feature is immediate visualization of retinal edema, whereas in OCT mapping and FA, the presence of edema is indicated only by phenomena, increased retinal thickness and dye leakage, respectively. When the entire edema zone was within a 5 mm × 5 mm region (thus corresponding to the limitation imposed by OCT), there was no statistically significant difference between the areas of retinal edema visualized by RM-SLO and that found by OCT (however, the average of the former area was somewhat higher than that of the latter).

Previous studies have revealed no advantage of FA-guided over OCT-guided MLP based on comparison of different characteristics including the area of retinal edema identified by the method [16]. Additionally, Vujosevic et al. [19] have confirmed that RM-SLO does not suffer from the disadvantages characteristic for FA. Therefore, it can be expected that RM-SLO-guided planning for MLP will show comparable results to those seen in FA-guided planning. Moreover, the use of RM-SLO images can offer some advantages in planning for navigated MLP compared with the use of OCT retinal thickness maps.

As opposed to the OCT retinal thickness map, the RM-SLO image, allows visualizing the edema within the central fundus, which is seen on the baseline image. A NAVILAS-obtained fundus photograph corresponds to the field of view of 50°, while a standard OCT retinal thickness map covers 18° or 22° (depending on the OCT system, this corresponds to 5 mm × 5 mm or 6 mm × 6 mm ETDRS macular maps), [23] and an RM-SLO image covers up to 60°. No possibility to visualize the entire retinal edema zone on the OCT retinal thickness map was found in 61.5% of the eyes of our study. At the same time, the RM-SLO image allows visualizing the retinal edema within the entire central fundus; consequently,

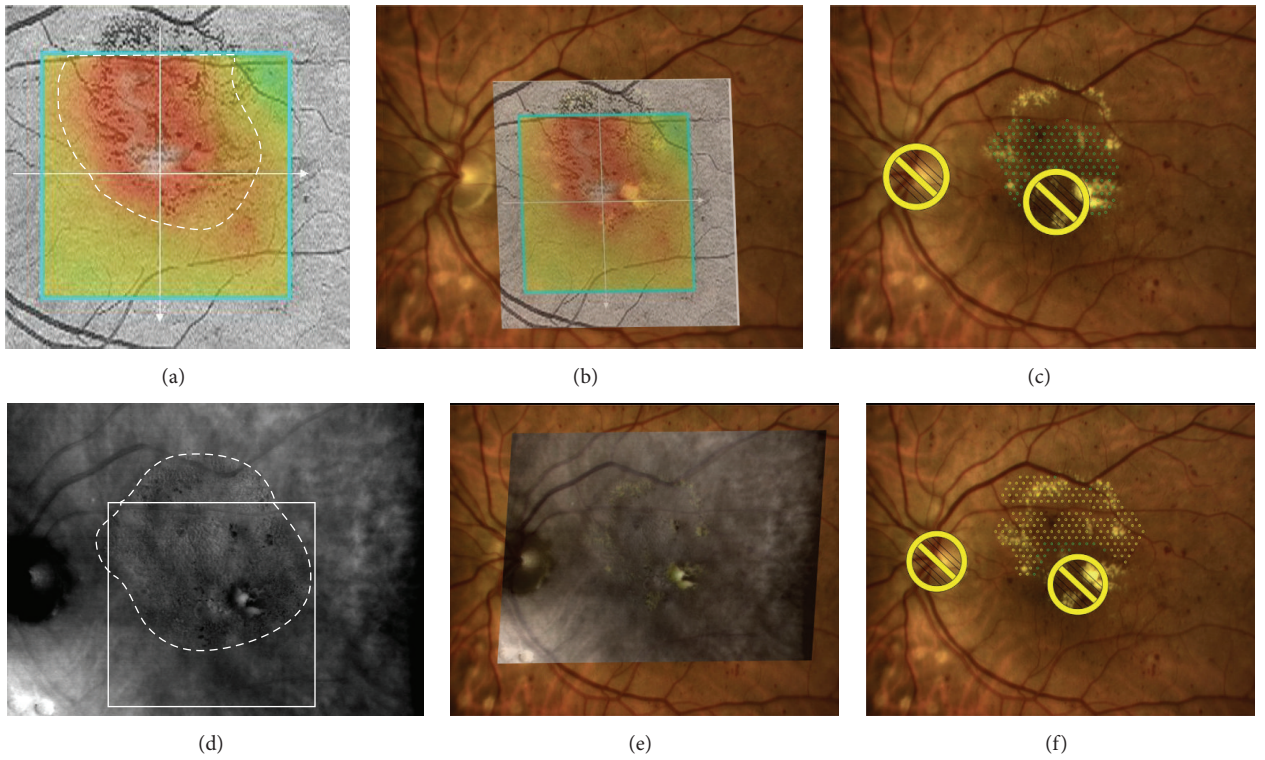

Figure 3: OCT- versus RM-SLO-guided treatment plan for macular laser photocoagulation. (a) OCT retinal thickness map fails to cover the entire zone of retinal edema (area, 9.33 mm^2). (b) OCT map superimposed onto the baseline image. (c) The number of laser spots placed in OCT-guided treatment planning is 149. (d) The entire zone of retinal edema is identified on RM-SLO image (entire edema area, 14.51 mm^2; white dashed line represents the edema zone boundary; white square represents a 5 mm × 5 mm zone involved into OCT retinal thickness map; the area of edema identified by RM-SLO within the 5 mm × 5 mm zone is 10.18 mm^2). (e) RM-SLO image superimposed onto the baseline image. (f) The number of laser spots placed in RM-SLO-guided treatment planning is 219 (i.e., more than that in OCT-guided treatment planning).

the area of edema measured in RM-SLO-guided treatment planning was found to be statistically significantly larger than that in OCT-guided treatment planning. Moreover, the RM-SLO image includes the optic nerve and the vascular arcades, thus facilitating the overlaying of images.

The average area of retinal edema revealed with RM-SLO within a 5 mm × 5 mm fundus zone was statistically insignificantly larger than that revealed with OCT. This difference may result from the fact that RM-SLO allows visualizing any small intraretinal microcysts located at the boundary of edema zone, with these microcysts either not increasing retinal thickness or increasing it insignificantly. Consequently, in OCT mapping, the retinal thickness in these microcystic regions is shown with a "nearly normal" color, and the regions may receive no spot marking at the time of planning for MLP.

Large cysts (such as those detected with RM-SLO in the foveal center in most of the eyes of our study) may serve as an additional landmark for identification of the foveal center, which has been confirmed by Yamamoto et al. [20]. Therefore, in RM-SLO-guided planning for MLP, the foveal center is identified not only on the baseline color image produced by NAVILAS system, but also with the help of additional landmarks, which allows avoiding its mistaken photocoagulation. At the same time, the foveal center is identified on the OCT retinal thickness map indirectly, using the fixation point.

A fixation error, if any, may cause the displacement of the foveal center marker from the true center and the displacement of the entire retinal thickness map with respect to the background SLO-type fundus photograph. Consequently, both the edema region and the foveal center will be identified incorrectly on the final retinal thickness map with respect to the background SLO-type fundus photograph. This may result in incorrect (e.g., outside-of-edema) placement of spot marks at the time of planning for MLP, since the retinal thickness map of the macula is superimposed onto the baseline color image (produced by NAVILAS system) using the landmarks of the background SLO-type fundus photograph. The requirements for a gaze fixation and no blinking during scan acquisition (acquisition time specified in the EMM5 protocol is 1.3 s) may be another cause for the above mentioned displacement of the foveal center from the true center. At the same time, acquisition of RM-SLO image occurs instantly, and requires neither a gaze fixation nor blinking inhibition, since the image covers most of the fundus area and can be aligned onto the baseline image.

If the edema results in an insignificant increase in retinal thickness (2 eyes of the study), the edema regions are not clearly defined on the OCT retinal thickness map and barely differ in color from non-edematous regions on the color map. Such edema regions become even less noticeable against the background SLO-type fundus photograph which is required for superimposition of the OCT retinal thickness map onto the baseline image.

In a considerable proportion of cases, OCT retinal thickness maps include underestimated areas of retinal thickening, which makes them inadequate for immediate import into the NAVILAS system and planning for MLP. This is associated with the attenuation of the signal by highly reflective intraretinal masses (hard exudates and hemorrhages which are often found in diabetic and proliferative retinopathy patients, potential candidates for MLP), with a correspondingly decreased signal of the retinal pigment epithelium. In such cases, the software algorithm misidentifies these highly reflective intraretinal masses as retinal pigment epithelium, uses them for segmentation of outer retinal layers, and computes underestimated retinal thickness values. Schneider et al. have found such errors in OCT images in 35.3% of examined patients with diabetic retinopathy [24], which is insignificantly less than the percentage found in our study. The difference may result from the inclusion of patients with RVO (because intraretinal hemorrhages are typical for central RVO pathology) and use of other OCT system in our study.

RM-SLO-guided planning for MLP has several disadvantages. First, a lower vessel contrast observed on the RM-SLO image compared to that on the SLO-type image produced by RTVue-100, resulting in an insignificant delay in the image superimposition process. Second, RM-SLO does not allow the physician to make an adequate conclusion about the post-treatment trends in edema-related parameters, since mean foveal thickness and macular volume, the indices providing the most valuable information for quantitative monitoring of ME, can be only measured with OCT. Hence, the use of RM-SLO does not exclude the need for the use of OCT. The correction of the automated segmentation boundaries and foveal center position for a later comparison of the pre-treatment OCT map with those obtained at different post-treatment time points, however, can be performed at any time before the comparison. Third, the measurement of retinal edema area based on RM-SLO images requires a certain level of expertise.

En face OCT imaging combines a number of advantages of both RM-SLO and OCT mapping. This approach allows the physician to visualize retinal microcysts in the macular region and to obtain quantitative data related to edema (e.g., mean foveal thickness) simultaneously. En face OCT, however, suffers all the disadvantages of conventional OCT related to the performance of scan protocol (automated segmentation errors, gaze fixation requirement, and a limited scan area).

The study has a number of limitations. First, we used only one OCT device. Since occurrence of different artifacts varies widely among OCT devices depending also on pathology, one may however expect occurrence of similar difficulties in planning for MLP when guided by the data derived from images taken with other OCT devices [25]. The limitation mentioned is not relevant to RM-SLO, since currently, F10 is the only commercially available scanning laser ophthalmoscope with retro-mode. Second, the study involved a relatively small number of eyes and did not involve controls for the comparison of anatomic and functional outcomes. Therefore, whether a larger photocoagulated area in MLP for ME results in better visual outcomes or a more sustained effect is so far unknown and warrants further investigation in a prospective controlled study.

In conclusion, our study demonstrates (1) the possibility of planning for navigated MLP based on the RM-SLO image overlayed on the fundus photograph of the same eye, (2) larger treatment areas suggested by RM-SLO-guided MLP plans for ME compared to those suggested by OCT-guided plans and (3) narrow variability in treatment planning among the retina specialists.

Disclosure

The authors have no proprietary or financial interest in any aspect of this report.

Conflict of Interests

The authors declare that there is no conflict of interests regarding the publication of this paper.

Acknowledgment

The authors thank O. V. Oleksiienko for his assistance in translating the article.

References

[1] The Branch Vein Occlusion Study Group, "Argon laser photocoagulation for macular edema in branch vein occlusion," *American Journal of Ophthalmology*, vol. 98, no. 3, pp. 271–282, 1984.

[2] A. Pielen, N. Feltgen, C. Isserstedt, J. Callizo, B. Junker, and C. Schmucker, "Efficacy and safety of intravitreal therapy in macular edema due to branch and central retinal vein occlusion: a systematic review," *PLoS ONE*, vol. 8, no. 10, Article ID e78538, 2013.

[3] Q. D. Nguyen, D. M. Brown, D. M. Marcus et al., "Ranibizumab for diabetic macular edema: results from 2 phase III randomized trials: RISE and RIDE," *Ophthalmology*, vol. 119, no. 4, pp. 789–801, 2012.

[4] P. Massin, F. Bandello, J. G. Garweg et al., "Safety and efficacy of ranibizumab in diabetic macular edema (RESOLVE study): a 12-month, randomized, controlled, double-masked, multicenter phase II study," *Diabetes Care*, vol. 33, no. 11, pp. 2399–2405, 2010.

[5] S. Day, K. Acquah, P. Mruthyunjaya, D. S. Grossman, P. P. Lee, and F. A. Sloan, "Ocular complications after antivascular endothelial growth factor therapy in medicare patients with age-related macular degeneration," *American Journal of Ophthalmology*, vol. 152, no. 2, pp. 266–272, 2011.

[6] V. Dewan, D. Lambert, J. Edler, S. Kymes, and R. S. Apte, "Cost-effectiveness analysis of ranibizumab plus prompt or deferred

laser or triamcinolone plus prompt laser for diabetic macular edema," *Ophthalmology*, vol. 119, no. 8, pp. 1679–1684, 2012.

[7] M. S. Ip, I. U. Scott, P. C. VanVeldhuisen et al., "A randomized trial comparing the efficacy and safety of intravitreal triamcinolone with observation to treat vision loss associated with macular edema secondary to central retinal vein occlusion: the Standard Care vs Corticosteroid for Retinal Vein Occlusion (SCORE) study report 5," *Archives of Ophthalmology*, vol. 127, no. 9, pp. 1101–1114, 2009.

[8] Y. G. Park, E. Y. Kim, and Y. J. Roh, "Laser-based strategies to treat diabetic macular edema: history and new promising therapies," *Journal of Ophthalmology*, vol. 2014, Article ID 769213, 9 pages, 2014.

[9] E. W. Schneider, P. Mruthyunjaya, and S. M. Hariprasad, "Combination therapy for macular edema secondary to retinal vein occlusion," *Ophthalmic Surgery Lasers and Imaging Retina*, vol. 44, no. 5, pp. 434–438, 2013.

[10] M. A. Leitritz, F. Gelisken, F. Ziemssen, P. Szurman, K. U. Bartz-Schmidt, and G. B. Jaissle, "Grid laser photocoagulation for macular oedema due to branch retinal vein occlusion in the age of bevacizumab? Results of a prospective study with crossover design," *British Journal of Ophthalmology*, vol. 97, no. 2, pp. 215–219, 2013.

[11] H. Schatz, D. Madeira, H. R. McDonald, and R. N. Johnson, "Progressive enlargement of laser scars following grid laser photocoagulation for diffuse diabetic macular edema," *Archives of Ophthalmology*, vol. 109, no. 11, pp. 1549–1551, 1991.

[12] K. Maeshima, N. Utsugi-Sutoh, T. Otani, and S. Kishi, "Progressive enlargement of scattered photocoagulation scars in diabetic retinopathy," *Retina*, vol. 24, no. 4, pp. 507–511, 2004.

[13] I. Kozak, S. F. Oster, M. A. Cortes et al., "Clinical evaluation and treatment accuracy in diabetic macular edema using navigated laser photocoagulator NAVILAS," *Ophthalmology*, vol. 118, no. 6, pp. 1119–1124, 2011.

[14] Early Treatment Diabetic Retinopathy Study Research Group, "Treatment techniques and clinical guidelines for photocoagulation of diabetic macular edema. Early Treatment Diabetic Retinopathy Study Report Number 2," *Ophthalmology*, vol. 94, no. 7, pp. 761–774, 1987.

[15] C. L. Lobo, R. C. Bernardes, J. R. F. de Abreu, and J. G. Cunha-Vaz, "One-year follow-up of blood-retinal barrier and retinal thickness alterations in patients with type 2 diabetes mellitus and mild nonproliferative retinopathy," *Archives of Ophthalmology*, vol. 119, no. 10, pp. 1469–1474, 2001.

[16] I. Kozak, S. Y. El-Emam, L. Cheng et al., "Fluorescein angiography versus optical coherence tomography-guided planning for macular laser photocoagulation in diabetic macular edema," *Retina*, vol. 34, no. 8, pp. 1600–1605, 2014.

[17] J. Y. Shin, S. H. Byeon, and O. W. Kwon, "Optical coherence tomography-guided selective focal laser photocoagulation: a novel laser protocol for diabetic macular edema," *Graefe's Archive for Clinical and Experimental Ophthalmology*, vol. 253, no. 4, pp. 527–535, 2015.

[18] R. Gallego-Pinazo, A. M. Suelves-Cogollos, R. Dolz-Marco et al., "Macular laser photocoagulation guided by spectral-domain optical coherence tomography versus fluorescein angiography for diabetic macular edema," *Clinical Ophthalmology*, vol. 5, no. 1, pp. 613–617, 2011.

[19] S. Vujosevic, P. Pucci, A. R. Daniele et al., "Extent of diabetic macular edema by scanning laser ophthalmoscope in the retromode and its functional correlations," *Retina*, vol. 34, no. 12, pp. 2416–2422, 2014.

[20] M. Yamamoto, S. Mizukami, A. Tsujikawa, N. Miyoshi, and N. Yoshimura, "Visualization of cystoid macular oedema using a scanning laser ophthalmoscope in the retro-mode," *Clinical and Experimental Ophthalmology*, vol. 38, no. 1, pp. 27–36, 2010.

[21] R. Ray, S. S. Stinnett, and G. J. Jaffe, "Evaluation of image artifact produced by optical coherence tomography of retinal pathology," *American Journal of Ophthalmology*, vol. 139, no. 1, pp. 18–29, 2005.

[22] J. Chhablani, T. Krishnan, V. Sethi, and I. Kozak, "Artifacts in optical coherence tomography," *Saudi Journal of Ophthalmology*, vol. 28, no. 2, pp. 81–87, 2014.

[23] A. C. Sull, L. N. Vuong, L. L. Price et al., "Comparison of spectral/Fourier domain optical coherence tomography instruments for assessment of normal macular thickness," *Retina*, vol. 30, no. 2, pp. 235–245, 2010.

[24] M. Schneider, A. Seres, G. Borgulya, and J. Nemeth, "Boundary detection errors on optical coherence tomography images in patients with diabetic retinopathy," *Ophthalmic Surgery Lasers and Imaging*, vol. 41, no. 1, pp. 54–59, 2010.

[25] A. Giani, M. Cigada, N. Choudhry et al., "Reproducibility of retinal thickness measurements on normal and pathologic eyes by different optical coherence tomography instruments," *American Journal of Ophthalmology*, vol. 150, no. 6, pp. 815–824, 2010.

Hindawi Publishing Corporation
Journal of Ophthalmology
Volume 2016, Article ID 8307639, 9 pages
http://dx.doi.org/10.1155/2016/8307639

Research Article

Comparison of Two Different OCT Systems: Retina Layer Segmentation and Impact on Structure-Function Analysis in Glaucoma

Livia M. Brandao,[1] Anna A. Ledolter,[2] Andreas Schötzau,[1] and Anja M. Palmowski-Wolfe[1]

[1]*Department of Ophthalmology, University of Basel, 4031 Basel, Switzerland*
[2]*Department of Ophthalmology, Medical University of Vienna, 1090 Vienna, Austria*

Correspondence should be addressed to Livia M. Brandao; livia.brandao@usb.ch

Received 23 September 2015; Revised 16 December 2015; Accepted 21 December 2015

Academic Editor: Gian M. Tosi

Copyright © 2016 Livia M. Brandao et al. This is an open access article distributed under the Creative Commons Attribution License, which permits unrestricted use, distribution, and reproduction in any medium, provided the original work is properly cited.

Purpose. To compare two different spectral-domain optical coherence tomography (OCT) systems in regard to full macular thickness (MT) and ganglion cell layer-inner plexiform layer (GCIPL) measures and in regard to structure-function correlation when compared to standard automated perimetry (SAP). *Methods*. Seventeen primary open angle glaucoma patients and 16 controls (one eye per subject) were enrolled. MT and GCIPL thicknesses were measured by Cirrus and Spectralis OCTs. Octopus Perimeter 101 (G2 protocol) reports sensitivity in mean defect (dB). Differences between measurements were assessed with Student's t-test and Bland Altman. Diagnostic performance was also compared between each parameter calculating the areas under the operator receiver (ROC). Linear models were used to investigate structure-function association between OCT and SAP. *Results*. Disagreement between OCTs in both MT and GCIPL values was significant. Spectralis values were thicker than Cirrus. Average difference between OCTs was 21.64 μm (SD 4.5) for MT and 9.8 μm (SD 5.4) for GCIPL ($p < 0.001$). Patients differed significantly from controls in both OCTs, in both measurements. MT and GCIPL were negatively associated with MD ($p < 0.001$). *Conclusions*. Although OCT values were not interchangeable, both machines differentiated patients from controls with statistical significance. Structure-function analysis results were comparable, when either OCT was compared to SAP.

1. Introduction

Glaucoma remains the third or fourth most common cause of blindness in different regions around the globe. Since this is a treatable disease, early diagnosis and adequate follow-up are gaining importance. Also, direct and indirect economic burdens tend to increase for governments with patients extended lifetime expectancy and complexity of disease stage [1].

So far standard automated perimetry (SAP) is still considered the "gold standard" method for function analysis even though defects are only detectable after substantial cell loss [2]. Since its introduction, optical coherence tomography (OCT) has turned into a fundamental tool in the evaluation of a variety of different retinal diseases, in particular primary open angle glaucoma (POAG). Thinning of the peripapillary retinal nerve fiber layer (RNFL) and full macular thickness (MT) have been largely used in POAG evaluation [3, 4]. In addition, recent improvements in OCT technology (i.e., Spectral OCT and software analysis) not only increased image resolution but also allowed customized analysis of the individual retinal layers. Glaucoma damage is primarily related to the ganglion cells [5]. Thus OCT retinal layer segmentation allows us to directly analyze the ganglion cell layer separately and thereby look directly at the site of damage. Indeed, ganglion cell-inner plexiform layer (GCIPL) segmentation can identify changes and correctly diagnose glaucoma with a similar sensitivity as the RNFL or optic nerve head (ONH) parameters [6–8]. Thus segmentation may allow a more sensitive structure-function correlation in different stages of disease. Although the increased number of OCT manufacturing

companies may contribute positively to price competition as well as hardware and software improvements, it also leads to variability in measurements and analysis methodology.

In this study, we determined if the brand of the spectral-domain OCT used and their respective segmentation programs influence structure-function analysis differently. To the best of our knowledge, this is the first study to compare two different OCT systems and their respective macula layer segmentation software and associate them with SAP in structure-function analysis.

2. Materials and Methods

The study protocol was approved by the Ethics Committee of the University of Basel, and informed consent was obtained from all participants before the examination. All procedures followed the tenets of the Declaration of Helsinki.

Patients with established glaucoma diagnosis and controlled IOP were recruited from the glaucoma ambulatory. The inclusion criteria included a visual acuity of 0.8 or better, and a refractive error between ±6 diopters of hyperopia or myopia. All glaucoma patients had a cup-to-disc ratio of at least 0.5 and a localized thinning of the neuroretinal rim on OCT (Cirrus) corresponding to the fundus examination. The OCT thinning should have at least one red sector or two yellow sectors on the thickness map (less than 1% and 5% of the normal population, resp., as by Cirrus software analysis). Preperimetric glaucoma was defined by the presence of optic nerve abnormalities consistent with glaucoma and a normal visual field as tested with SAP. Other glaucoma patients had to present a reproducible glaucomatous visual field defect on at least three examinations with a mean defect (MD) higher than 2.0 dB and/or a squared root of loss variance (sLV) over 2.5 dB. Individuals with previous ocular surgery, systemic diseases, or regular use of medications that could influence the eye (e.g., antidepressant, chloroquine) were excluded from the study.

The right eye was included in the study, if it did not fulfill any exclusion criteria. All OCT images were performed in the same day. When not possible, visual field examination was performed at a maximum interval of 7 months from OCT examination. Subjects underwent OCT imaging and SAP testing as described below. Data from the corresponding areas of the central 10° were analyzed.

Technical details from the two different commercially available OCT instruments used are displayed in Table 1. The pupil of the study eye was dilated with a solution of tropicamide 0.5% and phenylephrine 1% (Spital-Pharmazie USB, Switzerland) before examination. OCT images were obtained in Cirrus using the fast macular cube protocol 512 × 218 (128 horizontal scan lines each composed of 512 A-scans, Cirrus SD-OCT, Carl Zeiss, USA), and the fast volume scan in Spectralis HRA + OCT (25 section scans and 26 ART frames, Heidelberg Engineering, Inc., Heidelberg, Germany). The same specialist executed all OCT images. Both instruments have a scan area of 6 × 6 mm and macular retinal thickness is calculated in microns in an area correspondent to the Early Treatment Diabetic Retinopathy Study (ETDRS) grid. The MT values used in this study corresponded to the 1 and 3 mm circles of the ETDRS grid. GCIPL thickness is calculated by Cirrus software in the area of an elliptical annulus with a 2.0 mm vertical and 2.4 mm horizontal radius, excluding a central elliptical area (0.5 mm vertical and 0.6 mm horizontal radius) that corresponded to the foveola. According to studies of human retina, the highest density of ganglion cells occurs in this area [9]. As Spectralis software (version 6.0.3) uses the ETDRS grid also for GCIPL thickness calculation, values in the 3 mm circle were averaged, excluding the 1 mm circle, and compared to Cirrus (Figure 1, top).

Table 1: Technical characteristics from Cirrus and Spectralis OCT and acquisition protocol details of each device.

	Cirrus™	Spectralis™
Axial resolution	5 μm	4 μm
Scan speed (scan/sec)	27.000	40.000
Scan pattern	512 × 128	512 × 49
Scan area	6 × 6 mm	6 × 6 mm
Acquisition time	2.5 sec	5.0 sec
Software version	6.5.0	6.0.3

Also the segmentation software from each OCT calculates layer thickness differently. Cirrus software excluded the macular RNFL layer from the GCIPL analysis while Spectralis software calculated each retina layer separately (Figure 1, bottom). Therefore, in Spectralis, only the layers of interest in this study (ganglion cell and inner plexiform layers) were added in a separate Microsoft Excel spreadsheet. The exclusion of RNFL in Cirrus was based on the histologic observation that the macular GCIPL layer presents less variation than the RNFL among normal individuals [6]. Differences between the OCTs are that while both allow for manual corrections of the macular thickness boundaries, only Spectralis allows for manual correction of possible errors in GCIPL segmentation. Cirrus, but not Spectralis, separately analyses the minimum value of GCIPL thickness (mGCIPL) measured within the areas analyzed. Thus parameters included in this analysis were averaged MT and the GCIPL from both OCTs, and in addition, their average after manual correction (cMT and cGCIPL) in Spectralis and the mGCIPL value given in Cirrus. All images included in this study had signal strength over 7 for Cirrus and a quality score over 25 for Spectralis (limits considered as good/acceptable image quality for analysis, according to each instrument's manual).

Standard automated perimetry was performed using an Octopus Perimeter (Octopus 101, G2 Program, Haag-Streit AG, Switzerland). Total field MD (mean defect) values in dB were included in the analysis. All SAP exams used in this study were inside reliability parameters (fixation loss < 33%, false-positive and false-negative rates < 25%).

3. Statistical Analysis

Bland-Altman analysis was used to compare OCT results. Differences between measurements were compared using the paired t-test. Differentiation between glaucoma and controls within each measurement was assessed with a t-test and p values posteriorly adjusted with FDR (false discovery rate).

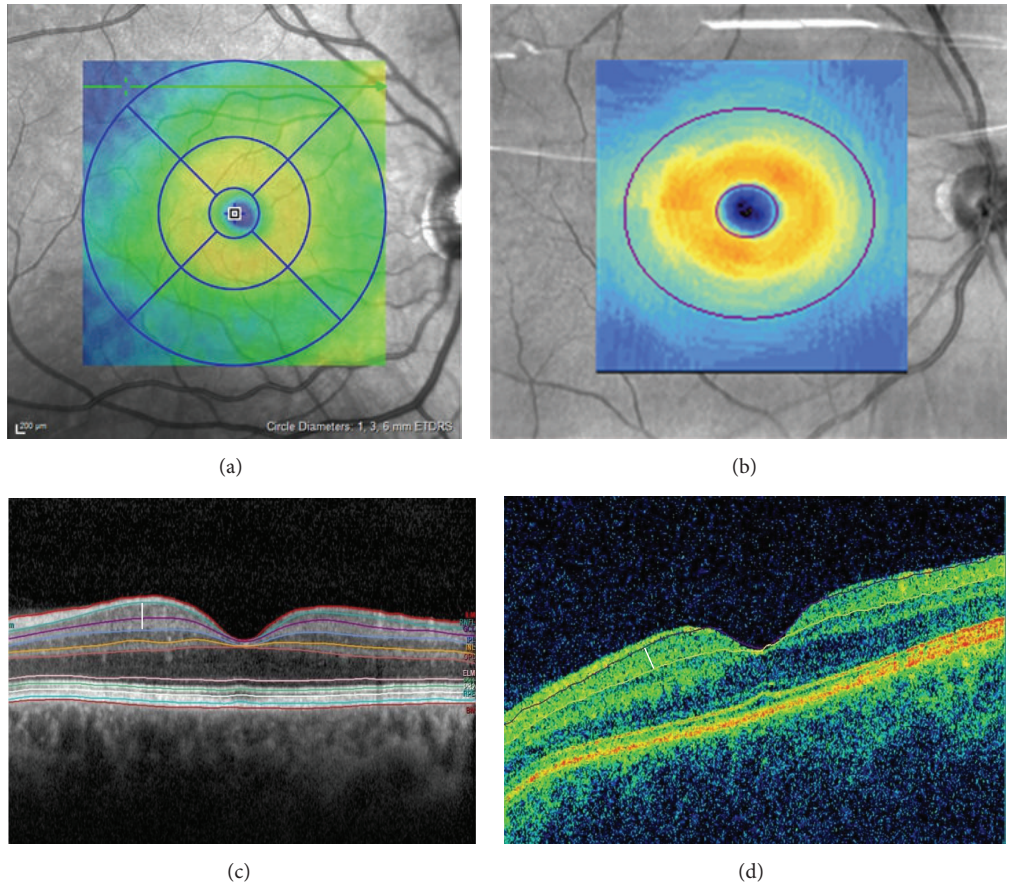

Figure 1: Top: (a) example from Early Treatment Diabetic Retinopathy Study (ETDRS) grid taken from Spectralis printout, used to calculate MT in both OCTs: scan area of 6 × 6 mm, divided into three concentric circles with 1 mm, 3 mm, and 6 mm diameter, respectively. Here, we used values from the 1 and 3 mm circles of the grid. (b) Area used in Cirrus to calculate GCIPL thickness corresponding to an elliptical annulus with a 2.0 mm vertical and 2.4 mm horizontal radius, excluding a central elliptical area (0.5 mm vertical and 0.6 mm horizontal radius) that corresponded to the foveola; in Spectralis GCIPL thickness was calculated with values in the 3 mm circle from ETDRS grid, excluding the 1 mm diameter circle. Bottom: OCT images using layer segmentation software from each instrument: (c) Spectralis, (d) Cirrus (same patient). While Cirrus software calculates only ganglion cell-inner plexiform layer (GCIPL) and excludes retina nerve fiver layer (RNFL), Spectralis software segments all retina layers and values from ganglion cell and inner plexiform layers were added manually. The white bar represents limits for thickness measurement of ganglion cell-inner plexiform layer in Spectralis (left) and Cirrus (right).

The predictive diagnostic performance for each parameter, that is, the ability to differentiate glaucoma from control, was assessed calculating the receiver operating characteristics (ROC) curves and the respective area under the ROC curve (AUC). A perfect predictive performance is represented by an AUC of 1.0 which means that this parameter can differentiate glaucoma from control with 100% sensitivity and specificity, while an AUC value of 0.5 means a prediction mostly influenced by chance. AUCs from different OCTs were compared with the DeLong test.

For prediction of structure-function relationship, linear models were performed. All calculations were adjusted to age. As OCT values are linear values but SAP are reported in dB, a logarithmic value, OCT values were transformed to logarithmic scale for better comparisons with SAP. Results were expressed as the regressive slope coefficients (on log-scale) with corresponding standard errors and p values.

Statistical analyses were performed using SPSS (IBM SPSS Statistics, version 22), and the statistical package R [10] (version 3.0.2). In this study, all p values <0.05 were considered as significant.

4. Results

A total of 33 eyes were included: 17 POAG and 16 controls. Complete demographic details are presented in Table 2. The mean age was 59.5 years (SD ± 13.9) for the glaucoma group and 49.2 years (SD ± 7.0) for the controls ($p = 0.013$). Median MD was 2.2 (range: −0.4–17.0) dB in POAG (including PPG) and −0.2 (range: −3.8–2.0) dB in controls ($p = 0.024$).

4.1. Macular and GCIPL Thickness in OCT. Table 3 shows averages from MT and GCIPL in both OCTs in the POAG and control groups. Spectralis and Cirrus showed a significant difference between patients and controls in both MT ($p = 0.018$, $p = 0.028$, resp.) and GCIPL ($p < 0.001$, both). Manual correction of the software segmentation parameters

Table 2

Group	POAG ($n = 17$)	Controls ($n = 16$)	p value*
Age (yrs) (mean ± SD)	59.5 ± 13.9	49.2 ± 7.0	$p = 0.029$
Gender (M/F)	12/5	4/12	
BVCA (decimal) (median, range)	1.0 (0.9–1.25)	1.2 (0.9–1.25)	$p = 0.030$
Refraction (mean ± SD)			
Diopters	−0.38 ± 2.0	−0.61 ± 2.1	$p > 0.05$
Cylinder	0.65 ± 0.72	0.72 ± 0.65	$p > 0.05$
MD (dB) (median, range)	2.2 (−0.4–17.0)	−0.2 (−3.8–2.0)	$p = 0.024$
RNFL (μm) (mean ± SD)	69.4 ± 11.1	90.0 ± 10.6	$p < 0.001$
IOP (mmHg) (mean ± SD)	12.8 ± 1.7	13.3 ± 2.7	$p = 0.811$
CDR (median, range)	0.8 (0.5–0.9)	0.3 (0.2–0.4)	$p < 0.0001$

POAG: primary open angle glaucoma, SD: standard deviation, BVCA: best corrected visual acuity (decimal), MD: mean defect (dB), RNFL: retinal nerve fiber layer average thickness, IOP: intraocular pressure under medication (mmHg), CDR: cup-to-disc ratio. * p values were obtained with t-test and posterior adjustment with FDR (false discovery rate).

Table 3: Total macula and ganglion cell layer mean thickness, in micrometers (μm), among groups and p values in the central 10°.

	POAG	Controls	p value*	AUC
MT (mean ± SD)				
Cirrus				
MT	297.6 ± 13.5	307.9 ± 12.1	**0.036**	0.789
Spectralis				
MT	319.0 ± 13.0	329.8 ± 11.7	**0.027**	0.801
cMT	319.0 ± 12.9	329.8 ± 11.7	**0.027**	0.805
GCIPL (mean ± SD)				
Cirrus				
GCIPL	68.5 ± 8.7	80.7 ± 4.7	<**0.01**	0.879
mGCIPL	61.2 ± 10.8	79.5 ± 4.7	<**0.01**	0.930
Spectralis				
GCIPL	75.7 ± 13.8	93.3 ± 4.6	<**0.01**	0.886
cGCIPL	76.1 ± 13.7	93.4 ± 4.6	<**0.01**	0.886

MT: full macular thickness, GCIPL: ganglion cell-inner plexiform layer thickness, cMT and cGCIPL: average values after manual correction of layer segmentation in Spectralis OCT, mGCIPL: minimum GCIPL value calculated by Cirrus software. AUC: area under the ROC curve. SD: standard deviation. * p values were obtained with paired t-test and posterior adjustment with FDR (false discovery rate).

in Spectralis produced a significant difference between measurements in GCIPL ($p < 0.05$) but not in MT ($p = 0.715$). A total of 2 controls (12.5%) and 7 patients (41.1%) needed posterior manual correction of retina thickness segmentation. No subject needed macula thickness segmentation correction in Cirrus analysis. Differences between OCT measurements per patient are shown in Figure 2(a).

Bland-Altman analysis showed disagreement between OCTs in MT and GCIPL values (Figure 2(b)). On average, measurements with Spectralis were thicker than with Cirrus. For MT the difference was 21.64 μm (SD ± 4.5) before and 21.65 μm (SD ± 4.5) after manual correction ($p < 0.001$). For average GCIPL thickness the difference was 9.8 μm (SD ± 5.4) before and 10.0 μm (SD ± 5.3) after manual correction ($p < 0.001$). With higher values measurements obtained with Spectralis tended to differ more from those measured with Cirrus. This difference increased when we compared Spectralis averages before (14.1 μm, SD ± 5.9) and after correction (14.4 μm, SD ± 5.8) with mGCIPL ($p < 0.001$).

There was no significant difference between the age-adjusted AUCs from MT in Cirrus (0.798) and Spectralis, before (0.801) and after (0.805) manual correction. This was also observed between OCTs for GCIPL measurements: 0.879 in Cirrus and 0.886 before and 0.886 after correction in Spectralis. Minimum GCIPL value in Cirrus had an AUC of 0.930 (Table 3; Figure 3).

4.2. Structure-Function Relationship. The association between SAP and OCT was assessed using a linear model. MT and GCIPL had a negative significant association with MD ($p < 0.001$), in both POAG ($p < 0.001$) and controls ($p < 0.001$) for Cirrus and Spectralis (Table 4, Figure 4).

5. Discussion

The aim of this study was to compare thickness measurements between two commercially available OCTs using their respective segmentation programs and assess if the brand of spectral-domain OCT used might influence structure function analysis differently in glaucoma. Using two different spectral-domain OCTs, Cirrus and Spectralis, we observed that there is a significant difference in full macula and GCIPL thickness measurements between machines. Therefore measurements are not interchangeable.

Nevertheless, when assessing structure function relationship individually, all measurements from both machines demonstrated a statistically significant relationship with function measured by standard automated perimetry. Further, age-adjusted AUCs demonstrated that all measurements had a similar predictive performance and could correctly differentiate patients from controls.

A literature review in PubMed using specific terms (optical coherence tomography, glaucoma, ganglion cell, macula, thickness, and segmentation software) did not reveal any other study which we could directly compare to this one. While we compared the entire area within the central 3 mm

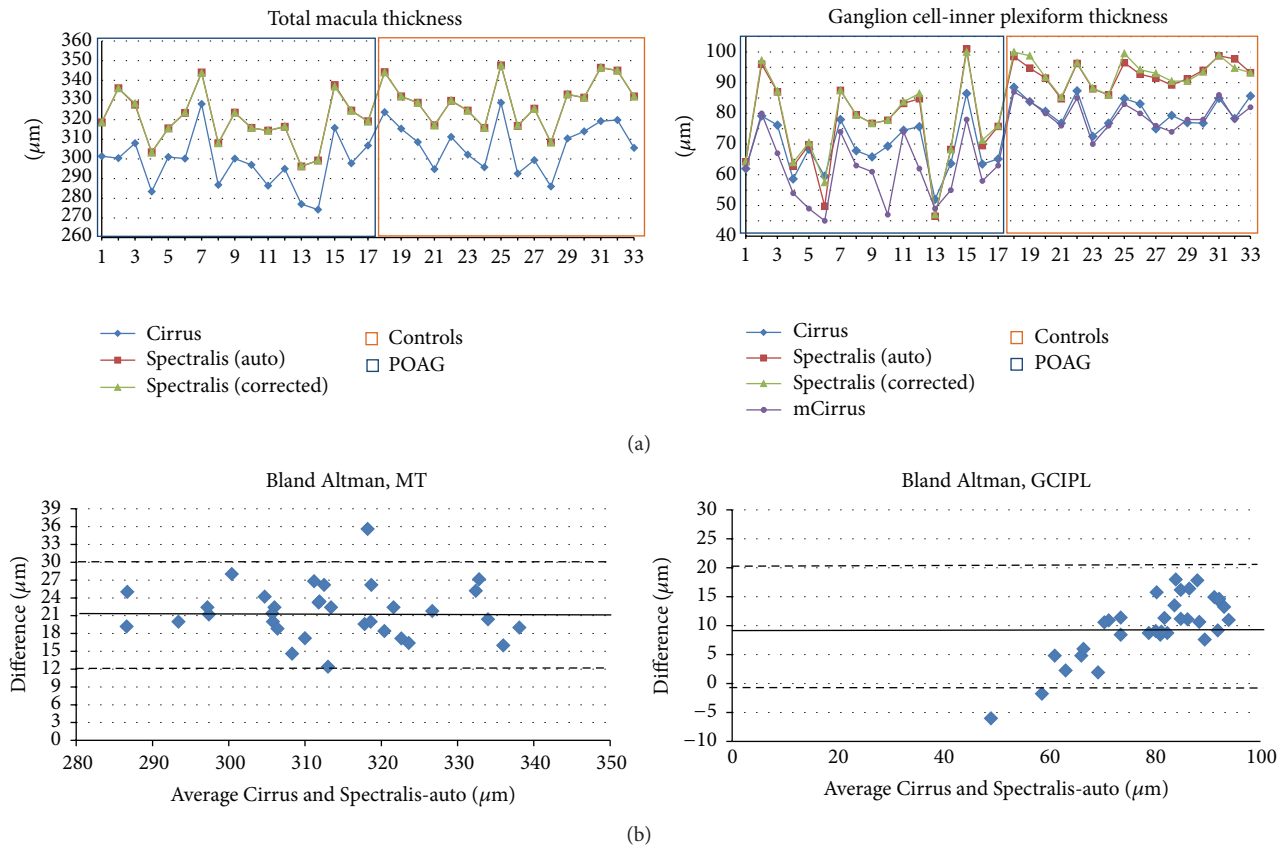

Figure 2: (a) This plot shows the measurements from both OCTs per patient: (left) total macula thickness; (right) ganglion cell-inner plexiform layer thickness. Comparison between these measurements allows visual appreciation of the difference per patient. (b) Respective Bland-Altman graphic representation comparing the difference between Cirrus and Spectralis MT (right) and GCIPL (left) to their mean. Auto: values using automatic segmentation in Spectralis; corrected: values after manual correction of retinal layer segmentation in Spectralis; mGCIPL: minimum GCIPL value calculated by Cirrus software. POAG: primary open angle glaucoma group; controls: control group.

diameters, most studies either refer to the central 1 mm area [11–16] or compare the areas within the ETDRS sectors calculated by the respective OCTs (i.e., the superior, inferior, temporal, and nasal sectors) [11, 16]. Here we showed that all thickness values from Spectralis were consistently higher than in Cirrus. This is in accordance with a study from Mylonas et al. [11], where Spectralis macula thickness also showed the highest values, in the central retinal thickness (CRT, 1 mm diameter) and individual sectors of the 3 mm area, in comparison to other OCTs (including Cirrus). Though the study was conducted in neovascular age-related macular degeneration patients (28 individuals), its control group (10 individuals) showed the same pattern. Other studies found the same difference between Cirrus and Spectralis in CRT [12, 14, 15].

There are numerous studies applying GCIPL thickness in glaucoma [6–8, 16–21]. The GCIPL average in early glaucoma patients from these studies (69.7 μm) is comparable to our study average (68.5 μm). A comparison of layer segmentation reproducibility was conducted at the IOWA University using Cirrus and their own segmentation software [22]. Here, the overall average from Cirrus GCIPL was reported as 70.0 μm (SD ± 11.4) in glaucoma, which also did not differ much from the patient group average in our study (Cirrus). Recently, Martinez-de-la-Casa et al. demonstrated that, using Spectralis layer segmentation software, macular RNFL thickness was the only parameter to differentiate healthy subjects from glaucoma suspects [21]. We have not found a study comparing Spectralis and Cirrus segmentation software, most probably because Spectralis software was made commercially available only recently.

The clear difference in macula thickness between OCTs could be explained analyzing the specific retina boundaries established by each manufacturer. While the inner boundary is always the vitreoretinal interface, the outer retinal boundary varies between manufacturers. For Cirrus the outer boundary corresponds to the level of the interdigitations of the external layers of the photoreceptors in the retinal pigment epithelium (Verhoeff's membrane), while in Spectralis it is at Bruch membrane [11, 13, 15]. Nevertheless, the establishment of different boundaries for total macula thickness calculation cannot explain the significant difference between GCIPL thicknesses we found in this study. Different image resolution, intrinsic reflectance, and analysis algorithms within each software may influence this calculation. We also cannot exclude an influence from the different areas analyzed, that is,

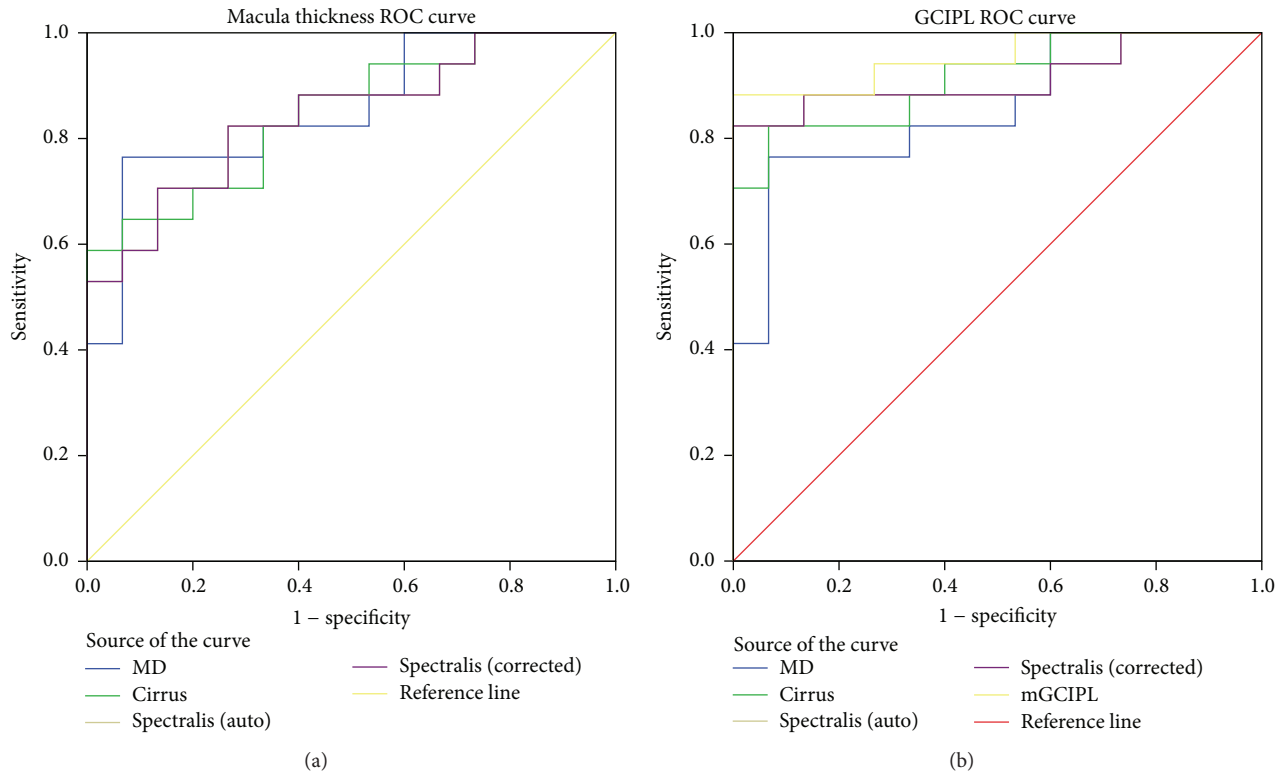

Figure 3: Age-adjusted ROC curves from Cirrus and Spectralis: (a) total macula thickness, (b) GCIPL. Auto: values using automatic segmentation in Spectralis; corrected: values after manual correction of retinal layer segmentation in Spectralis; mGCIPL: minimum GCIPL value calculated by Cirrus software; MD: mean defect.

Table 4: Structure-function relationship expressed as regression coefficients and corresponding p values.

Independent variable	Dependent variable	Regressive slope	Std. error	p value
Cirrus MT	MD	−7.459	1.552	<0.001
Spectralis MT	MD	−9.590	1.656	<0.001
Spectralis cMT	MD	−9.559	1.671	<0.001
Cirrus GCIPL	MD	−4.623	0.445	<0.001
Cirrus mGCIPL	MD	−3.206	0.374	<0.001
Spectralis GCIPL	MD	−3.053	0.336	<0.001
Spectralis cGCIPL	MD	−3.548	0.315	<0.001

OCT values were transformed to logarithmic scale. MT: full macular thickness, GCIPL: ganglion cell-inner plexiform layer, cMT and cGCIPL: average values after manual correction of layer segmentation in Spectralis OCT, mGCIPL: minimum GCIPL value calculated by Cirrus software, MD: mean defect.

ellipsoid in Cirrus versus the annular in Spectralis. However both areas differ only slightly and include the highest density area for ganglion cells.

While total macula thickness boundaries can be manually corrected in both Cirrus and Spectralis, individual layer segmentation correction is possible only in Spectralis. We did not observe a significant difference in total macula averages before and after manual correction of inner and outer retinal boundaries in Spectralis. This could be explained by the observation that, specifically for the internal limiting membrane and Bruch's membrane, delineation errors occurred mostly in the extreme periphery of the image slice. However, for the GCIPL segmentation errors also occur within the 3 mm ring averages. Thus GCIPL layer segmentation corrections made in Spectralis resulted in significantly different values, while values remained significantly higher than with Cirrus. In addition, the same difference in thickness measure will impact less on the thicker total macula thickness but more on the thinner GCIPL thickness. This probably explains the significant difference we found.

A significant correlation between function (global MD) and morphology (MT [23, 24] or GCIPL [20, 25, 26]) has been demonstrated previously. In agreement, despite the significant difference between Cirrus and Spectralis measurements,

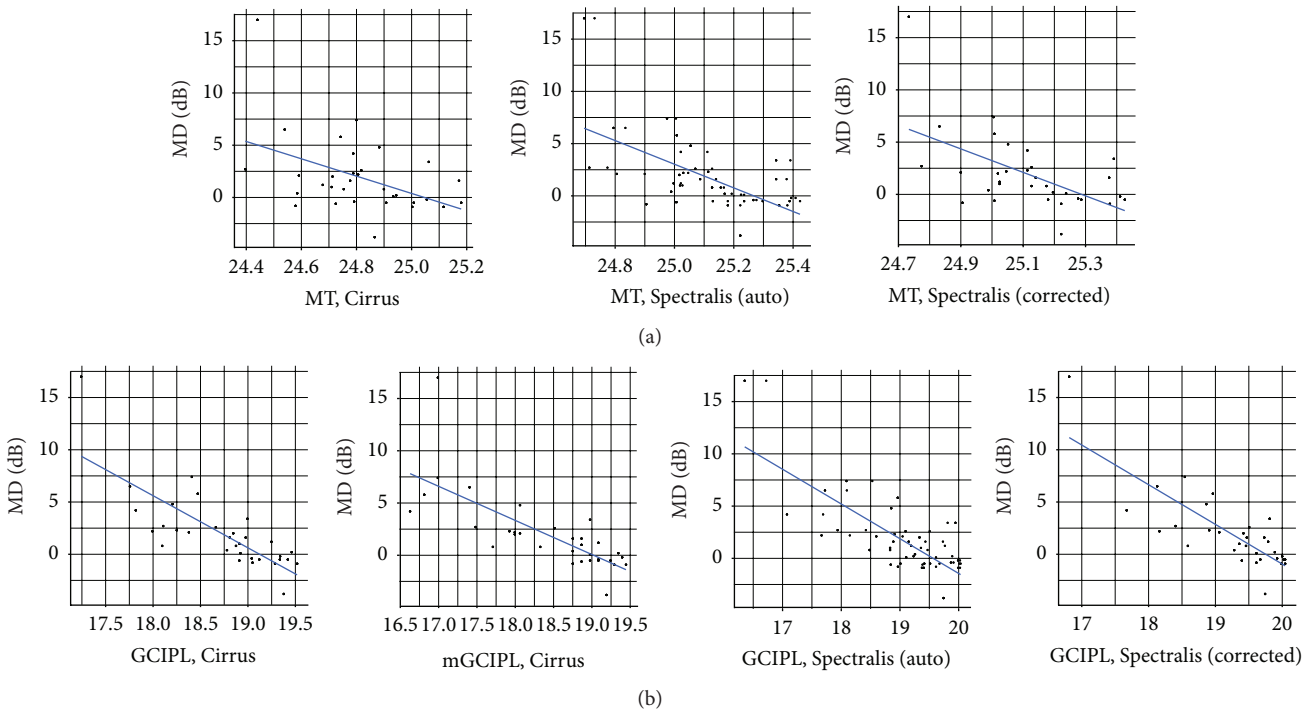

Figure 4: Scattered plots showing the structure-function relationship were obtained using linear models analysis. Age adjustment was applied in all calculations: top row from left to right: MD versus macular thickness from Cirrus, Spectralis (automatic values), and Spectralis (manually corrected values). Bottom row from left to right: MD versus ganglion cell-inner plexiform layer thickness from Cirrus (average and minimum value), Spectralis (automatic values), and Spectralis (manually corrected values). MD: mean defect.

both OCTs demonstrated a significant positive association with global MD. We are not aware of studies directly comparing the diagnostic performance between MT and GCIPL in glaucoma. When compared to RNFL, MT had an inferior diagnostic performance in Cirrus [27] and in Stratus [3, 23]. In our study, Spectralis MT showed similar diagnostic performance to Cirrus. However both were outperformed by GCIPL measurements, especially mGCIPL. Even though we found no other studies directly comparing AUC between MT and GCIPL, the AUC values found in this study are in accordance with findings from other studies using MT [27] and GCIPL [7, 8, 17, 20, 28].

Though we found a significant difference between OCT measurements, the small population analyzed here may limit our findings. Also, stage of disease might influence results given that the relationship between structural and functional damage is still not completely understood. Including more patients and later stages of disease glaucoma could give us additional information. In addition, knowing that age may influence our results, we adjusted all calculations for age.

Difference in gender distribution is also a concern: Cohn et al. did not observe a significant difference between males and females when comparing total dB from SAP [29]. However according to Ooto et al. total macular thickness is about 7.5 μm thicker in men than in women [30]. While age and sex differences should be considered when performing disease diagnostics, this is not the main scope of this study as we aimed to analyze measurements from two different OCTs within the same subject.

In contrast to Cirrus, Spectralis software does not yet include a normative databank. Once this is incorporated, comparison between deviation maps from these OCTs could contribute to understanding differences between calculations. Finally, the Spectralis segmentation software used here is a beta version. A definite version, without many changes, was recently made commercially available by the company.

In conclusion, the significant difference between measurements from Cirrus and Spectralis OCTs does not allow free interchange of machines, for instance, in the follow-up of patients. In a clinical setting, clinicians must be aware that once you change the machine and software analysis, a new baseline for the patient is needed. Nevertheless both machines showed similar capability of diagnostic performance in early glaucoma and also in their correlation to functional changes such as standard automated perimetry.

Ethical Approval

All subjects from this research read, signed, and gave the researcher their informed consent prior to their inclusion in the study. All procedures followed the tenets of the Declaration of Helsinki.

Disclosure

Funding organizations had no role in the design or conduct of this research.

Conflict of Interests

The authors declare that there is no conflict of interests regarding the publication of this paper.

Acknowledgments

This study was supported by Swiss National Science Foundation (SNF NMS 1823), LHW Stiftung Lichtenstein, and Freiwillige Akademische Gesellschaft Basel (FAG).

References

[1] K. Lorenz, C. Wolfram, L. Breitscheidel, M. Shlaen, Y. Verboven, and N. Pfeiffer, "Direct cost and predictive factors for treatment in patients with ocular hypertension or early, moderate and advanced primary open-angle glaucoma: the CoGIS study in Germany," *Graefe's Archive for Clinical and Experimental Ophthalmology*, vol. 251, no. 8, pp. 2019–2028, 2013.

[2] H. A. Quigley, G. R. Dunkelberger, and W. R. Green, "Retinal ganglion cell atrophy correlated with automated perimetry in human eyes with glaucoma," *American Journal of Ophthalmology*, vol. 107, no. 5, pp. 453–464, 1989.

[3] F. A. Medeiros, L. M. Zangwill, C. Bowd, R. M. Vessani, R. Susanna Jr., and R. N. Weinreb, "Evaluation of retinal nerve fiber layer, optic nerve head, and macular thickness measurements for glaucoma detection using optical coherence tomography," *American Journal of Ophthalmology*, vol. 139, no. 1, pp. 44–55, 2005.

[4] G. Wollstein, J. S. Schuman, L. L. Price et al., "Optical Coherence Tomography (OCT) macular and peripapillary retinal nerve fiber layer measurements and automated visual fields," *American Journal of Ophthalmology*, vol. 138, no. 2, pp. 218–225, 2004.

[5] L. A. Kerrigan-Baumrind, H. A. Quigley, M. E. Pease, D. F. Kerrigan, and R. S. Mitchell, "Number of ganglion cells in glaucoma eyes compared with threshold visual field tests in the same persons," *Investigative Ophthalmology & Visual Science*, vol. 41, no. 3, pp. 741–748, 2000.

[6] J.-C. Mwanza, D. L. Budenz, D. G. Godfrey et al., "Diagnostic performance of optical coherence tomography ganglion cell—inner plexiform layer thickness measurements in early glaucoma," *Ophthalmology*, vol. 121, no. 4, pp. 849–854, 2014.

[7] J.-C. Mwanza, M. K. Durbin, D. L. Budenz et al., "Glaucoma diagnostic accuracy of ganglion cell-inner plexiform layer thickness: comparison with nerve fiber layer and optic nerve head," *Ophthalmology*, vol. 119, no. 6, pp. 1151–1158, 2012.

[8] M.-S. Sung, J.-H. Yoon, and S.-W. Park, "Diagnostic validity of macular ganglion cell-inner plexiform layer thickness deviation map algorithm using cirrus HD-OCT in preperimetric and early glaucoma," *Journal of Glaucoma*, vol. 23, no. 8, pp. e144–e151, 2014.

[9] C. A. Curcio and K. A. Allen, "Topography of ganglion cells in human retina," *The Journal of Comparative Neurology*, vol. 300, no. 1, pp. 5–25, 1990.

[10] *R: A Language and Environment for Statistical Computing*, R Foundation for Statistical Computing, Vienna, Austria, 3.0.2 edition, 2008.

[11] G. Mylonas, C. Ahlers, P. Malamos et al., "Comparison of retinal thickness measurements and segmentation performance of four different spectral and time domain OCT devices in neovascular age-related macular degeneration," *The British Journal of Ophthalmology*, vol. 93, no. 11, pp. 1453–1460, 2009.

[12] L. Pierro, S. M. Giatsidis, E. Mantovani, and M. Gagliardi, "Macular thickness interoperator and intraoperator reproducibility in healthy eyes using 7 optical coherence tomography instruments," *American Journal of Ophthalmology*, vol. 150, no. 2, pp. 199–204, 2010.

[13] Z. Bentaleb-Machkour, E. Jouffroy, M. Rabilloud, J.-D. Grange, and L. Kodjikian, "Comparison of central macular thickness measured by three OCT models and study of interoperator variability," *The Scientific World Journal*, vol. 2012, Article ID 842795, 6 pages, 2012.

[14] U. E. K. Wolf-Schnurrbusch, L. Ceklic, C. K. Brinkmann et al., "Macular thickness measurements in healthy eyes using six different optical coherence tomography instruments," *Investigative Ophthalmology and Visual Science*, vol. 50, no. 7, pp. 3432–3437, 2009.

[15] A. Giani, M. Cigada, N. Choudhry et al., "Reproducibility of retinal thickness measurements on normal and pathologic eyes by different optical coherence tomography instruments," *American Journal of Ophthalmology*, vol. 150, no. 6, pp. 815.e1–824.e1, 2010.

[16] H.-Y. Shin, H.-Y. L. Park, K.-I. Jung, J.-A. Choi, and C. K. Park, "Glaucoma diagnostic ability of ganglion cell-inner plexiform layer thickness differs according to the location of visual field loss," *Ophthalmology*, vol. 121, no. 1, pp. 93–99, 2014.

[17] J. W. Jeoung, Y. J. Choi, K. H. Park, and D. M. Kim, "Macular ganglion cell imaging study: glaucoma diagnostic accuracy of spectral-domain optical coherence tomography," *Investigative Ophthalmology & Visual Science*, vol. 54, no. 7, pp. 4422–4429, 2013.

[18] M. Francoz, J.-R. Fenolland, J.-M. Giraud et al., "Reproducibility of macular ganglion cell-inner plexiform layer thickness measurement with cirrus HD-OCT in normal, hypertensive and glaucomatous eyes," *The British Journal of Ophthalmology*, vol. 98, no. 3, pp. 322–328, 2014.

[19] J.-C. Mwanza, J. D. Oakley, D. L. Budenz, R. T. Chang, O. J. Knight, and W. J. Feuer, "Macular ganglion cell-inner plexiform layer: automated detection and thickness reproducibility with spectral domain-optical coherence tomography in glaucoma," *Investigative Ophthalmology & Visual Science*, vol. 52, no. 11, pp. 8323–8329, 2011.

[20] J. S. Jeong, M. G. Kang, C. Y. Kim, and N. R. Kim, "Pattern of macular ganglion cell-inner plexiform layer defect generated by spectral-domain OCT in glaucoma patients and normal subjects," *Journal of Glaucoma*, vol. 24, no. 8, pp. 583–590, 2015.

[21] J. M. Martinez-de-la-Casa, P. Cifuentes-Canorea, C. Berrozpe et al., "Diagnostic ability of macular nerve fiber layer thickness using new segmentation software in glaucoma suspects," *Investigative Ophthalmology and Visual Science*, vol. 55, no. 12, pp. 8343–8348, 2014.

[22] M. K. Garvin, K. Lee, T. L. Burns, M. D. Abràmoff, M. Sonka, and Y. H. Kwon, "Reproducibility of SD-OCT-based ganglion cell-layer thickness in glaucoma using two different segmentation algorithms.," *Investigative Ophthalmology & Visual Science*, vol. 54, no. 10, pp. 6998–7004, 2013.

[23] C. K. S. Leung, W.-M. Chan, W.-H. Yung et al., "Comparison of macular and peripapillary measurements for the detection of glaucoma: an optical coherence tomography study," *Ophthalmology*, vol. 112, no. 3, pp. 391–400, 2005.

[24] D. S. Greenfield, H. Bagga, and R. W. Knighton, "Macular thickness changes in glaucomatous optic neuropathy detected using optical coherence tomography," *Archives of Ophthalmology*, vol. 121, no. 1, pp. 41–46, 2003.

[25] K. Mathers, J. A. Rosdahl, and S. Asrani, "Correlation of macular thickness with visual fields in glaucoma patients and suspects," *Journal of Glaucoma*, vol. 23, no. 2, pp. e98–e104, 2014.

[26] H.-Y. Shin, H.-Y. L. Park, K. I. Jung, and C. K. Park, "Comparative study of macular ganglion cell-inner plexiform layer and peripapillary retinal nerve fiber layer measurement: structure-function analysis," *Investigative Ophthalmology and Visual Science*, vol. 54, no. 12, pp. 7344–7353, 2013.

[27] J. H. Na, K. R. Sung, S. Baek, J. H. Sun, and Y. Lee, "Macular and retinal nerve fiber layer thickness: which is more helpful in the diagnosis of glaucoma?" *Investigative Ophthalmology & Visual Science*, vol. 52, no. 11, pp. 8094–8101, 2011.

[28] K. Nouri-Mahdavi, S. Nowroozizadeh, N. Nassiri et al., "Macular ganglion cell/inner plexiform layer measurements by spectral domain optical coherence tomography for detection of early glaucoma and comparison to retinal nerve fiber layer measurements," *American Journal of Ophthalmology*, vol. 156, no. 6, pp. 1297.e2–1307.e2, 2013.

[29] H. Cohn, M. DeAgostini, D. Aron-Rosa, L. Laloum, and F. Boller, "Sex differences in the left and right hemifields of normal subjects with computerised static perimetry," *British Journal of Ophthalmology*, vol. 78, no. 11, pp. 837–841, 1994.

[30] S. Ooto, M. Hangai, and N. Yoshimura, "Effects of sex and age on the normal retinal and choroidal structures on optical coherence tomography," *Current Eye Research*, vol. 40, no. 2, pp. 213–225, 2015.

Hindawi Publishing Corporation
Journal of Ophthalmology
Volume 2016, Article ID 1628469, 8 pages
http://dx.doi.org/10.1155/2016/1628469

Research Article

Ocular Surface Epithelial Thickness Evaluation in Dry Eye Patients: Clinical Correlations

Qingfeng Liang,[1] Hong Liang,[1,2,3,4] Hanruo Liu,[1] Zhiqiang Pan,[1] Christophe Baudouin,[2,3,4,5,6] and Antoine Labbé[1,2,3,4,5,6]

[1]*Beijing Institute of Ophthalmology, Beijing Tongren Eye Center, Beijing Tongren Hospital, Capital Medical University, Beijing Key Laboratory of Ophthalmology and Visual Sciences, Beijing 100005, China*
[2]*INSERM, U968, 75012 Paris, France*
[3]*UPMC Université Paris 06, UMR_S 968, Institut de la Vision, 75012 Paris, France*
[4]*CNRS, UMR_7210, 75012 Paris, France*
[5]*Quinze-Vingts National Ophthalmology Hospital, 75012 Paris, France*
[6]*Versailles Saint-Quentin-en-Yvelines University, 78000 Versailles, France*

Correspondence should be addressed to Qingfeng Liang; lqflucky@163.com

Received 31 October 2015; Revised 31 December 2015; Accepted 31 December 2015

Academic Editor: Taras Ardan

Copyright © 2016 Qingfeng Liang et al. This is an open access article distributed under the Creative Commons Attribution License, which permits unrestricted use, distribution, and reproduction in any medium, provided the original work is properly cited.

Purpose. To evaluate the relationship between corneal and conjunctival epithelium thickness and ocular surface clinical tests in dry eye disease (DED) patients. *Patients and Methods.* Fifty-four patients with DED and 32 control subjects were included. Each patient underwent an ocular surface evaluation using the ocular surface disease index (OSDI), tear film break-up time (TBUT), corneal and conjunctival staining, tear film lipid layer analysis, and Schirmer test. The central corneal (CET), limbal (LET), and bulbar conjunctival epithelium thickness (BET) were acquired using spectral-domain optical coherence tomography (SD-OCT). *Results.* Compared to control subjects, mean BET was significantly thicker and mean LET was significantly lower in the DED group. There was no significant difference in mean CET between the two groups. The mean LET was correlated with OSDI and TBUT. The inferior LET was correlated with OSDI, Schirmer I test, TBUT, Oxford score, and corneal sensitivity. Mean BET was correlated with OSDI and TBUT, but not with Schirmer I test and Oxford score. *Conclusions.* In dry eye patients, a thinner limbal epithelium and a thicker bulbar conjunctival epithelium were observed. These changes were correlated to the severity of dry eye symptoms and tear film alterations.

1. Introduction

Dry eye disease (DED) is a multifactorial disease of the tears and ocular surface resulting in tear film instability with potential damage to conjunctival and corneal epithelium [1]. It results from a disturbance of the lacrimal functional unit that includes the tear film, the lacrimal and meibomian glands, the ocular surface epithelium, and the sensory and motor nerves that connect them [2]. Inflammation with inflammatory cell infiltration and cytokine production are also common features of DED, found in the lacrimal glands, the cornea, and the conjunctiva [3]. In association with the mechanical and desiccating stress induced by the lack and/or the poor quality of tears, inflammation further damages ocular surface epithelia. Considering the central role of these tissues in the pathophysiology of DED, several imaging techniques have been developed to evaluate and grade the alterations of ocular surface epithelia *in vivo* [4, 5]. Despite lower resolution than *in vivo* confocal microscopy (IVCM), SD-OCT has numerous advantages over other imaging techniques, such as slit-lamp or ultrasound biomicroscopy [6]. OCT is a noninvasive imaging method that allows high-resolution analysis and quantification without the need for ocular anesthesia or contact procedures. In a preliminary study, we used SD-OCT to noninvasively evaluate ocular surface epithelial thickness [4]. In DED patients and patients

using IOP-lowering eye drops, we observed a decreased limbal-conjunctival epithelial thickness and an increased bulbar conjunctival epithelial thickness. The epithelial thickness measurement of ocular surface tissues with SD-OCT seemed to be an advantageous new parameter during ocular surface evaluation. However, the number of patients in each group was limited and correlations were not evaluated between epithelium thickness changes and ocular surface clinical tests. Thus, the objective of the present study was to compare the results of corneal, limbal, and conjunctival epithelium thicknesses obtained with SD-OCT in normal subjects and non-Sjögren dry eye patients and to evaluate the relationship between these parameters and the results of ocular surface clinical tests.

2. Patients and Methods

2.1. Subjects. This study was conducted at the Beijing Institute of Ophthalmology with approval of the Medical Ethics Committee of Beijing Tongren Hospital (TREC-2013-KY012). All patients were informed of the aims of the study and their consent was obtained according to the declaration of Helsinki. A total of 54 patients with DED not associated with Sjögren syndrome (36 women and 18 men; mean age: 44.59 ± 10.08 years; range: 24–68 years) were consecutively recruited from the Cornea Unit of Beijing Tongren Hospital from June 2013 to February 2014 (DED group). The sample size was calculated according to the results of Cui et al.'s study [7] with 80% power level. DED was defined as Schirmer I testing <5 mm and/or tear film break-up time (TBUT) <10 s, accompanied by complaints of ocular irritation in the absence of other ocular (in particular meibomian gland disease) or systemic diseases [1]. Thirty-two age- and gender-matched control subjects (20 women and 12 men; mean age: 43.34 ± 10.81 years; range: 19–67 years) were also recruited (control group). All control subjects had no complaint of ocular surface irritation and no anterior segment abnormality on biomicroscopic examination and ocular surface tests. Exclusion criteria for both groups were as follows: age <18 years, subject unable to complete the questionnaire or understand the procedures, the presence of ocular or systemic disease or the use of topical or systemic medications that may affect the cornea and the ocular surface (except the use of nonpreserved tear substitutes in the DED group), and previous eye surgery or contact lens wear.

2.2. Clinical Evaluation. Demographic information and medical history were obtained from the patients' medical records. Each subject underwent quantification of ocular surface symptoms with the Ocular Surface Disease Index (OSDI) questionnaire (range: 0–100). Then, the subjects underwent ocular surface examinations in the following order: tear film break-up time (TBUT), corneal and conjunctival fluorescein staining, tear film lipid layer analysis, Schirmer test without anesthesia, and corneal sensation measured with the Cochet-Bonnet esthesiometer.

TBUT was measured by instilling fluorescein into the inferior cul-de-sac and calculating the average of three consecutive break-up times. Corneal and conjunctival staining was evaluated under a yellow filter using the Oxford scale and after instillation of fluorescein. Tear film lipid layer analysis was performed using interferometry (DR-1, Kowa, Tokyo, Japan) and evaluated semiquantitatively from 1 to 5 (grade 5 being the most severe) [5]. Schirmer I test was performed without anesthesia for 5 min with the patient's eyes closed. Corneal sensation was measured using the contact nylon thread Luneau 12/100 mm Cochet-Bonnet esthesiometer (Luneau, Prunay-Le-Gillon, France) in the central cornea and in the superior, inferior, nasal, and temporal quadrants. Mean corneal sensitivity (MCS) was defined as the mean of the measures obtained in the five different areas.

2.3. SD-OCT Examination and Image Analysis. SD-OCT fitted with an anterior segment module (Optovue Corporation, Fremont, CA, USA) was used. This SD-OCT has a scan rate of 26,000 axial scans per second. Its axial and transverse optical resolution were 5 μm and 15 μm, respectively. An add-on lens (CAM-L mode: 6.0–2.0 mm) was used to assess the regional corneal and conjunctival architecture and epithelial thickness. Because SD-OCT examination is a noncontact technique, it was performed before ophthalmological examinations in order to avoid potential epithelium alterations.

The specific imaging capture technique for this study has been previously described [4]. Briefly, patients were asked to fixate on the target light source, and consecutive images were acquired with the patient's forehead and chin stabilized by a headrest. Corneal epithelium thickness (CET) was defined as the epithelium thickness in the 2 mm central zone of the cornea; limbal epithelium thickness (LET) was defined as the limbal-conjunctival epithelium thickness in each quadrant (superior, inferior, temporal, and nasal); bulbar conjunctival epithelial thickness (BET) was defined as the bulbar conjunctival epithelial thickness located between 2 and 3 mm from the limbus of each quadrant (Figure 1).

The cursors were placed perpendicular to the ocular surface epithelium from a point located just beneath the tear film (first hyperreflective layer) to the basal membrane (second hyperreflective layer). For every quadrant, three measurements were taken (if the difference between measurements exceeded 3 μm, the measurement was repeated in order to confirm thickness measurement reproducibility; the measurement needed to be confirmed in less than 5% of cases), and the results were expressed as mean ± SD. The measurements were taken by one researcher (HL) who was masked to patient demographic data and the results of ophthalmologic examinations. To evaluate interobserver variability, a second examiner (QL), who was masked to the results of the first SD-OCT analyses, assessed CET, LET, and BET from the same images of 20 randomized patients.

2.4. Statistical Analysis. Statistical analyses were performed with SPSS for Windows version 16.0 (SPSS Inc., Chicago, IL, USA). For each patient, one eye was randomly chosen for statistical analysis. The mean ± SD values of each epithelial thickness variable were calculated for both the DED and control groups. To compare ocular surface parameters and epithelial thickness, measured in normal and DED eyes, two-tailed Student's t-tests were performed. The Pearson

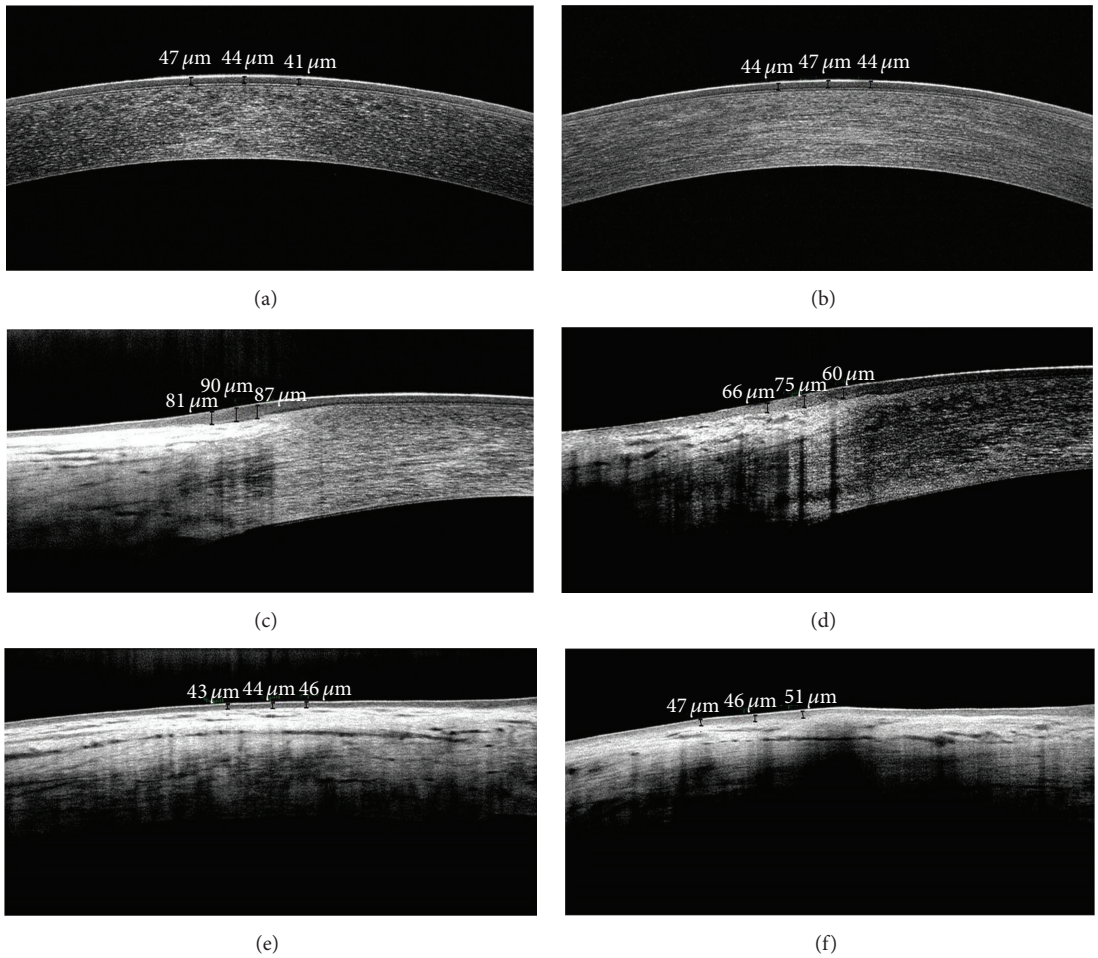

Figure 1: SD-OCT images of ocular surface epithelial thickness measurement in a healthy control subject (a, c, e) and a dry eye patient (b, d, f). Corneal epithelium thickness measurement with software cursors (a, b), limbus and conjunctiva epithelium thickness analysis (c, d), and conjunctiva epithelium thickness measurement (e, f).

correlation coefficient was used in DED patients to investigate the correlation between the quantitative measurements of epithelial thicknesses and the results of other ocular surface evaluations. P values less than 0.05 were considered statistically significant.

3. Results

There was no difference in terms of gender ($P = 0.699$) and age ($P = 0.503$) between the DED and control groups. Concerning ocular surface clinical evaluation, DED patients had significantly more symptoms (OSDI) (35.46 ± 14.94 versus 1.52 ± 3.96, $P < 0.001$), lower TBUT (4.67 ± 2.30 s versus 13.31 ± 2.54 s, $P < 0.001$), a lower Schirmer I test score (4.11 ± 6.98 mm versus 12.56 ± 6.99 mm, $P < 0.001$), and a higher Oxford score (1.06 ± 1.73 versus 0.00, $P = 0.001$) as compared to the control group. Mean corneal sensitivity was significantly decreased in the DED group (5.74±0.41 mm versus 5.98 ± 0.07 mm, $P = 0.002$), while tear film lipid layer interferometry was not statistically different between the two groups (2.43 ± 0.71 mm versus 2.28 ± 0.52, $P = 0.323$). Results of clinical data are presented in Table 1.

Mean CET, LET, and BET were 50.23 ± 4.42 μm, 81.37 ± 6.21 μm, and 50.44 ± 5.25 μm in the DED group and 49.76 ± 3.15 μm, 87.14 ± 9.98 μm, and 44.62 ± 5.04 μm in the control group, respectively. Compared to control subjects, mean BET was significantly thicker ($P < 0.001$) and mean LET was significantly lower ($P = 0.009$) in the DED group. There was no significant difference in CET between the two groups ($P = 0.103$). In addition, dry eyes had a significantly thicker BET in each quadrant region (superior, $P = 0.005$; inferior, $P = 0.014$; temporal, $P < 0.001$; and nasal, $P = 0.003$) than that of normal subjects. In dry eyes, the LET was also significantly thinner in the inferior ($P = 0.011$), temporal ($P = 0.008$), and nasal regions ($P < 0.001$) but not in the superior region ($P = 0.152$) as compared to control subjects (Table 2, Figure 2).

Within the DED group, there were significant correlations between symptoms (OSDI) and Schirmer I test ($r = -0.312$, $P = 0.003$), TBUT ($r = -0.720$, $P < 0.001$), and Oxford score ($r = 0.340$, $P = 0.001$). TBUT was also correlated with Schirmer I test and Oxford score ($r = 0.436$, $P < 0.001$ and $r = -0.504$, $P < 0.001$, resp.). Tear film lipid layer interferometry was correlated with TBUT, Oxford score, and MCS

Table 1: Demographic and clinical test results.

Parameters	DED group	Control group	*P*value
Number of patients	54	32	
Gender			
Female	36 (66.7%)	20 (62.5%)	0.699
Male	18 (33.3%)	12 (37.5%)	
Age (years)	44.59 ± 10.08	43.34 ± 10.81	0.503
OSDI	35.46 ± 14.94	1.52 ± 3.96	<0.001
Schirmer I test (mm)	4.11 ± 6.98	12.56 ± 6.99	<0.001
TBUT (seconds)	4.67 ± 2.30	13.31 ± 2.54	<0.001
Oxford scale	1.06 ± 1.73	0.00 ± 0.00	0.001
MCS (mm)	5.74 ± 0.41	5.98 ± 0.07	0.002
TFL	2.43 ± 0.71	2.28 ± 0.52	0.323

DED: dry eye disease; OSDI: Ocular Surface Disease Index; TBUT: tear film break-up time; MCS: mean corneal sensitivity; TFL: tear film lipid layer interferometry.

Table 2: Comparison of ocular surface epithelium thickness (μm) between DED and control groups.

Parameters	DED group	Control group	*P* value
Number of patients	54	32	
CET	50.23 ± 4.42	49.76 ± 3.15	0.103
LET	81.37 ± 6.21	87.14 ± 9.98	0.009
LET (N)	80.60 ± 9.27	89.95 ± 15.23	<0.001
LET (T)	80.73 ± 8.91	87.65 ± 11.19	0.008
LET (S)	82.10 ± 8.48	84.64 ± 6.75	0.152
LET (I)	80.12 ± 7.84	86.74 ± 14.45	0.011
BET	50.44 ± 5.25	44.62 ± 5.04	<0.001
BET (N)	50.99 ± 5.26	43.45 ± 4.99	0.003
BET (T)	50.37 ± 6.14	42.57 ± 5.00	<0.001
BET (S)	50.10 ± 5.13	43.99 ± 5.54	0.005
BET (I)	51.35 ± 5.27	46.48 ± 8.83	0.014

CET: corneal epithelium thickness; LET: limbal epithelium thickness; BET: bulbar conjunctival epithelium thickness; N: nasal; T: temporal; S: superior; I: inferior.

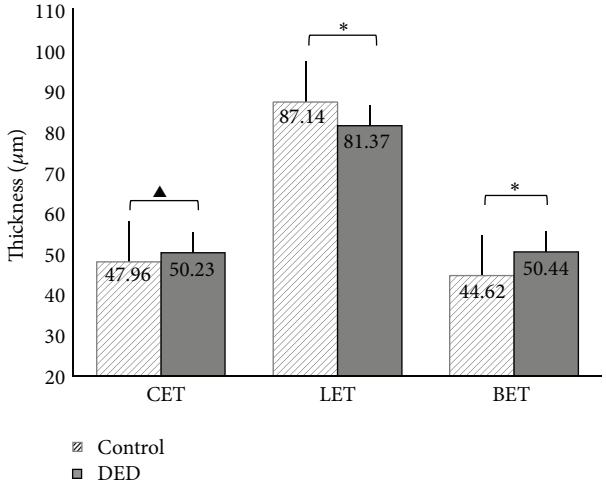

Figure 2: Comparison of CET, LET, and BET data between DED and control group. ∗ represents a significant difference between the indicated groups, $P \leq 0.05$; ▲ represents no significant difference. ANOVA with Tukey's post hoc test.

($r = -0.236$, $P = 0.029$; $r = -0.389$, $P < 0.001$; and $r = 0.259$, $P = 0.016$, resp.) (Table 3).

When evaluating the relationship between dry eye clinical tests and ocular surface epithelium thickness parameters, mean BET was correlated with OSDI ($r = 0.362$, $P < 0.001$) and TBUT ($r = -0.428$, $P < 0.001$) but not with Schirmer I test ($r = -0.165$, $P = 0.290$) and Oxford score ($r = 0.134$, $P = 0.392$). The mean LET was correlated with OSDI and TBUT ($r = -0.305$, $P = 0.047$ and $r = 0.378$, $P = 0.012$, resp.). Interestingly, the inferior quadrant LET was correlated with OSDI ($r = -0.519$, $P < 0.001$), Schirmer I test ($r = 0.271$, $P = 0.012$), TBUT ($r = 0.638$, $P < 0.001$), Oxford score ($r = -0.256$, $P = 0.017$), and MCS ($r = -0.519$, $P < 0.001$) (Table 4).

4. Discussion

Several studies have been conducted to measure the thickness and morphology of ocular surface epithelium with OCT, IVCM, or ultrasound, in order to better understand

Table 3: Statistical results of correlations between dry eye clinical tests.

Parameters	Gender	Age	OSDI	Schirmer 1 test	TBUT	Oxford scale	MCS
Age							
r	0.162						
P	0.136						
OSDI							
r	−0.048	0.071					
P	0.659	0.514					
Schirmer 1 test							
r	−0.098	−0.192	−0.312				
P	0.371	0.077	**0.003**				
TBUT							
r	−0.025	−0.201	−0.720	0.436			
P	0.817	0.063	<**0.001**	<**0.001**			
Oxford scale							
r	0.105	0.098	0.340	−0.274	−0.504		
P	0.337	0.370	**0.001**	**0.011**	<**0.001**		
MCS							
r	−0.155	−0.177	−0.137	0.111	0.211	−0.185	
P	0.155	0.103	0.209	0.309	0.054	0.089	
TFL							
r	0.044	0.053	0.163	−0.207	−0.236	−0.389	0.259
P	0.689	0.630	0.134	0.056	**0.029**	<**0.001**	**0.016**

DED: dry eye disease; OSDI: Ocular Surface Disease Index; TBUT: tear film break-up time; MCS: mean corneal sensitivity; TFL: tear film lipid layer interferometry.

epithelial alterations in DED [7–13]. With Fourier-domain OCT, Cui et al. evaluated for the first time the features of the corneal epithelial thickness map within the central 5 mm zone and the correlation with symptoms in dry eye patients [7]. Yang et al. [14] and our group [4] reported the evaluation with SD-OCT of ocular surface epithelia including the bulbar conjunctival epithelium, the limbal epithelium, and the central corneal epithelium thicknesses in normal subjects and dry eye patients. However, no studies reported the correlations between DED clinical features and ocular surface epithelial thicknesses, including the limbal and the conjunctival epithelium. In accordance with our previous results [4], we observed a thinner limbal epithelium and a thicker conjunctival epithelium in patients with dry eye. Moreover, we observed that the severities of symptoms (OSDI) and tear film alterations (TBUT) were correlated to both LET and BET.

When evaluating the CET of DED patients, some authors observed a decrease, while others found no change or even an increase as compared with the control group [4, 7, 8, 15]. Comparison between studies was made difficult by the different durations and severities of the disease, the varying ages of DED patients, and the different techniques used to measure CET. Fabiani et al. [15] established a mouse model of dry eye and detected that the average CET became significantly thicker in dry eye mice as compared to the controls after 7 days. These results demonstrated that the inflammatory processes and epithelial proliferation had a significant impact on the average CET in the early stage of DED. The studies from Chen et al. [16] and Kanellopoulos and Asimellis [17] indicated that increased epithelial thickness might be used as an objective clinical indicator of dry eye. Conversely, Cui et al. [7] found that the superior corneal epithelium was thinner in DED patients than in normal subjects. Erdélyi et al. [18] and Villani et al. [19] also showed that the CET tends to be thinner in DED patients, which was attributed to the destruction of stem cells at the limbus. In the present study, there was no significant difference in CET between DED patients and the control group, consistent with our previous results [4] and the results from Tuominen et al. [20]. This may be explained by the moderate severity of DED (average OSDI 35.46 and TBUT 4.67 s) and the location of CET evaluation in the central cornea (central 2 mm diameter area), away from the limbus.

Considering the role of limbal epithelial stem cells (LESCs) in corneal epithelium homeostasis, the limbal region is essential in dry eye physiopathology [21]. Several factors might explain the reduced thickness of the limbal epithelium in DED. First, stem cell metabolism can be directly affected in DED patients [22–24]. Infiltration of $CD4^+$ T cells at the limbus and the levels of inflammatory cytokines in tears may play an important role in inhibiting corneoscleral stem cell metabolism in dry eye patients. This downregulation of limbal stem cells in DED patients could influence the development of corneal limbal epithelial layers and result in a thinner LET. Increased turnover of corneal epithelial cells might also explain limbal epithelial cell depletion in DED [4]. Limbal microenvironment inflammation could also

Table 4: Correlations of ocular surface epithelial thickness with the result of clinical tests in the DED group.

Parameters	Gender	Age	OSDI	Schirmer I test	TBUT	Oxford scale	MCS	TFL
CET								
r	0.079	0.036	0.047	−0.109	−0.087	−0.104	−0.034	0.003
P	0.468	0.743	0.668	0.318	0.424	0.342	0.755	0.975
LET								
r	−0.178	−0.105	−0.305	0.263	0.378	−0.154	0.113	−0.081
P	0.252	0.504	**0.047**	0.089	**0.012**	0.325	0.469	0.607
LET (nasal)								
r	−0.043	−0.137	−0.322	0.209	0.311	−0.114	0.112	0.000
P	0.694	0.182	**0.022**	0.054	**0.004**	0.295	0.304	0.999
LET (temporal)								
r	−0.150	0.162	−0.169	0.059	0.280	0.062	0.003	−0.004
P	0.167	0.135	0.119	0.592	**0.009**	0.573	0.976	0.968
LET (superior)								
r	−0.001	−0.103	0.009	0.198	0.101	0.105	0.054	−0.043
P	0.995	0.343	0.933	0.067	0.354	0.335	0.623	0.694
LET (inferior)								
r	0.054	0.006	−0.519	0.271	0.638	−0.256	0.273	−0.066
P	0.429	0.953	<**0.001**	**0.012**	<**0.001**	**0.017**	**0.011**	0.548
BET								
r	0.157	0.085	0.362	−0.165	−0.428	0.134	−0.178	−0.105
P	0.314	0.588	<**0.001**	0.290	<**0.001**	0.392	0.252	0.504
BET (nasal)								
r	0.041	0.053	0.452	−0.116	−0.500	0.130	−0.105	−0.026
P	0.705	0.627	<**0.001**	0.254	<**0.001**	0.233	0.334	0.815
BET (temporal)								
r	0.023	0.295	0.497	−0.153	−0.479	0.132	−0.152	0.069
P	0.833	**0.006**	<**0.001**	0.326	<**0.001**	0.225	0.319	0.529
BET (superior)								
r	0.097	0.060	0.384	−0.075	−0.410	0.118	−0.286	−0.010
P	0.372	0.581	<**0.001**	0.493	<**0.001**	0.280	0.063	0.930
BET (inferior)								
r	0.191	−0.027	0.281	−0.049	−0.288	0.092	−0.184	0.097
P	0.078	0.807	**0.009**	0.651	**0.007**	0.401	0.089	0.376

DED: dry eye disease; OSDI: Ocular Surface Disease Index; TBUT: tear film break-up time; MCS: mean corneal sensitivity; TFL: tear film lipid layer interferometry; CET: corneal epithelium thickness; LET: limbal epithelium thickness; BET: bulbar conjunctival epithelium thickness.

directly alter limbal stem cells and their functions, resulting in various degrees of stem cell deficiency [25]. The inferior and superior limbal areas are thought to be the largest reservoirs of limbal stem cells as compared to the nasal and temporal quadrants. With confocal microscopy and scanning electron microscopy, Shortt et al. [26] showed more limbal crypts in the superior and inferior limbal regions. Similarly, Thoft et al. found a larger number of stem cells in the superior and inferior limbus than in the medial and lateral areas [27]. Interestingly, in the present study, the inferior LET seemed to be the most sensitive parameter because it was directly correlated to the OSDI, the Schirmer test, TBUT, the Oxford score, and mean corneal sensitivity. The greatest changes observed for the inferior LET could be explained by the prolonged contact between epithelial cells and altered tears within the inferior lacrimal river containing inflammatory factors such as cellular debris or proinflammatory cytokines. Decreased corneal sensitivity correlated to the inferior LET was also observed in DED patients. Corneal nerves are implicated in DED pathophysiology and DED patients exhibit nerves alterations [5]. These nerves changes have been correlated to the severity of the ocular surface lesions and might be in part responsible for corneal sensitivity alterations. As observed with corneal nerves, a thinner inferior LET might represent a marker of DED severity and emphasized the role of LESCs in ocular surface diseases.

The bulbar conjunctiva is an essential tissue of the ocular surface with numerous ocular surface cell populations including inflammatory cells and goblet cells [28, 29]. In this study, the mean BET in dry eye patients was significantly increased as compared to normal eyes. Moreover, the thickness of the conjunctival epithelium layers was directly

correlated to symptoms (OSDI) and tear film alterations (TBUT). The infiltration of inflammatory cells and tissue edema observed within the conjunctiva in DED patients might explain, at least in part, the thickening of the conjunctival epithelium [30].

Although the changes in ocular surface epithelium thickness evaluated with SD-OCT are not specific of a particular etiology of DED and may also be observed in other ocular surface diseases, this parameter is providing useful information for the evaluation of ocular surface tissue changes. Given that it is already used for the evaluation of keratoconus, ocular surface epithelial mapping, especially corneal limbus epithelial mapping, might be used in association with other clinical parameters to monitor DED ocular surface changes and the benefit of different treatments in the future.

Conflict of Interests

No conflicting relationship exists for any author.

Acknowledgment

This study is supported by the Central Health Research Project Fund (W2013BJ47), China.

References

[1] "The definition and classification of dry eye disease: report of the definition and classification subcommittee of the international Dry Eye WorkShop (2007)," *Ocular Surface*, vol. 5, no. 2, pp. 75–92, 2007.

[2] M. E. Stern, R. W. Beuerman, R. I. Fox, J. Gao, A. K. Mircheff, and S. C. Pflugfelder, "The pathology of dry eye: the interaction between the ocular surface and lacrimal glands," *Cornea*, vol. 17, no. 6, pp. 584–589, 1998.

[3] Y. Wei and P. A. Asbell, "The core mechanism of dry eye disease is inflammation," *Eye and Contact Lens*, vol. 40, no. 4, pp. 248–256, 2014.

[4] M. Francoz, I. Karamoko, C. Baudouin, and A. Labbé, "Ocular surface epithelial thickness evaluation with spectral-domain optical coherence tomography," *Investigative Ophthalmology & Visual Science*, vol. 52, no. 12, pp. 9116–9123, 2011.

[5] A. Labbé, Q. Liang, Z. Wang et al., "Corneal nerve structure and function in patients with non-sjögren dry eye: clinical correlations," *Investigative Ophthalmology and Visual Science*, vol. 54, no. 8, pp. 5144–5150, 2013.

[6] A. Yagci and C. Gurdal, "The role and treatment of inflammation in dry eye disease," *International Ophthalmology*, vol. 34, no. 6, pp. 1291–1301, 2014.

[7] X. Cui, J. Hong, F. Wang et al., "Assessment of corneal epithelial thickness in dry eye patients," *Optometry & Vision Science*, vol. 91, no. 12, pp. 1446–1454, 2014.

[8] D. Z. Reinstein, T. E. Yap, T. J. Archer, M. Gobbe, and R. H. Silverman, "Comparison of corneal epithelial thickness measurement between fourier-domain OCT and very high-frequency digital ultrasound," *Journal of Refractive Surgery*, vol. 31, no. 7, pp. 438–445, 2015.

[9] K.-S. Na, J.-W. Mok, J. Y. Kim, C. R. Rho, and C.-K. Joo, "Correlations between tear cytokines, chemokines, and soluble receptors and clinical severity of dry eye disease," *Investigative Ophthalmology & Visual Science*, vol. 53, no. 9, pp. 5443–5450, 2012.

[10] A. Alhatem, B. Cavalcanti, and P. Hamrah, "In vivo confocal microscopy in dry eye disease and related conditions," *Seminars in Ophthalmology*, vol. 27, no. 5-6, pp. 138–148, 2012.

[11] J. A. Hallak, S. Jassim, V. Khanolkar, and S. Jain, "Symptom burden of patients with dry eye disease: a four domain analysis," *PLoS ONE*, vol. 8, no. 12, Article ID e82805, 2013.

[12] G. Cardona, C. García, C. Serés, M. Vilaseca, and J. Gispets, "Blink rate, blink amplitude, and tear film integrity during dynamic visual display terminal tasks," *Current Eye Research*, vol. 36, no. 3, pp. 190–197, 2011.

[13] K. S. Na, K. Han, Y. G. Park, C. Na, and C. K. Joo, "Depression, stress, quality of life, and dry eye disease in Korean women: a population-based study," *Cornea*, vol. 34, no. 7, pp. 733–738, 2015.

[14] Y. Yang, J. Hong, S. X. Deng, and J. Xu, "Age-related changes in human corneal epithelial thickness measured with anterior segment optical coherence tomography," *Investigative Ophthalmology and Visual Science*, vol. 55, no. 8, pp. 5032–5038, 2014.

[15] C. Fabiani, S. Barabino, S. Rashid, and M. R. Dana, "Corneal epithelial proliferation and thickness in a mouse model of dry eye," *Experimental Eye Research*, vol. 89, no. 2, pp. 166–171, 2009.

[16] W. Chen, Z. Li, J. Hu et al., "Corneal alternations induced by topical application of benzalkonium chloride in rabbit," *PLoS ONE*, vol. 6, no. 10, Article ID e26103, 2011.

[17] A. J. Kanellopoulos and G. Asimellis, "In vivo 3-dimensional corneal epithelial thickness mapping as an indicator of dry eye: preliminary clinical assessment," *American Journal of Ophthalmology*, vol. 157, no. 1, pp. 63.e2–68.e2, 2014.

[18] B. Erdélyi, R. Kraak, A. Zhivov, R. Guthoff, and J. Németh, "In vivo confocal laser scanning microscopy of the cornea in dry eye," *Graefe's Archive for Clinical and Experimental Ophthalmology*, vol. 245, no. 1, pp. 39–44, 2007.

[19] E. Villani, D. Galimberti, F. Viola, C. Mapelli, and R. Ratiglia, "The cornea in Sjögren's syndrome: an in vivo confocal study," *Investigative Ophthalmology and Visual Science*, vol. 48, no. 5, pp. 2017–2022, 2007.

[20] I. S. J. Tuominen, Y. T. Konttinen, M. H. Vesaluoma, J. A. O. Moilanen, M. Helintö, and T. M. T. Tervo, "Corneal innervation and morphology in primary Sjögren's syndrome," *Investigative Ophthalmology and Visual Science*, vol. 44, no. 6, pp. 2545–2549, 2003.

[21] M. Dogru and K. Tsubota, "New insights into the diagnosis and treatment of dry eye," *Ocular Surface*, vol. 2, no. 2, pp. 59–75, 2004.

[22] L. S. Vera, J. Gueudry, A. Delcampe, J.-C. Roujeau, G. Brasseur, and M. Muraine, "In vivo confocal microscopic evaluation of corneal changes in chronic Stevens-Johnson syndrome and toxic epidermal necrolysis," *Cornea*, vol. 28, no. 4, pp. 401–407, 2009.

[23] B. Steger, L. Speicher, W. Philipp, and N. E. Bechrakis, "In vivo confocal microscopic characterisation of the cornea in chronic graft-versus-host disease related severe dry eye disease," *British Journal of Ophthalmology*, vol. 99, no. 2, pp. 160–165, 2015.

[24] M. J. Lee, A. Y. Ko, J. H. Ko et al., "Mesenchymal stem/stromal cells protect the ocular surface by suppressing inflammation in an experimental dry eye," *Molecular Therapy*, vol. 23, no. 1, pp. 139–146, 2015.

[25] C. Baudouin, "A new approach for better comprehension of diseases of the ocular surface," *Journal Français d'Ophtalmologie*, vol. 30, pp. 239–246, 2007.

[26] A. J. Shortt, S. J. Tuft, and J. T. Daniels, "Corneal stem cells in the eye clinic," *British Medical Bulletin*, vol. 100, no. 1, pp. 209–225, 2011.

[27] R. A. Thoft, L. A. Wiley, and N. Sundarraj, "The multipotential cells of the limbus," *Eye*, vol. 3, no. 2, pp. 109–113, 1989.

[28] J. T. Henriksson, C. S. De Paiva, W. Farley, S. C. Pflugfelder, A. R. Burns, and J. P. G. Bergmanson, "Morphologic alterations of the palpebral conjunctival epithelium in a dry eye model," *Cornea*, vol. 32, no. 4, pp. 483–490, 2013.

[29] P. Argüeso, M. Balaram, S. Spurr-Michaud, H. T. Keutmann, M. R. Dana, and I. K. Gipson, "Decreased levels of the goblet cell mucin MUC5AC in tears of patients with Sjögren syndrome," *Investigative Ophthalmology & Visual Science*, vol. 43, no. 4, pp. 1004–1011, 2002.

[30] P. Chhadva, A. Alexander, A. L. McClellan et al., "The impact of conjunctivochalasis on dry eye symptoms and signs," *Investigative Ophthalmology & Visual Science*, vol. 56, no. 5, pp. 2867–2871, 2015.

Hindawi Publishing Corporation
Journal of Ophthalmology
Volume 2015, Article ID 981274, 6 pages
http://dx.doi.org/10.1155/2015/981274

Clinical Study

An Evaluation of Effects of Different Mydriatics on Choroidal Thickness by Examining Anterior Chamber Parameters: The Scheimpflug Imaging and Enhanced Depth Imaging-OCT Study

İsa Yuvacı,[1] Emine Pangal,[1] Sümeyra Yuvacı,[1] Nurettin Bayram,[1] Mustafa Ataş,[1] Burhan Başkan,[1] Süleyman Demircan,[1] and Ali Akal[2]

[1]*Department of Ophthalmology, Kayseri Training and Research Hospital, 38000 Kayseri, Turkey*
[2]*Department of Ophthalmology, School of Medicine, Harran University, 63300 Sanliurfa, Turkey*

Correspondence should be addressed to İsa Yuvacı; mdisay@hotmail.com

Received 11 April 2015; Accepted 19 May 2015

Academic Editor: Lisa Toto

Copyright © 2015 İsa Yuvacı et al. This is an open access article distributed under the Creative Commons Attribution License, which permits unrestricted use, distribution, and reproduction in any medium, provided the original work is properly cited.

Aim. To assess the effects of mydriatics commonly used in clinical practice on choroidal thickness and anterior chamber change. *Methods*. This was a prospective, randomized, controlled, double-blinded study including a single eye of the participants. The subjects were assigned into 4 groups to receive tropicamide 1%, phenylephrine 2.5%, cyclopentolate 1%, and artificial tears. At the baseline, anterior chamber parameters were assessed using a Pentacam Scheimpflug camera system, and choroidal thickness (CT) was measured using a spectral-domain OCT with Enhanced Depth Imaging (EDI) modality. All measurements were repeated again after drug administration. *Results*. Increases in pupil diameter, volume, and depth of anterior chamber were found to be significant ($p = 0.000$, $p = 0.000$, and $p = 0.000$, resp.), while decreases in the choroidal thickness were found to be significant in subjects receiving mydriatics ($p < 0.05$). *Conclusions*. The study has shown that while cyclopentolate, tropicamide, and phenylephrine cause a decrease in choroidal thickness, they also lead to an increase in the volume and depth of anterior chamber. However, no correlation was detected between anterior chamber parameters and choroidal changes after drug administration. These findings suggest that the mydriatics may affect the choroidal thickness regardless of anterior chamber parameters. This study was registered with trial registration number 2014/357.

1. Introduction

Mydriatics have a broad range of applications in ocular examination and treatment to allow for pupil dilatation and/or cycloplegia. In clinical practice, these agents are used to achieve cycloplegia before refraction examination; to achieve pupil dilatation before fundus examination, surgery, and angiography; or to prevent synechia in the management of uveitis. After administration, many changes occur in the iris root, anterior chamber angle, anterior chamber depth, iris thickness, and iris volume as well as pupil dilatation [1–3].

The choroidea is a vascular layer localized in the outer sclera and inner retinal layers. It has many major functions, including oxygenation of inner nuclear layers and retinal pigment epithelium [4]. Greater understanding of the choroidal structure may contribute to the diagnosis and management of several eye disorders. Enhanced Deep Imaging-Optical Coherence Tomography (EDI-OCT) allows a detailed evaluation of choroidea and theoretically contributes to better understanding of a wide range of disorders. In several studies using EDI-OCT, it has been shown that choroidal thickness is affected by many diseases such as age related macular degeneration [5], degenerative myopia [6], and central serous retinopathy [7] and several conditions such as smoking [8], caffeine intake [9], and time of day [10]. There are studies evaluating anterior chamber changes, visual field, and the retinal nerve fiber layer [11, 12].

It is possible that the choroidea, a part of uvea like iris, may display certain changes after mydriatic use. There have been a limited number of studies measuring choroidal

thickness after mydriatic use. In these studies, conflicting results were reported after measurements with sufficient dilatation in healthy individuals, suggesting no change [13, 14] or thinning [15] in choroidea by mydriatics. In our study, we have tested the hypothesis that choroidal changes will occur with the administration of 3 commonly used mydriatics and investigated whether these potential changes may be assessed through evaluation of anterior chamber changes.

2. Methods

Subjects: this was designed as a randomized, placebo-controlled, double-blinded study including a single eye of participants. The study followed the tenets of the Declaration of Helsinki and was approved by the Local Ethics Committee of Erciyes University (2014/357). All individuals received both oral information and written information about the study, and each was provided with written and informed consent before participation to the study.

All individuals underwent a screening process involving a complete ophthalmologic examination, including visual acuity and refraction, slit-lamp biomicroscopy, fundus examination, and intraocular pressures measured using noncontact tonometry. Axial length was measured using an IOL Master (Carl Zeiss Meditec, Dublin, CA). Anterior chamber parameters were measured using a Pentacam rotating Scheimpflug camera (Oculus, Wetzlar, Germany). The retina nerve fiber layer and choroidal thickness measurements were obtained through the Spectralis OCT (Heidelberg Engineering, Heidelberg, Germany).

All individuals required a best corrected visual acuity of 20/25 or better, with refractive error <5 diopters, 3 diopters of cylinder, and absence of glaucomatous optic disc changes. Exclusion criteria included any retinal diseases, history of ocular injury or surgery, any reasons for poor image quality of OCT such as unstable fixation or severe cataract, and age younger than 18 years.

Two hundred and forty eyes of 120 individuals satisfying the inclusion criteria were enrolled in the study between May 2014 and September 2014. Both eyes were enrolled, and one eye of each individual was randomly selected. A double-blinded protocol was used, and those who evaluated the EDI-OCT did not know which drug was administered to each patient.

All individuals were randomly assigned into 4 groups based on the application of drops. Subjects who received a drop of tropicamide 1% 3 times at 5 min intervals were referred to as the tropicamide group, while subjects who received a drop of 2.5% phenylephrine 3 times at 5 min intervals were the phenylephrine group. Subjects who received a drop of cyclopentolate 1% 3 times at 5 min intervals were defined as the cyclopentolate group, and subjects who received a drop of artificial tears 3 times at 5 min intervals were defined as the control group.

Procedure of image acquisition: the procedure of obtaining EDI-OCT has been previously described [16]. The subfoveal, temporal, and nasal fovea choroidal thicknesses (CTs) were measured by using spectral-domain OCT (Spectralis, wavelength: 870 nm) with EDI modality. Subfoveal, temporal, and nasal fovea CTs were defined as the vertical distance from the hyperreflective line of Bruch's membrane to the hyperreflective line of the inner surface of the sclera. All subjects were imaged by the same experienced retina specialist (İsa Yuvacı). Two independent clinicians (Emine Pangal and Nurettin Bayram) measured CT, and the average of these measurements was used in the analysis. These clinicians did not know about the other's measurements and were also not aware of the group divisions. EDI-OCT images of each subject were obtained before the administration of drops and 50 min after instillation. All scans were performed around the same time of the day, between 11:00 and 12:00, to minimize the possibility of CT changes attributable to diurnal CT fluctuations [17].

Ocular biometrics before and after application of drops in each subject were also assessed with the IOL Master. The measures of axial length (AXL), lens thickness, and anterior chamber depth (ACD) along the visual axis were obtained through a single measurement procedure.

For each subject, corneal thickness, anterior chamber depth (ACD), corneal volume, anterior chamber angle (ACA), corneal curvature, and anterior chamber volume (ACV) were obtained through Pentacam before and after instillation of drops.

Statistical analysis: all data analyses were performed by using the Statistical Package for the Social Sciences (SPSS) for Windows version 22.0 (SPSS Inc., Chicago, IL, USA). The Pearson chi-square test was used to assess qualitative variables. Continuous variables were presented as mean ± standard deviation. Correlation coefficient (CC) was calculated for each of the ocular parameters. The measurement reliability of CC was considered "excellent" if the values of CC > 0.75, "good" if the values of CC > 0.4, and "poor" if the values of CC < 0.4.

For each continuous variable, normality was checked by Kolmogorov-Smirnov test, and it did not depart significantly from a normally distributed sample ($p > 0.05$). Homogeneity of variances was tested by using Levene's test. For parametric statistics, data with normal distribution were analyzed using one-way ANOVA test to compare the groups. When a significant result was obtained, the Tukey test was used for post hoc comparisons. Repeated measurements of anterior chamber parameters, choroidal thickness, and intraocular pressure of the groups were compared by a Paired t-test. For nonparametric statistics, data with skewed distribution were analyzed by using Kruskal-Wallis test. When a significant result was obtained, Mann-Whitney U test with Bonferroni's correction was used for post hoc comparisons. A p value < 0.05 was considered statistically significant.

3. Results

Overall, 120 patients (59 males and 61 females) were included in the study. The mean age was 30.9 ± 9.7 years (age range: 18–56 years). All patients were randomly divided into 4 groups. Groups were comprised of the tropicamide group ($n = 29$; 24%), the phenylephrine group ($n = 29$; 24%),

Table 1: A summary of demographics and ocular parameters in all groups.

	Tropicamide ($n = 29$)	Phenylephrine ($n = 29$)	Cyclopentolate ($n = 32$)	Control ($n = 30$)	p value
Age (year)	32.9 ± 1.4	31.8 ± 1.5	28.9 ± 1.6	30.1 ± 1.4	0.382[a]
Gender (male : female)	17 : 12	16 : 13	14 : 18	12 : 18	0.561[b]
BCVA (Snellen)	1.05 ± 0.12	1.05 ± 0.15	1.04 ± 0.15	1.09 ± 0.15	0.628[a]
SEQ of manifest refraction (diopters)	−0.55 ± 1.49	−0.73 ± 1.60	0.01 ± 2.24	−1.0 ± 1.20	0.117[a]
AXL (mm)	23.4 ± 0.63	23.7 ± 0.81	23.3 ± 0.88	23.5 ± 0.86	0.425[a]

BCVA: Best Corrected Visual Acuity; SEQ: mean spheric equivalent, AXL: mean axial length.
Variables are expressed as mean ± standard deviation; Level of significance $p < 0.05$.
[a]One-way ANOVA test; [b]Pearson chi-squared test.

the cyclopentolate group ($n = 32$; 27%), and the control group ($n = 30$; 25%). The mean spheric equivalent was measured as −0.55 ± 1.49 diopters in the tropicamide group, −0.73 ± 1.60 diopters in the phenylephrine group, 0.01 ± 2.24 diopters in the cyclopentolate group, and −1.0 ± 1.20 diopters in the control group. There were no significant differences in the demographic characteristics and ocular parameters between those who received mydriatics and those who were in the control group. Demographics and ocular parameters in all groups were summarized in Table 1. Pupil diameter increased from 3.08 ± 0.53 mm at baseline to 6.47 ± 0.69 mm after drug administration in the tropicamide group, from 3.02 ± 0.50 mm to 5.80 ± 0.89 mm in the phenylephrine group, from 3.36 ± 0.72 mm to 6.79 ± 0.74 mm in the cyclopentolate group, and from 3.19 ± 0.52 mm to 3.20 ± 0.51 mm in the control group, respectively. Pupil diameter increased significantly in the subjects who received mydriatics ($p = 0.000$), but the extent of pupil diameter was found to be higher in the tropicamide and the cyclopentolate groups than in the phenylephrine group. The anterior chamber depth increased from 2.88 ± 0.33 mm at baseline to 2.96 ± 0.34 mm after drug administration in the tropicamide group, from 3.03 ± 0.32 mm to 3.11 ± 0.34 mm in the phenylephrine group, from 3.09 ± 0.33 mm to 3.22 ± 0.31 in the cyclopentolate group, and from 3.11 ± 0.34 mm to 3.14 ± 0.38 mm in the control group, respectively.

These results demonstrate that the anterior chamber depth increased significantly in the subjects who received mydriatics when compared to the control group ($p = 0.000$). When it comes to the anterior chamber volume, the study found that it increased from 154.76 ± 34.99 mm^3 at baseline to 171.90 ± 31.52 mm^3 after drug administration in the tropicamide group, from 178.28 ± 39.43 mm^3 to 193.97 ± 34.69 mm^3 in the phenylephrine group, from 187.93 ± 35.38 mm^3 to 203.84 ± 30.06 mm^3 in the cyclopentolate group, and from 184.66 ± 38.97 mm^3 to 185.10 ± 38.94 mm^3 in the control group, respectively. These results also show that the anterior chamber volume increased significantly in the subjects who received mydriatics when compared to the control group ($p = 0.000$).

The central EDI-OCT measurements before and after drug administration were 328.65 ± 87.88 μ and 302.10 ± 74.29 in the tropicamide group, 341.83 ± 73.36 μ and 316.11 ± 68.70 μ in the phenylephrine group, 312.28 ± 84.94 μ and 292.81 ± 88.69 μ in the cyclopentolate group, and 326.53 ± 67.20 μ and 316.57 ± 75.51 μ in the control group, respectively. These findings indicate that the central EDI-OCT measurements decreased significantly in the subjects who received mydriatics when compared to the control group ($p = 0.000$), but no significant difference was detected among the tropicamide, phenylephrine, and cyclopentolate groups in terms of choroidal thinning. Moreover, no significant difference was also detected in the central choroidal thickness before and after drug administration in the control group ($p = 0.172$).

The temporal EDI-OCT measurements before and after drug administration were 308.90 ± 79.36 μ and 291.48 ± 72.80 in the tropicamide group, 324.34 ± 79.36 μ and 305.58 ± 66.94 μ in the phenylephrine group, 291.41 ± 85.32 μ and 280.12 ± 84.30 μ in the cyclopentolate group, and 297.47 ± 68.72 μ and 305.47 ± 67.87 μ in the control group, respectively. Thus, the temporal EDI-OCT measurements saw a significant decrease in the participants who received mydriatics when compared to the participants in the control group ($p = 0.000$). On the other hand, no significant difference was detected in the central choroidal thickness in the control group ($p = 0.072$). The nasal EDI-OCT measurements before and after drug administration were 302.10 ± 84.48 μ and 286.03 ± 74.78 in the tropicamide group, 313.45 ± 66.98 μ and 296.86 ± 64.30 μ in the phenylephrine group, 290.34 ± 85.89 μ and 276.87 ± 86.52 μ in the cyclopentolate group, and 305.53 ± 81.13 μ and 300.77 ± 75.79 μ in the control group, respectively. The nasal EDI-OCT measurements significantly decreased in the subjects receiving mydriatics when compared to the control group ($p = 0.000$). No significant differences were detected in the central choroidal thickness in the control group ($p = 0.232$). Changes in the anterior chamber parameters, choroidal thickness, and intraocular pressure before and after drug administration in all groups are summarized in Table 2.

No statistical difference in the choroidal thickness was observed for subjects with an increase in anterior chamber depth and subjects with changes in anterior chamber depth were compared ($r = -0.136$, $p = 0.200$). The same was also true for anterior chamber volume ($r = 0.071$, $p = 0.505$).

In general, the mean for the pupil diameter increased from 3.17 ± 0.85 mm at baseline to 5.57 ± 1.59 mm after drug

Table 2: Changes of anterior chamber parameters, choroidal thickness, and intraocular pressure before and after drug administration.

Dilated eye	Tropicamide ($n = 29$)	Phenylephrine ($n = 29$)	Cyclopentolate ($n = 32$)	Control ($n = 30$)
PD (mm)				
Before	3.08 ± 0.53	3.02 ± 0.50	3.36 ± 0.72	3.19 ± 0.52
After	6.47 ± 0.69	5.80 ± 0.89	6.79 ± 0.74	3.20 ± 0.51
Difference	−3.39 ± 0.55	−2.78 ± 0.90	−3.42 ± 0.68	−0.01 ± 0.01
Pa value	0.000	0.000	0.000	0.054
ACD (mm)				
Before	2.88 ± 0.33	3.03 ± 0.32	3.09 ± 0.33	3.11 ± 0.34
After	2.96 ± 0.34	3.11 ± 0.34	3.22 ± 0.31	3.14 ± 0.38
Difference	−0.80 ± 0.05	−0.80 ± 0.08	−0.13 ± 0.09	−0.03 ± 0.17
Pa value	0.000	0.000	0.000	0.290
ACV (mm^3)				
Before	154.76 ± 34.99	178.28 ± 39.43	187.93 ± 35.38	184.66 ± 38.97
After	171.90 ± 31.52	193.97 ± 34.69	203.84 ± 30.06	185.10 ± 38.94
Difference	−17.14 ± 11.53	−15.69 ± 12.17	−15.91 ± 13.44	−0.44 ± 1.16
Pa value	0.000	0.000	0.000	0.051
CEDİ (μ)				
Before	328.65 ± 87.88	341.83 ± 73.36	312.28 ± 84.94	326.53 ± 67.20
After	302.10 ± 74.29	316.11 ± 68.70	292.81 ± 88.69	316.57 ± 75.51
Difference	26.55 ± 33.85	25.72 ± 32.66	19.47 ± 19.41	9.97 ± 38.98
Pa value	0.000	0.000	0.000	0.172
TEDİ (μ)				
Before	308.90 ± 79.36	324.34 ± 79.36	291.41 ± 85.32	297.47 ± 68.72
After	291.48 ± 72.80	305.58 ± 66.94	280.12 ± 84.30	305.47 ± 67.87
Difference	17.42 ± 42.70	18.76 ± 38.87	11.29 ± 16.40	−8.00 ± 39.15
Pa value	0.037	0.015	0.000	0.272
NEDİ (μ)				
Before	302.10 ± 84.48	313.45 ± 66.98	290.34 ± 85.89	305.53 ± 81.13
After	286.03 ± 74.78	296.86 ± 64.30	276.87 ± 86.52	300.77 ± 75.79
Difference	16.07 ± 40.51	16.59 ± 34.03	13.47 ± 18.06	4.76 ± 21.36
Pa value	0.042	0.014	0.000	0.232
IOP (mmHg)				
Before	14.90 ± 2.94	14.48 ± 2.94	14.97 ± 2.72	14.27 ± 1.53
After	14.34 ± 2.11	14.52 ± 2.10	14.66 ± 2.51	14.10 ± 1.86
Difference	0.55 ± 3.01	−0.40 ± 1.92	0.31 ± 1.59	0.17 ± 1.91
Pa value	0.332	0.924	0.276	0.637

PD: pupil diameter, ACD: anterior chamber depth, ACV: anterior chamber volume, CEDİ: central, subfoveal, choroidal thickness, TEDİ, temporal choroidal thickness, and NEDİ: nasal choroidal thickness.
Variables are expressed as mean ± standard deviation. Level of significance $p < 0.05$, a Paired t-test.

administration, while the means for the central, subfoveal, and choroidal thicknesses decreased from 326.94 ± 78.59 μ at baseline to 308.29 ± 75.55 μ. Overall, no statistically significant change was detected between the decrease in the choroidal thickness and the extent of increase in the pupil diameter (PD) ($p = 0.086$). No significant difference was found between the subjects with PD > 6.0 mm and with PD < 6.0 mm in the groups receiving tropicamide 1% and phenylephrine 2.5%, but the extent of the choroidal thinning was found to be higher in the subjects with PD > 6.0 mm in the cyclopentolate group. Overall, no significant correlations were detected between the central choroidal thickness and pupil diameter ($r = 0.033$, $p = 0.754$).

4. Discussion

Mydriatics induce pupil dilatation or cycloplegia through several mechanisms, including sympathomimetic and anti-muscarinic activities. In Turkey, there are three commercially

available mydriatic preparations in common use. Of these, cyclopentolate 1% and tropicamide 1% have antimuscarinic (parasympatholytic) effects. The major difference between these antimuscarinic drugs is the duration of action. Phenylephrine 2.5% is an α-agonist with sympathomimetic effects. Generally, sympathomimetic agents have shorter onset and duration of action than antimuscarinic agents. There may be changes in several parameters, such as the iris configuration and angle, the volume and the depth of anterior chamber during pupil dilatation, and cycloplegia induced by mydriatics [1–3]. Length of these changes can cause some mechanical effects on a fixed eye. In addition, the contraction of nonvascular smooth muscle cells innervated by sympathetic and parasympathetic stimuli in choroidea can lead to fluid efflux from choroidea and choroidal thinning by constriction [18–20]. Parasympathetic effects occur in the perivascular plexus, which affects choroidal blood flow and acts as vasodilator [21]. Both drug classes act to increase sympathetic effect. These potential mechanisms suggest that the effects induced by mydriatic agent include choroidal thinning. Theoretically, the mechanical effects of anterior chamber changes induced by drug use, the effect of drugs on choroidea, or both can cause choroidal changes. In the present study, we evaluated pre- and posttreatment choroidal and anterior chamber changes and relationships among these parameters, in order to investigate the effects of mydriatic agents.

In our study, it was found that all mydriatic agents led to significant choroidal thinning. No correlation was demonstrated between choroidal changes and pupil diameter or volume and depth of anterior chamber. In the cyclopentolate group, it was found that the extent of thinning was significantly higher in the subjects with PD > 6,0 mm than those with PD < 6.0 mm. However, no such differences were observed in the tropicamide and phenylephrine groups.

Similarly, Kara et al. [15] found choroidal thinning after administration of 2 different mydriatic agents in their study that measured choroidal thickness. In that study [15], dilatation was performed in one eye, while no drug was administered to the other eye. The authors emphasized that both agents induced choroidal thinning without statistically significant difference between the agents. In that study [15], measurements were performed 60 minutes after drug administration, while choroidal and anterior chamber measurements were repeated 50 minutes after drug administration. However, in our study, we used an additional mydriatic agent, namely, cyclopentolate 1%. Again, the subjects with PD < 6.0 were also included in our study. As a result, choroidal thinning was observed in both drug classes after administration.

Contrary to our results, it was shown that there was no change in choroidal thickness in 2 studies using mydriatic agents [13, 14]. In their study in which choroidal thicknesses were assessed in several quadrants of the central choroidal region before and after Mydrin P (phenylephrine plus tropicamide), Kim et al. [14] reported no significant difference between the results. In their study using tropicamide 1% in healthy and glaucomatous subjects, Mwanza et al. [13] reported that there was no significant difference between the results. In our study, a significant choroidal thickness was detected after drug use. Not only regional differences but also differences in time to measurement after drug administration and active substances used may be a factor of variation for study results. All subjects meeting the eligibility criteria after drug administration were included in our study. Although mydriatics exert similar effects in different individuals, not all individuals have equivalent susceptibility to mydriatics. For example, variation in the extent of increases in pupil diameter comprises a good sample, which is commonly observed in clinical studies. In a study by Kim et al. [14], both parasympatholytic and sympathomimetic effects of drug used in the study may have caused variation in mechanisms acting on choroidea. Manual measurements may have also contributed to these results, which may be completely incidental.

Sander et al. [22] state that according to results of their study in which they examine the anterior chamber and choroidal changes after a single drop mydriatic application there exists no significant statistical difference between pre- and postdrug anterior chamber parameters and choroidal thickness values for placebo and phenylephrine groups. On the contrary, in our study, we observed statistically significant changes in phenylephrine groups, anterior chamber parameters, and choroidal thickness values after mydriatic use. Both individual and/or regional differences and the extent of the penetration of drug into intraocular structures of eyes might be the effective factors for the existence of such different results. This is because, in this study [22], drug application was made as a single drop. Further, the results are not different compared to ones of placebo group. In our study, at least three doses of drug are applied and the measurement is made after 50 minutes. Unlike our study and a few studies dealing with the same issue, in the same study of Sander et al. [22], choroidal thickness is observed for the group where 2% homatropine is used. The author of [22] noted that this observation could be explained by the change in the parasympathetic effect, more dominant in the posterior, owing to drug. Except this [22], there are no studies known about homatropine; however this drug's mechanism of action resembles tropicamide and the effects of both drugs on the anterior chamber are close to each other [3]. Besides different drug usage and individual and/or regional differences, the variation with regard to effective concentration of drug in eyes, aforementioned above, might be explanatory factors for different results.

In conclusion results have failed to demonstrate a correlation between the pupil diameter and choroidal changes in the subjects with PD > 6.0 mm receiving tropicamide 1% and phenylephrine. Only in the group that received cyclopentolate was choroidal thinning found to be significantly different in the subjects with PD > 6.0 mm compared to those with PD < 6.0 mm. The most important difference of cyclopentolate, an antimuscarinic agent, is a longer duration of action than the other agents used. Thus, it may have longer effect in tissue. Given the smaller number of subjects with PD < 6.0 mm, we think it appropriate to reevaluate these results in studies with larger sample size, as these results may be completely incidental.

To the best of our knowledge, ours is the first study comparing anterior chamber changes and choroidal thickness after mydriatic use to be found in the literature. Our results

have demonstrated that mydriatic drug use resulted in choroidal thinning, which was found to be independent from both anterior chamber depth and volume.

Although the choroidal effect that resulted from mydriatic use was thinning on average, it was not observed in all participants in the same way. While there was no significant change in some participants, there was an increase in some others. Excluding pupil diameter changes, anterior chamber parameters also displayed individual differences. There was no statistically significant relationship between anterior chamber parameters and choroidal changes. This might lead us to think that there might be some other factors causing changes in individual CT as a result of mydriatic use. This may also explain why there are conflicting findings in the literature. We are in the opinion that this subject should be further analyzed by large-scale works that utilize different types of data.

In the studies on choroidal thickness, it is important to indicate whether results are obtained before or after mydriatic use in order to assess study. Based on these results, it appears to be impossible to determine the extent of drug effects on the choroidea through evaluation of anterior chamber data.

Conflict of Interests

None of the authors has conflict of interests with the submission of this paper.

References

[1] S. W. Cheung, R. Chan, R. C. S. Cheng, and P. Cho, "Effect of cycloplegia on axial length and anterior chamber depth measurements in children," *Clinical and Experimental Optometry*, vol. 92, no. 6, pp. 476–481, 2009.

[2] F. Aptel and P. Denis, "Optical coherence tomography quantitative analysis of iris volume changes after pharmacologic mydriasis," *Ophthalmology*, vol. 117, no. 1, pp. 3–10, 2010.

[3] A. P. Ribeiro, R. M. Crivelaro, P. P. M. Teixeira et al., "Effects of different mydriatics on intraocular pressure, pupil diameter, and ruminal and intestinal motility in healthy sheep," *Veterinary Ophthalmology*, vol. 17, no. 6, pp. 397–402, 2014.

[4] D. L. Nickla and J. Wallman, "The multifunctional choroid," *Progress in Retinal and Eye Research*, vol. 29, no. 2, pp. 144–168, 2010.

[5] R. F. Spaide, "Enhanced depth imaging optical coherence tomography of retinal pigment epithelial detachment in age related macular degeneration," *The American Journal of Ophthalmology*, vol. 147, no. 4, pp. 644–652, 2009.

[6] T. Fujiwara, Y. Imamura, R. Margolis, J. S. Slakter, and R. F. Spaide, "Enhanced depth imaging optical coherence tomography of the choroid in highly myopic eyes," *The American Journal of Ophthalmology*, vol. 148, no. 3, pp. 445–450, 2009.

[7] I. Maruko, T. Iida, Y. Sugano, A. Ojima, and T. Sekiryu, "Subfoveal choroidal thickness in fellow eyes of patients with central serous chorioretinopathy," *Retina*, vol. 31, no. 8, pp. 1603–1608, 2011.

[8] S. Sızmaz, C. Küçükerdönmez, E. Y. Pınarcı, A. Karalezli, H. Canan, and G. Yılmaz, "The effect of smoking on choroidal thickness measured by optical coherence tomography," *British Journal of Ophthalmology*, vol. 97, no. 5, pp. 601–604, 2013.

[9] A. D. Vural, N. Kara, N. Sayin, D. Pirhan, and H. B. A. Ersan, "Choroidal thickness changes after a single administration of coffee in healthy subjects," *Retina*, vol. 34, no. 6, pp. 1223–1228, 2014.

[10] R. Chakraborty, S. A. Read, and M. J. Collins, "Diurnal variations in axial length, choroidal thickness, intraocular pressure, and ocular biometrics," *Investigative Ophthalmology and Visual Science*, vol. 52, no. 8, pp. 5121–5129, 2011.

[11] G. C. Massa, V. G. Vidotti, F. Cremasco, A. P. C. Lupinacci, and V. P. Costa, "Influence of pupil dilation on retinal nerve fibre layer measurements with spectral domain OCT," *Eye*, vol. 24, no. 9, pp. 1498–1502, 2010.

[12] G. Savini, M. Carbonelli, V. Parisi, and P. Barboni, "Effect of pupil dilation on retinal nerve fibre layer thickness measurements and their repeatability with Cirrus HD-OCT," *Eye*, vol. 24, no. 9, pp. 1503–1508, 2010.

[13] J.-C. Mwanza, F. E. Sayyad, M. R. Banitt, and D. L. Budenz, "Effect of pupil dilation on macular choroidal thickness measured with spectral domain optical coherence tomography in normal and glaucomatous eyes," *International Ophthalmology*, vol. 33, no. 4, pp. 335–341, 2013.

[14] M. Kim, H. J. Kwon, and S. C. Lee, "Influence of mydriatics on choroidal thickness measurement using enhanced depth imaging-OCT," *Optometry and Vision Science*, vol. 89, no. 8, pp. 1150–1155, 2012.

[15] N. Kara, A. Demircan, G. Karatas et al., "Effects of two commonly used mydriatics on choroidal thickness: direct and crossover effects," *Journal of Ocular Pharmacology and Therapeutics*, vol. 30, no. 4, pp. 366–370, 2014.

[16] R. F. Spaide, H. Koizumi, and M. C. Pozonni, "Enhanced depth imaging spectral-domain optical coherence tomography," *American Journal of Ophthalmology*, vol. 146, no. 4, pp. 496–500, 2008.

[17] S. Usui, Y. Ikuno, M. Akiba et al., "Circadian changes in subfoveal choroidal thickness and the relationship with circulatory factors in healthy subjects," *Investigative Ophthalmology & Visual Science*, vol. 53, no. 4, pp. 2300–2307, 2012.

[18] C. A. May, W. Neuhuber, and E. Lütjen-Drecoll, "Immunohistochemical classification and functional morphology of human choroidal ganglion cells," *Investigative Ophthalmology and Visual Science*, vol. 45, no. 2, pp. 361–367, 2004.

[19] D. L. Nickla, X. Zhu, and J. Wallman, "Effects of muscarinic agents on chick choroids in intact eyes and eyecups: evidence for a muscarinic mechanism in choroidal thinning," *Ophthalmic and Physiological Optics*, vol. 33, no. 3, pp. 245–256, 2013.

[20] E. Lütjen-Drecoll, "Choroidal innervation in primate eyes," *Experimental Eye Research*, vol. 82, no. 3, pp. 357–361, 2006.

[21] W. Neuhuber and F. Schrödl, "Autonomic control of the eye and the iris," *Autonomic Neuroscience: Basic and Clinical*, vol. 165, no. 1, pp. 67–79, 2011.

[22] B. P. Sander, M. J. Collins, and S. A. Read, "The effect of topical adrenergic and anticholinergic agents on the choroidal thickness of young healthy adults," *Experimental Eye Research*, vol. 128, pp. 181–189, 2014.